NASA TECHNICAL NOTE

NASA TN D-6985

NASA TN D-6985

ION HEATING MECHANISM IN A MODIFIED PENNING DISCHARGE

by J. Reece Roth

Lewis Research Center
Cleveland, Ohio 44135

NATIONAL AERONAUTICS AND SPACE ADMINISTRATION • WASHINGTON, D. C. • SEPTEMBER 1972

1. Report No.	2. Government Accession No.	3. Recipient's Catalog No.
NASA TN D-6985		

4. Title and Subtitle	5. Report Date
ION HEATING MECHANISM IN A MODIFIED PENNING DISCHARGE	September 1972
	6. Performing Organization Code

7. Author(s)	8. Performing Organization Report No.
J. Reece Roth	E-7003
	10. Work Unit No. 503-10
9. Performing Organization Name and Address	11. Contract or Grant No.
Lewis Research Center National Aeronautics and Space Administration Cleveland, Ohio 44135	
	13. Type of Report and Period Covered
12. Sponsoring Agency Name and Address	Technical Note
National Aeronautics and Space Administration Washington, D.C. 20546	14. Sponsoring Agency Code

15. Supplementary Notes

16. Abstract

Ions with Maxwellian energy distributions and kinetic temperatures ranging from 20 eV to 7 keV have been observed in a modified Penning discharge operating in the steady state. Investigation of the plasma revealed two distinct spoke-like concentrations of charge rotating with different velocities in the sheath between the plasma and the anode ring. The faster spoke consists of electrons rotating with the E/B drift velocity, where E is the electric field and B is the magnetic field strength. The slow spoke consists of ions, the thermal velocity of which is observed to be proportional to the spoke velocity. The experimental data are consistent with a model whereby the ion drift velocity in this spoke, corresponding to kilovolt ion energies, is Maxwellianized by strong electrostatic turbulence in the sheath. Theoretical expressions are derived for the frequency of the electron and ion spoke rotation, for the ion kinetic temperature, and for the ion heating efficiency as functions of the discharge parameters. These expressions are shown to be consistent with extensive experimental data.

17. Key Words (Suggested by Author(s))	18. Distribution Statement
Ion heating; Plasma heating; Penning discharge; Plasma generation; Hot ions; Rotating spokes	Unclassified - unlimited

19. Security Classif. (of this report)	20. Security Classif. (of this page)	21. No. of Pages	22. Price*
Unclassified	Unclassified	86	$3.00

* For sale by the National Technical Information Service, Springfield, Virginia 22151

CONTENTS

ION HEATING MECHANISM IN A MODIFIED PENNING DISCHARGE

by J. Reece Roth

Lewis Research Center

SUMMARY

Ions with Maxwellian energy distributions and kinetic temperatures up to 7 keV have been observed in a modified Penning discharge. Investigation of the plasma with capacitive probes at several azimuthal locations revealed two distinct spoke-like concentrations of charge rotating with different velocities in the sheath between the plasma and the anode ring. The faster spoke consists of electrons rotating with the E/B drift velocity, where E is the electric field and B is the magnetic field strength. The slow spoke consists of ions, the measured thermal velocity of which is proportional to the spoke velocity. The ion spoke is caused to rotate in the crossed electric and magnetic fields between the anode ring, which is at high positive potential, and the plasma, which is near cathode potential. The interaction of the electron and ion spokes appears to be responsible for the violent electrostatic "turbulence" observed and for the Maxwellianization of the ions. The experimental observations are consistent with an anode sheath thickness proportional to the ion Debye length, which is smaller than the ion gyrodiameter in this plasma. The E/B drift (spoke) velocity of the ions is smaller than that of the electrons, since the former are in the electric field of the sheath for only a fraction of their orbits.

Theoretical expressions are derived for the frequency of the ion and electron spoke rotation, for the ion kinetic temperature, and for the ion heating efficiency. These are expressed in terms of the discharge parameters. An extensive series of experimental measurements was made to test these theoretical expressions. Good agreement between experiment and theory was observed within error limits imposed by the nature of the experiment. It is shown that the ion kinetic temperature in the modified Penning discharge V_i scales according to the relation

$$V_i \sim \frac{V_a n_i^{1/4}}{B^{1/2}}$$

where V_a is the applied anode voltage, n_i is the ion density in the sheath, and B is the magnetic field strength. The observed data demonstrate that the ion heating efficiency can be as high as several tens of percent.

INTRODUCTION

History of the Penning Discharge

The Penning discharge was first extensively developed by F. M. Penning and his coworkers at the Philips Corporation (ref. 1). The objective of this early work was the development of a low-pressure ion gage tube, for which the anode current was directly proportional to neutral gas pressure. During the decade of the 1950's, the potential of the Penning discharge as an ion source was exploited by Gow and Foster (ref. 2) and also by Meyerand and Brown (ref. 3). A review of Penning discharges has been published by Hooper (ref. 4) and by Hopfgarten (ref. 5), who have summarized the extensive recent literature on the Penning discharge and its operating characteristics.

Observation of Hot Ions From Penning Discharges

There have been many reports of hot ion and even neutron production from Penning discharges. Hot ions and neutron production were first reported from a Penning-discharge-like configuration by K. A. George in 1961 (ref. 6). A second early paper reporting hot ion production was that of Angerth, Ehrensvard, and Persson (ref. 7) at the Culham conference in 1965. Several more recent investigations (refs. 8 to 13) have confirmed the production of hot ions in Penning discharges. In some cases ions with kinetic temperatures of several kilovolts (refs. 8 and 10 to 13) have been observed. Although the existence of hot ions in Penning discharges may be regarded as well-established, the physical processes responsible for ion heating are not understood.

Observation of Rotating Spokes in Penning Discharges

An entirely separate body of literature on the Penning discharge has reported a single rotating spoke in the anode sheath (refs. 4 and 14 to 23). This rotating spoke has been identified as a spoke of electrons rotating with E/B drift energies which are of the order of the ionization potential of the neutral gas investigated. Ionizing collisions of electrons in this rotating spoke with neutral gas molecules are generally regarded as the ionization mechanism by which the Penning discharge sustains itself at gas pressures below 10^{-3} torr. In none of the investigations discussed in references 14 to 23 was a second spoke of rotating ions also observed. This may have happened because these investigations involved Penning discharges of small radial dimensions, 1 to 2

centimeters, and/or very low magnetic fields, which would have been inadequate to confine ions of any significant kinetic temperature.

A few experiments have reported rotating spokes and/or hot ions in a modified Penning discharge (refs. 13, 24, and 25). Bannenberg and Brakenhoff (ref. 24) observed a single rotating spoke, but they were unable to make a direct measurement of the ion energy, or to determine whether the spoke consisted of ions, electrons, or both. Hopfgarten, Johansson, Nilsson, and Persson (ref. 13) have found one set of operating conditions for which the ion thermal velocity may have been comparable to the velocity of a spoke near the cathode of their device. Roth (ref. 25) has shown in preliminary work with a 15-centimeter-diameter anode ring that two distinct spokes exist and that the ion thermal velocity is directly proportional to the ion spoke velocity over more than an order of magnitude in these quantities.

Rotating Spokes and Hot Ions in Ion Magnetrons and Other Crossed-Field Devices

Hot ion and neutron production have also been observed in ion magnetrons and other similar devices based on crossed electric and magnetic fields (refs. 26 to 40). Some early work in which hot ions were observed in an ion magnetron geometry is discussed by Bishop (ref. 26), Neidigh and Weaver (ref. 27), and Boyer et al. (ref. 28). The hot ion and neutron production observed in these early experiments was not followed up in the controlled fusion program, nor were the physical mechanisms responsible for the ion heating identified.

Other devices in which ion heating is associated with crossed electric and magnetic fields have been investigated by Fahleson (ref. 29) and by Lehnert (refs. 30 and 31). In these devices a plasma is formed in contact with end electrodes that intercept the magnetic field lines, and the magnetic field is normal to the applied electric field. A plasma spoke rotates in the resulting crossed electric and magnetic field much in the manner of a homopolar motor. A velocity limit was observed in homopolar plasmas which held over a wide range of plasma conditions (refs. 29 to 31). Fahleson (ref. 29) found that the rotating spoke accelerated until the ion energies become comparable to the ionization potential of the gas used, not more than 10 to 20 electron volts per ion. It did not appear possible to heat ions above this limit under the conditions of the Fahleson experiment (ref. 29). Lehnert (refs. 30 and 31) remarked that if this limit could be overcome, a very attractive ion heating method for controlled fusion research would result.

Another approach to ion heating by crossed electric and magnetic fields is the BURNOUT series of experiments of the Oak Ridge National Laboratory (refs. 32

to 37). These investigators have developed a steady-state ion magnetron device in which hot electrons, hot ions, and steady-state neutron production have been observed under various operating conditions. The heating mechanism in this device has been variously attributed to electron cyclotron resonance heating of the electrons by internally generated radiofrequency fields (ref. 32), to beam-plasma interactions in the case of ion heating (refs. 32 to 34), and more recently to various instabilities in the vicinity of the ion plasma frequency (refs. 35 to 37).

Another class of crossed-field device that produces higher ion than electron energies is the magnetoplasmadynamic (MPD) thruster, which is under development as a possible space propulsion system (refs. 38 and 40). Ion energies of 10 to 100 eV are commonly reported (refs. 38 and 40), and the spoke rotation velocity has been observed to be equal to the ion thermal velocity for a few operating conditions in which both parameters were simultaneously measured (ref. 40). In view of the extensive theoretical and experimental work available on the MPD thruster (see refs. 38 and 40, for example) and other space-related devices (ref. 39), it is surprising that the space-related MPD arc literature has been overlooked in reviews of Penning discharges and other crossed-field devices (refs. 4, 5, and 31).

OBSERVATION OF ION HEATING AND THERMALIZATION

Description of Experiment

The present experiment is an extension of earlier work in which hot ions were reported (refs. 8, 10, 12, 41, and 42) and of a preliminary paper in which the origin of the high ion thermal velocities was traced to a rotating ion spoke in the anode sheath (ref. 25). The present report extends the investigations reported in reference 25 to four anode rings with different diameters and also includes a theoretical and experimental study of the rotating spoke dynamics.

In figure 1 is shown an isometric cutaway drawing of the superconducting magnetic mirror facility used in the present experimental investigation (ref. 43). The anode ring is located at the midplane of the magnetic mirror. The two superconducting magnet Dewars are located in a vacuum tank 1 meter in diameter and 2 meters long. The walls of the vacuum tank are at least 50 centimeters from the plasma, along the magnetic field lines, and the surfaces of the superconducting magnet Dewars are at liquid nitrogen temperatures. These features, in addition to operation in the steady state, reduced the level of background impurities to a negligible level, such that contaminants could not be detected with an optical bench spectrometer in this series of experiments. Deuterium gas was introduced into the vacuum tank at a location remote from the plasma, and the

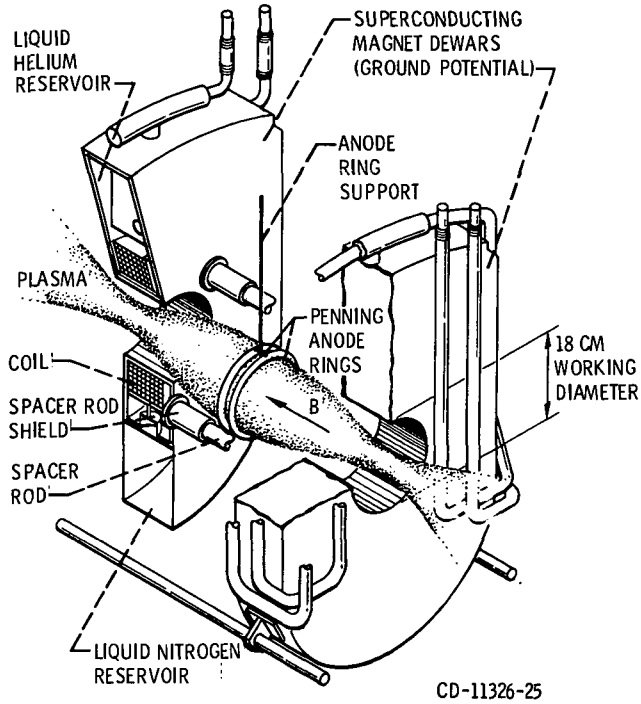

Figure 1. - Isometric cut-away drawing of the modified Penning discharge in a superconducting magnetic mirror facility. The anode ring is normally operated at positive dc potentials up to several tens of kilovolts.

entire vacuum tank was at essentially the same background pressure. The background pressure was measured with a commercial ion gage tube, and the indicated gage pressure is quoted in this report. Absolute pressures may be obtained by multiplying by a gage factor of 2.6, appropriate to deuterium gas.

In figure 2 is a photograph of the plasma taken under relatively low ion temperature and high density conditions. The boundary of the plasma follows the magnetic field lines. The plasma is optically hollow in the center, and the radial distribution of ion energy and density have a dip on the axis of the plasma. The vertical element in the midplane is a single, circular, water-cooled, anode ring of 15.2-centimeter inside diameter, which is operated at positive direct-current potentials of up to 40 kilovolts. Occasional arcing from the anode ring support rod to nearby sheet metal made it necessary to limit experimental runs to anode voltages below 30 kilovolts. In this series of investigations, the mirror ratio was 2.64:1. The "standard" maximum magnetic field at the mirror throats was 1 tesla, and the magnetic field at the midplane, where the anode rings are located, was 0.38 tesla. Note that there are no hot, electron-emitting cathodes on the axis of the magnetic field. The discharge is sustained by a cascading ionization process in the anode sheath. The electrons produced in the sheath migrate to the anode ring. The ions are lost through the mirrors of the magnetic bottle and impinge

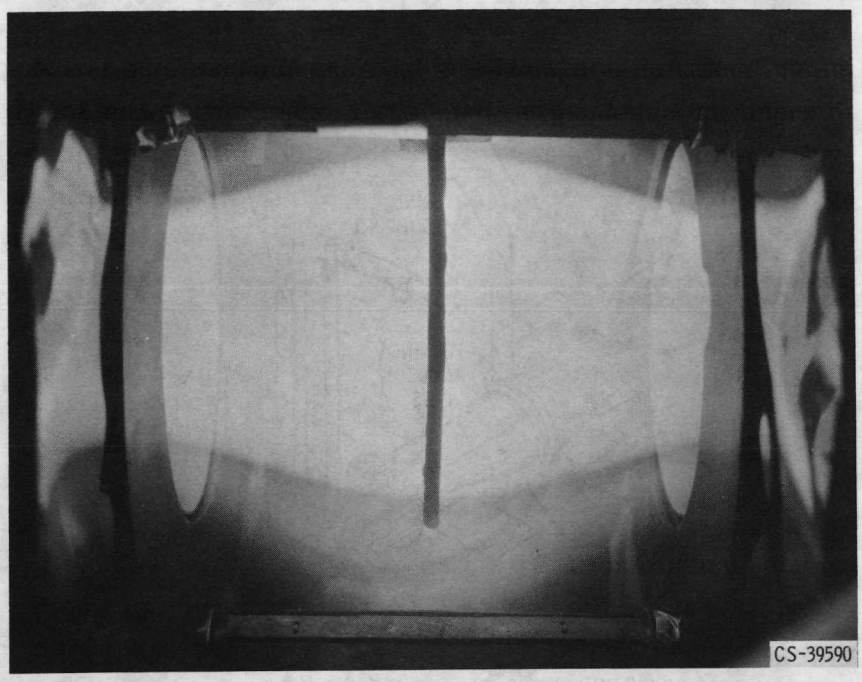

Figure 2. - Plasma in modified Penning discharge. Vertical element in center is single anode ring with inside diameter of 15.2 centimeters (6 in.).

on the walls of the vacuum tank about 50 centimeters away from the center of the plasma and thus complete the electrical circuit to the power supply. The plasma volume is approximately 2.5×10^3 cubic centimeters for a 15.2-centimeter-diameter anode ring.

The anode assemblies used in this investigation are shown in figure 3. These double anode rings were used to increase the axial width of the anode sheath, and thus improve the coherence and signal-to-noise ratio of signals associated with rotating spoke phenomena, and to make the plane of symmetry accessible to diagnostic instruments. These anode rings are 5.1, 10.2, 15.2 and 20.3 centimeters in diameter. Each anode assembly consists of two circular rings of 0.63-centimeter (1/4-in.) copper tubing through which cooling water flows. The two rings of each assembly were spaced approximately 1.3 centimeters on either side of the magnetic field midplane. As is evident in figure 2, the plasma diameter at the midplane is never greater than the inner diameter of the anode ring, and this latter dimension was therefore used to characterize the plasma diameter.

Figure 4 shows the retarding potential energy analyzer, which was used to measure the component of ion energy parallel to the magnetic field lines as the ions left the magnetic mirror (ref. 10). For a 15.2-centimeter-diameter anode ring, the retarding potential energy analyzer was spaced approximately 10 centimeters from the magnetic field axis and 20 centimeters outside the magnetic mirror throat. The radial position of the analyzer was adjusted for other anode ring diameters in such a way that the mag-

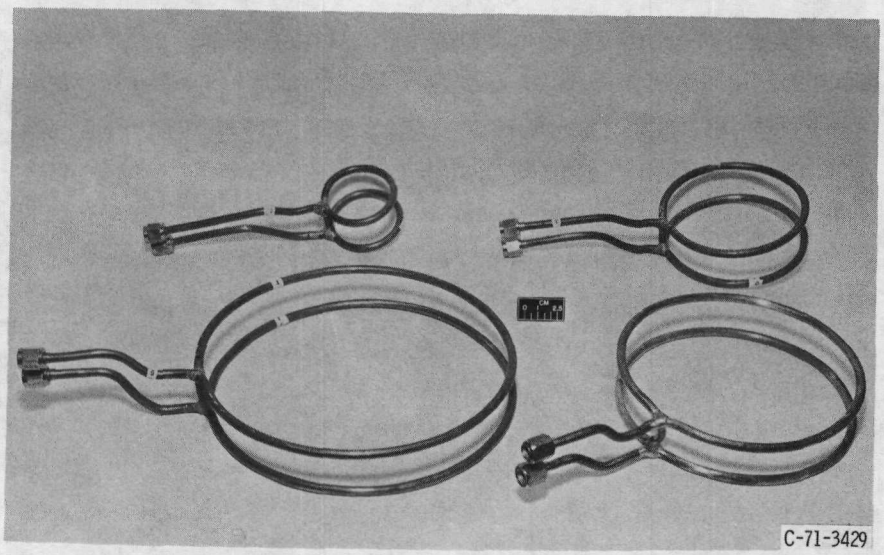

Figure 3. - Four anode rings used in this investigation. Anode rings had inner radii of 2.54, 5.08, 7.62, and 10.16 centimeters (1, 2, 3, and 4 in.).

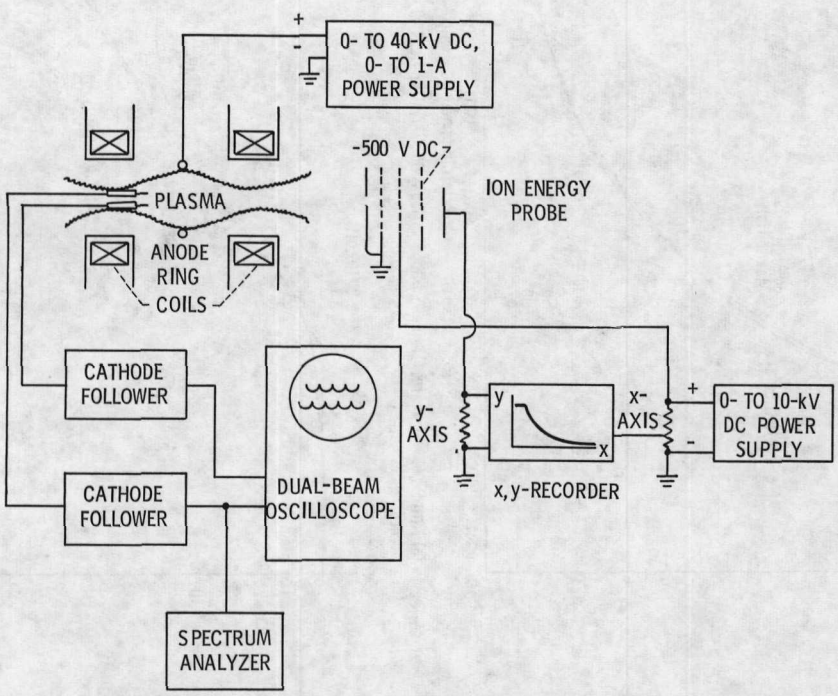

Figure 4. - Schematic of principal plasma diagnostics used in this investigation. Assembly of five capacitive probes was inserted in left throat of magnetic mirror to detect azimuthally rotating electrostatic potential fluctuations. Ion energies were measured with retarding potential energy analyzer.

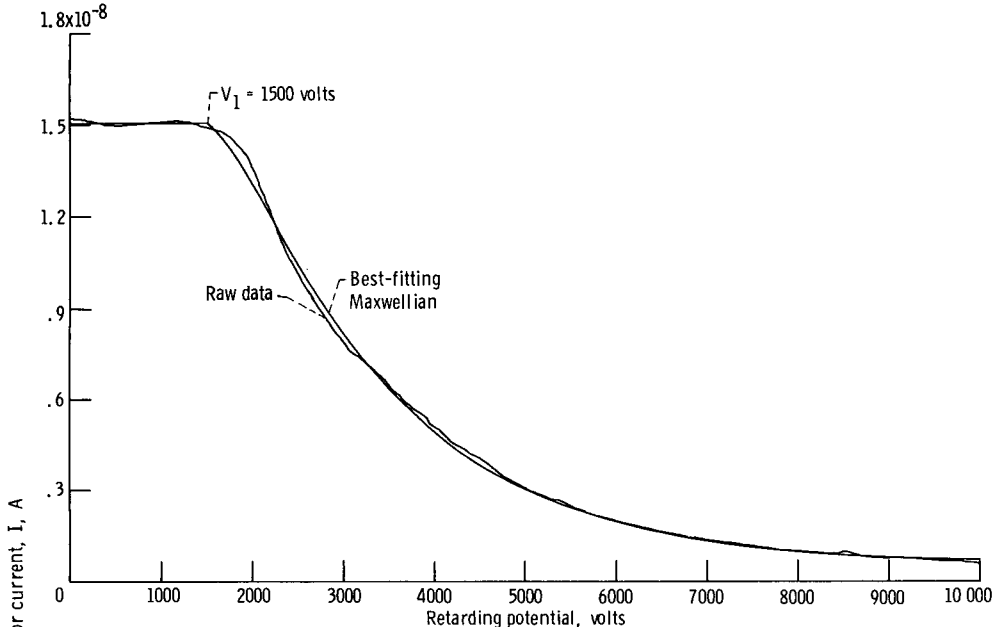

(a) Kinetic temperature, 1740 eV; anode voltage, 15 kilovolts; neutral gas pressure, 4.2×10^{-6} torr; anode current, 5 milliamperes.

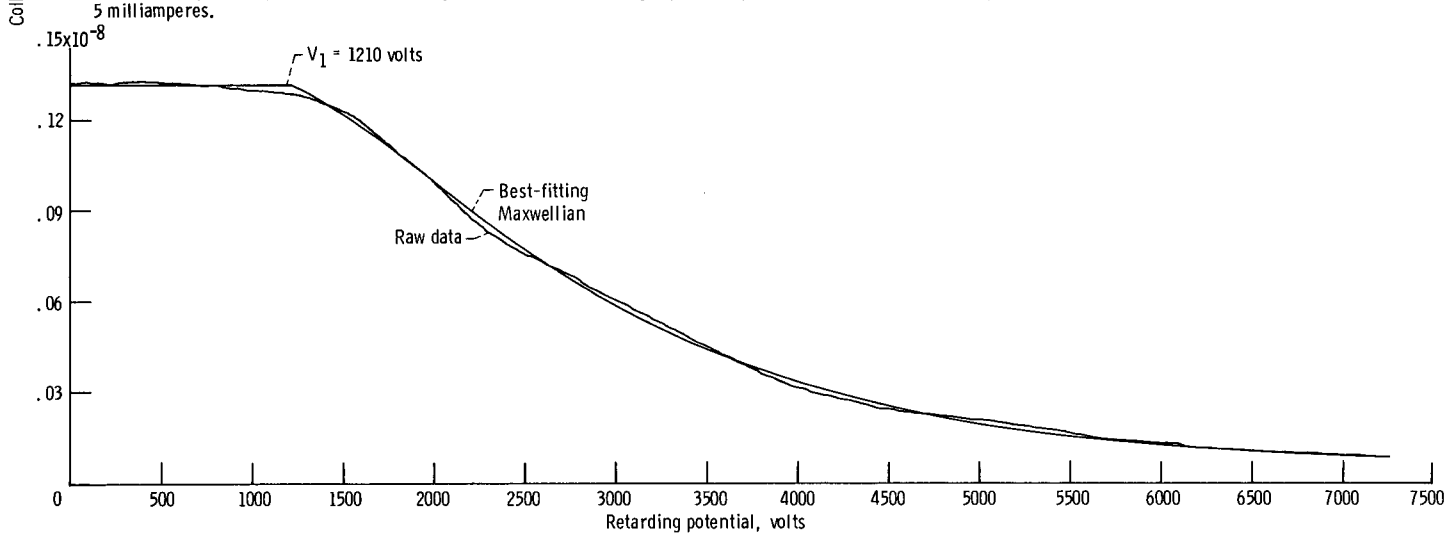

(b) Kinetic temperature, 1600 eV; anode voltage, 10 kilovolts; neutral gas pressure, 9×10^{-7} torr; anode current, 2 milliamperes.

Figure 5. - Two examples of deuterium ion energy spectra taken with retarding potential energy analyzer. Shown are raw data and best-fitting integrated Maxwellian distribution for pulsed efflux of particles. Minimum magnetic field strength, 0.38 tesla; maximum magnetic field strength, 1.0 tesla; anode ring diameter, 15.2 centimeters.

netic field line on which the anlyzer is located passes approximately within 1 centimeter of the inner radius of the anode ring. This radial position was intended to sample the efflux of ions from the anode ring sheath. The axis of the analyzer was alined with the direction of the magnetic field at the analyzer location. By sweeping the intermediate grid of the retarding potential energy analyzer through positive potentials, one obtains a collector current that is an integrated energy distribution function of ions reaching the energy analyzer (ref. 10). Also shown schematically in figure 4 is the capacitive probe assembly, which is discussed in the next section. The power supply was capable of 40 kilovolts of direct current at 1 ampere.

Observed Ion Energy Spectra

Figure 5 shows two ion energy spectra obtained with the retarding potential energy analyzer. Plotted over the raw data is the best-fitting integrated Maxwellian distribution. In both cases, the energy is Maxwellianized along a radius in velocity space, even in the high energy tail of the distribution (ref. 10). The kinetic temperature which best fits the data is 1740 and 1600 eV for figures 5(a) and (b), respectively. In this investigation, ion kinetic temperatures from 20 eV to 7 keV were observed, and the ions had Maxwellian energy distributions.

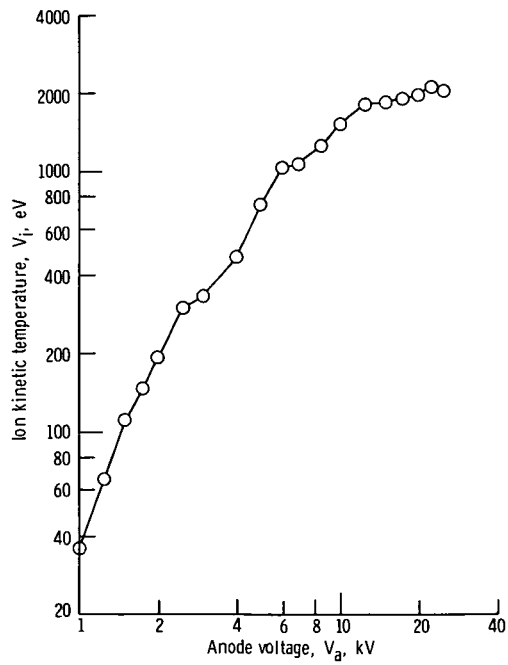

Figure 6. - Ion kinetic temperature as function of positive anode voltage. Neutral gas pressure, 5×10^{-6} torr; anode ring diameter, 15.2 centimeters.

Ion Energy as a Function of Anode Voltage and Gas Pressure

Retarding potential energy spectra were taken for a variety of operating conditions, and some typical results are illustrated in figure 6. These were taken with an anode ring 15.2 centimeter in diameter. The ion kinetic temperature is plotted as a function of the anode voltage for a background pressure of deuterium gas of 5×10^{-5} torr. The ion kinetic temperatures vary with plasma conditions other than the anode voltage, and nonadiabatic effects may be expected to influence data above ion energies of 300 eV in this apparatus.

OBSERVATION OF TWO DISTINCT ROTATING SPOKES

Diagnostic Equipment

The data presented in the previous section demonstrate the existence of thermalized hot ions in this modified Penning discharge. In an attempt to identify the physical mechanism responsible for these ions, a number of diagnostic probes were tested. The most satisfactory are capacitive probes, the performance and characteristics of which

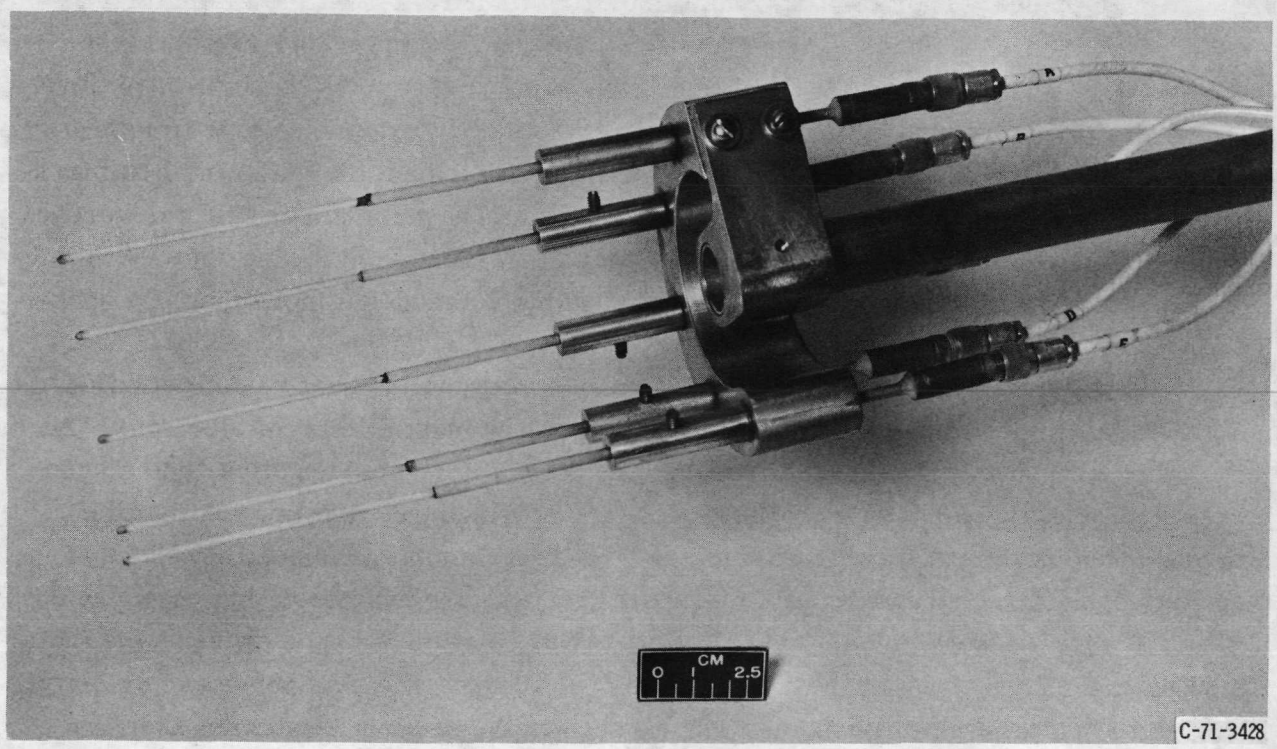

Figure 7. - Capacitive probe assembly.

have been described elsewhere (ref. 44). One of the capacitive probe assemblies used in this investigation is shown in figure 7. The five capacitive probes shown are mounted on a 7.6-centimeter diameter and were used with the anode ring of 15.2-centimeter inside diameter. The capacitive probes were located at the magnetic mirror throat. For all anode rings, the magnetic field lines on which the probes were located passed through a point approximately 1 centimeter from the inner surface of the anode ring at the midplane. This was accomplished by varying the radius at which the five probes were mounted. The capacitive probes could not be moved closer to the midplane, for a large portion of the data, because damage would have resulted from plasma bombardment of the probe. The five capacitive probes were mounted at 45° increments in azimuth. During normal operation signals from probes at opposite ends of a diameter were monitored by a dual-beam oscilloscope to verify that the signals were 180° out of phase. Rotating spokes with mode numbers higher than $m = 1$ could be identified with the other three capacitive probes attached to the assembly when the nature of the waveform was ambiguous.

Physical Model of Sheath Phenomena

Figure 8 shows three examples of waveforms of electrostatic potential fluctuations, taken from probes at opposite ends of a diameter, with a 10.2-centimeter-diameter anode ring. Each of the photographs shown in figure 8(a), (b), or (c) was taken under the same set of plasma operating conditions, but with different time scales. The waveform in the top photograph is the electrostatic potential waveform on a fast time scale. The signal was 180° out of phase at opposite ends of the diameter, which implies that a concentration of charge or "spoke" was rotating about the plasma axis. It was verified by observing the phase from probes at other azimuthal positions that the data shown in figure 8 refer to a single rotating spoke, although higher modes - more than one spoke - were observed in isolated cases.

The sign convention for potential in figure 8 is such that a negative deflection is upward. The rotating spoke illustrated in the first row must consist of electrons. As the spoke approached and passed the probe, the potential became negative, and a cusp-like peak on the waveform was produced. This cusp-like peak also implies that the electron spoke is narrow in azimuthal extent. In this example, the rotating spoke of electrons had a frequency of about 3 megahertz and was therefore rotating with a velocity of about 1.1×10^{6} meters per second. The energy of rotation is of the order of the ionization potential of the gas, that is, of the order of 10 eV. The electron spoke velocity varies with operating conditions. As will be seen in the section Relation of Electron Energy to Electron Spoke Velocity the electron spoke velocity and electron thermal

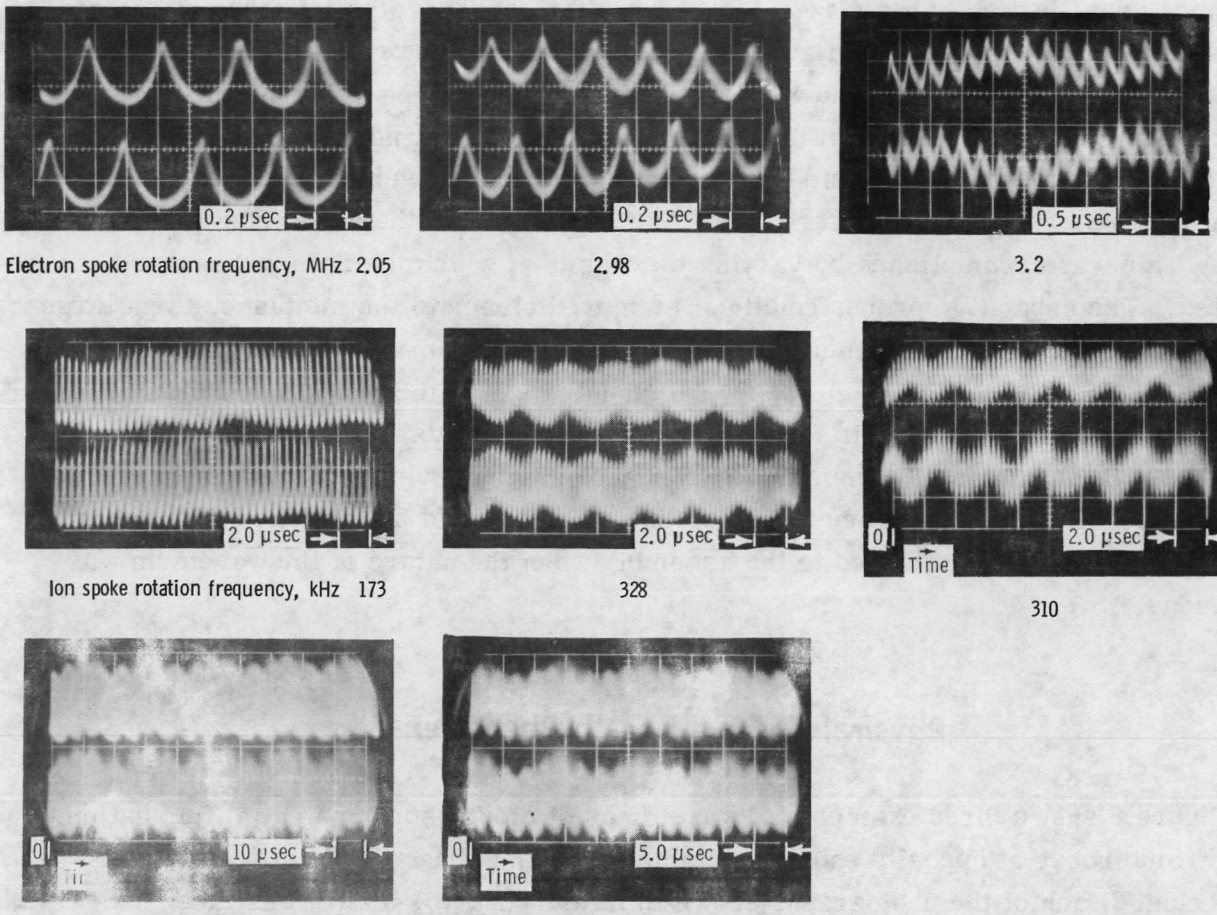

(a) Neutral gas pressure, 6.1×10^{-6} torr; anode voltage, 8 kilovolts; anode current, 4 milliamperes.

(b) Neutral gas pressure, 1.25×10^{-5} torr; anode voltage, 10.7 kilovolts; anode current, 12 milliamperes.

(c) Neutral gas pressure, 1.55×10^{-5} torr; anode voltage, 10 kilovolts; anode current, 16.5 milliamperes.

Figure 8. - Multiple-sweep waveforms of electrostatic potential fluctuations detected by capacitive probes at opposite ends of a diameter, taken under conditions of unusual oscillation coherence. Waveforms taken in deuterium gas; minimum magnetic field strength, 0.38 tesla; anode ring diameter, 10.2 centimeters.

velocity are approximately proportional to one another.

The data in the middle row of figure 8 show that there was a modulation of the signal amplitude at a frequency of about 300 kilohertz in these examples. This modulated waveform is also 180° out of phase at opposite ends of the diameter. It was verified with probes at other azimuthal locations that this slower rotating concentration of charge was a single "spoke" in the cases shown, although $m = 2$ and $m = 4$ spokes were also observed under other conditions. Under conditions shown in figure 8(c), downward-pointing cusps were observed on the ion waveform, which indicate a spoke of positive ions approaching the probe. The rarity of cusps on the ion waveform suggests that the ion spoke has a significant azimuthal spread or that it is located at a smaller radius.

The ion and electron spokes both rotate in the $\underline{E} \times \underline{B}/B^2$ drift direction. The rotational frequencies of the ion spokes were typically a factor of 5 or 10 less than the rotational frequency of the electron spoke. It was verified by placing two probe arrays at various axial stations that both the electron and ion spokes are in phase along the axis of the discharge, so that each behaves as if it obeys Ferraro's law of isorotation (ref. 45).

In the bottom row of figure 8(a) is shown the potential waveform on the slowest time scale. A third frequency, which modulates the data, is apparent below 100 kilohertz. These oscillations are in phase throughout the plasma volume. This in-phase oscillation is the continuity-equation oscillation which has been reported previously (refs. 46 and 47).

The physical picture adopted to explain the data in figure 8 is indicated schematically in figure 9. The outer circle represents the anode ring, and the interior is occupied by the confined plasma. The interior plasma is quasi-neutral and is typically observed to be a few hundred volts positive with respect to ground potential. Figures 5(a) and (b) are exceptional in that they indicate floating potentials of more than 1 kilovolt. A sheath is assumed to exist between the plasma and the anode ring, with a voltage drop across it that varies from 1 to 30 kilovolts in this investigation. The electrons are highly magnetized in this plasma, since they are in magnetic fields of at least several tenths of a tesla. The ions are therefore the more mobile species in directions normal to the magnetic field lines. This implies that the radial anode sheath thickness is determined by the ion Debye length (ref. 48, p. 162) rather than the electron Debye length. As will become evident, the observed data are best fit by theoretical expressions which incoroprate the ion Debye length as the sheath thickness, but are inconsistent with expressions that assume a sheath thickness given by the electron Debye length, or the ion gyroradius.

The ion Debye length is of the order of 1 centimeter at the midplane of this discharge. The electrons in the thick anode sheath experience an electric field which gives

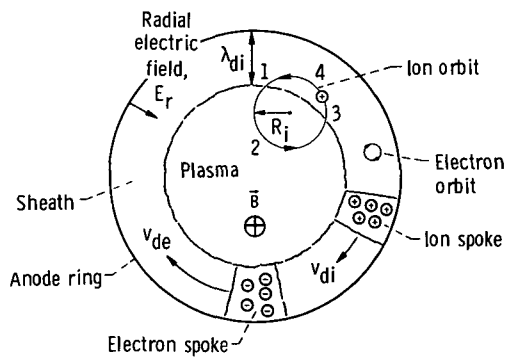

Figure 9. - Schematic drawing illustrating phenomena in sheath between anode ring and plasma. Electron drift velocity $v_{de} = E_r/B$; ion drift velocity $v_{di} = \delta E_r/B$.

them an E/B drift velocity. The electrons do not leave the electric field of the sheath because their gyrodiameters are smaller than the sheath thickness. The operating conditions of this discharge are such that the ion gyrodiameter is larger than the ion Debye length at the midplane, where the anode ring is located. A consequence of this, indicated in figure 9, is that ions will be in the sheath for only a part of their orbit. The ion spoke then moves at a slower drift velocity than the electron spoke, because the ions experience the sheath electric field only part of the time.

Relation of Ion Energy to Ion Spoke Rotation

This section discuses the relation between the velocity of the rotating spoke and the ion energies which was first reported in reference 25. The experimental data have been reduced on the assumption that the strong electrostatic turbulence reported in reference 12 results in equipartition of energy between the parallel, perpendicular, and guiding center (spoke) velocities such that the total energy is given by

$$W_i = \frac{1}{2} m_i v_i^2 = \frac{1}{2} m_i \left(v_{\perp i}^2 + v_{\parallel i}^2 + v_s^2 \right) = 2 m_i v_s^2 \tag{1}$$

(Symbols are defined in appendix A.) Since the ion energy was acquired from the ion spoke rotational velocity, it also appeared likely that the total velocity v_i is the velocity which corresponds to the most probable energy,

$$\frac{1}{2} m_i v_i^2 = \frac{1}{2} eV_i \tag{2}$$

If the guiding centers of the ions are assumed to be at the inner radius of the anode ring R, the expected ion spoke rotation frequency for ions with kinetic temperature v_i in electron volts is given by

$$\nu_1 = \frac{1}{4\pi R} \sqrt{\frac{eV_i}{m_i}} \tag{3}$$

Figure 10 shows the observed frequency of the ion spoke ν_{io} as a function of ν_1 predicted from equation (3), where V_i was measured by the retarding potential energy analyzer. In figure 10 are data for the four anode ring radii investigated, with the observed frequency divided by the mode number (number of spokes). If there were a one-

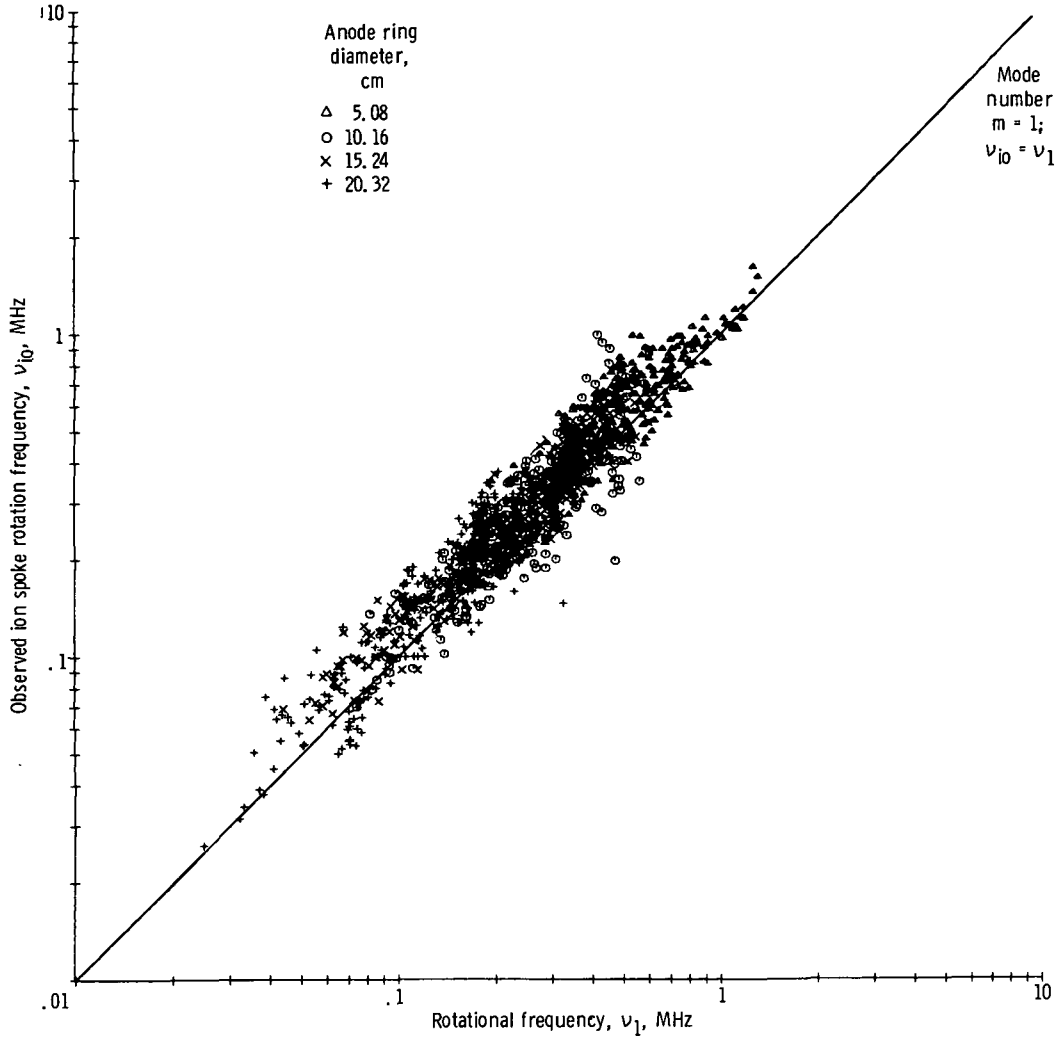

Figure 10. - Relation of observed ion spoke rotation frequency to rotational frequency calculated from measured ion kinetic temperature given by equation (3) for four anode ring radii.

to-one correspondence between the observed ion spoke frequency and the ion spoke frequency calculated from equation (3), the data would lie on the straight line of slope 45°. The frequency ν_i was calculated on the assumption that the guiding centers were located on the inner surface of the anode ring. In general, most of the data lie slightly above the 45° line, as a result of the finite gyroradius of the ions. An effective spoke radius of about 0.85 R best fits the data. The trend of the data has a slope of 45°. This is very significant, since it implies that the E/B drift velocity of the ions is directly proportional to the ion thermal velocity, as was assumed in deriving equation (3). It is plausible that this rotating spoke is driven by the electric field of the sheath and is the physical mechanism by which the ions are raised to high energies.

In figure 11 is shown all of the data from figure 10 plotted in raw form, without

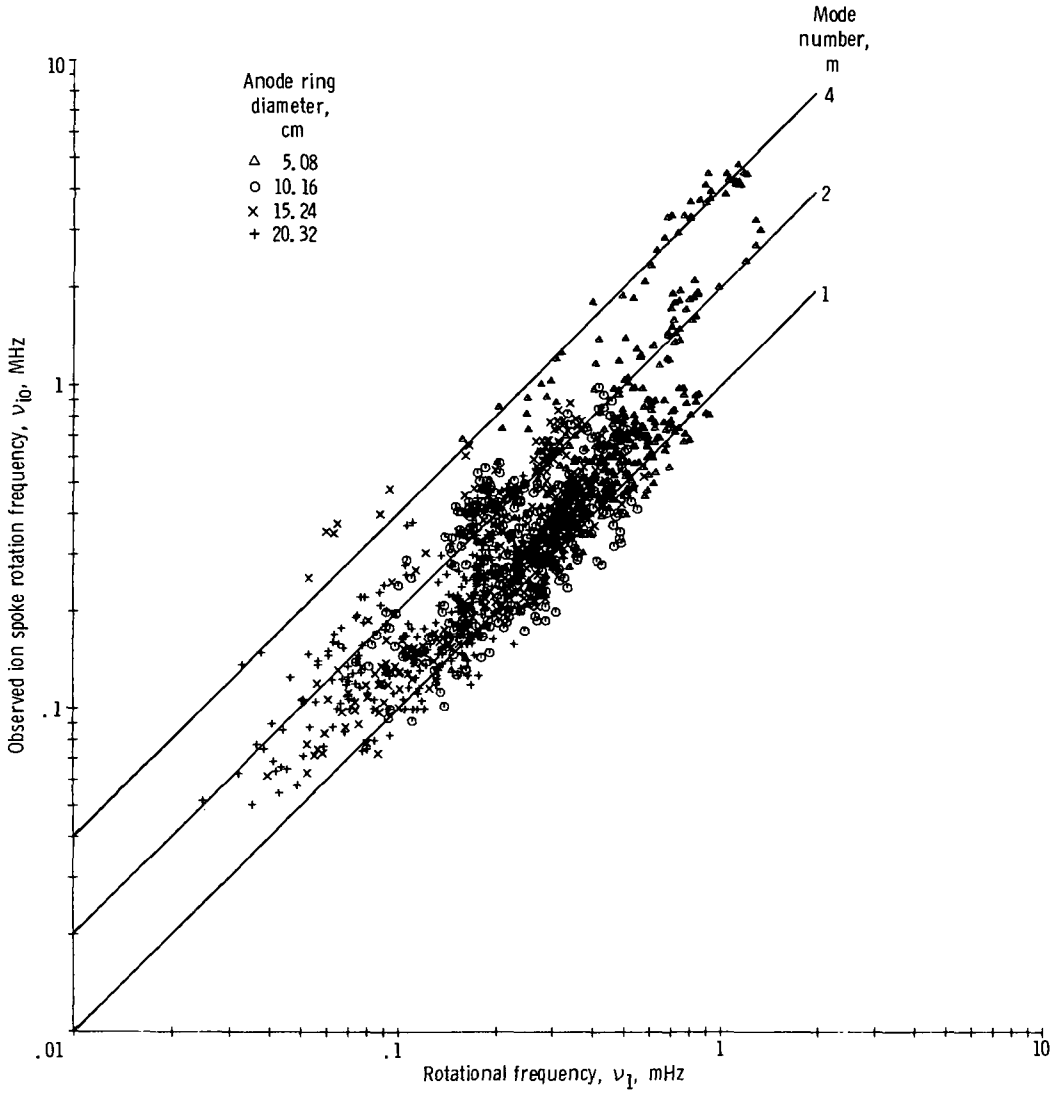

Figure 11. - Relation of observed ion spoke rotation frequency to rotation frequency calculated from measured ion kinetic temperature given by equation (3) for four anode ring radii and entire data population without division by mode number.

division by the mode number. Harmonics of the fundamental ion spoke rotation frequency, sidebands, and peaks due to radiofrequency interference were omitted from these graphs. Some of the data in figure 11 reveal that two (m = 2) or four (m = 4) spokes equally spaced in azimuth, were simultaneously present. These higher order modes are shown schematically in figure 12. These data lie adjacent to the lines designated m = 2 and m = 4 in figure 11. Graphs of the data for individual modes are given in appendix B. A few of the m = 2 and m = 4 data may be harmonics of m = 1 spokes, the fundamental frequency of which was buried in the background turbulent spectrum. However, this explanation cannot hold for the majority of the m = 2 and m = 4 data shown

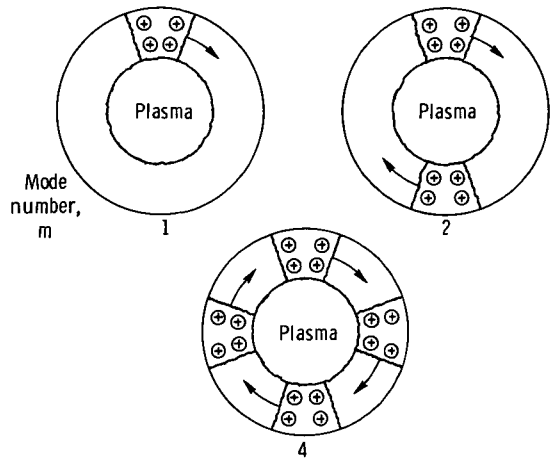

Figure 12. - Schematic showing physical significance of oscillations for mode numbers 1, 2, and 4 from figure 11.

in figure 11. Experimental spot checks with the capacitive probes not at opposite ends of a diameter were made when higher mode numbers were observed. It was confirmed that the data designated $m = 2$ and $m = 4$ were higher order modes in these cases.

Energy Cascading in Turbulent Spectrum

The Maxwellianization of the ion energy may be understood as resulting from the interaction of the ion and electron spokes. On the average, the electron spoke will pass through or near the ion spoke several times each microsecond. One would expect two spokes consisting of charge concentrations of opposite sign to interact very strongly and to give rise to electrostatic turbulence involving high electric fields. Such violent electrostatic turbulence was observed in this discharge and has been reported previously (ref. 12).

In figure 13 is shown the spectrum of electrostatic potential fluctuations φ from 100 kilohertz to 1 megahertz, as measured with a capacitive probe (ref. 12). The spectrum has been plotted on log-log axes, and the peak is at the ion spoke rotation frequency, about 300 kilohertz, in the two examples shown. The turbulence spectrum in figure 13 may be understood by assuming that energy is injected into the spectrum at the peak frequency, corresponding to the ion spoke rotation frequency. The energy then cascades upward in frequency and downward in scale size, as indicated by the enhancement of the spectrum above the energy input frequency. It is characteristic of this strong electrostatic turbulence that, when plotted on log-log axes, the spectrum follows a power law relation (ref. 12). Below the energy input frequency, the spectrum approximates a straight line. Above the input frequency the spectrum is also a straight line

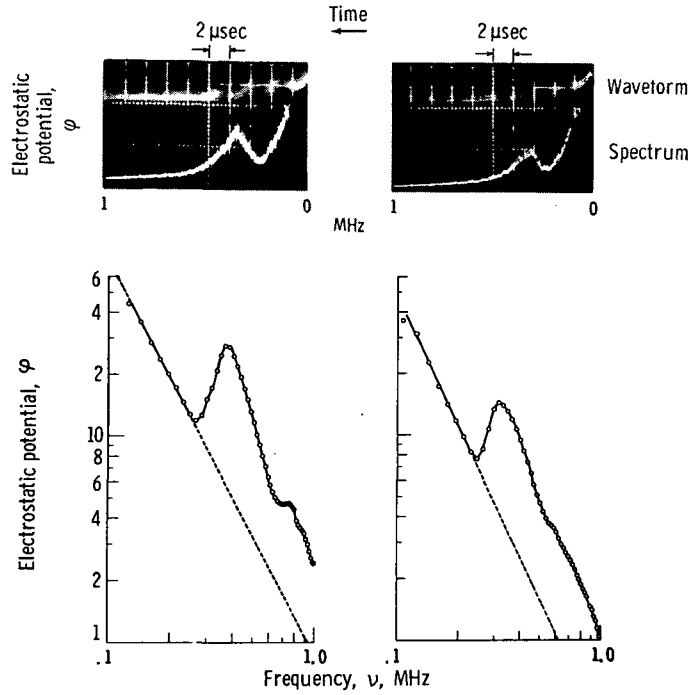

Figure 13. - Two examples showing energy cascading in spectrum of electrostatic potential fluctuations.

with the same slope, but there is a considerable enhancement of the spectrum above the input frequency. This enhancement of the spectrum results from the energy cascading upward in frequency and downward in scale size as the ion energy is degraded into random thermal motions of the ions. This randomization of the ion energy is evident in the Maxwellian energy distributions illustrated in figure 5.

DYNAMICS OF PARTICLE MOTION IN SHEATH

Description of Sheath

The proportionality of the observed intermediate spoke rotation frequency to the frequency calculated from the ion kinetic temperature in equation (3) is consistent with the hypothesis that the intermediate frequency represents a rotating spoke of ions in the sheath. It is possible to extract further information about the nature of the rotating spokes from information contained in the electrostatic potential waveforms in figure 8. The waveforms shown in figure 8 are multiple-sweep traces. It is evident, in the examples shown in this figure, that the multiple-sweep traces quite accurately retrace one another. This implies coherence in phase, amplitude, and frequency of the spoke

rotation over many periods of rotation. Other data, not shown in figure 8, were taken under conditions for which the coherence time was not more than 6 or 10 periods of rotation. In the examples shown in figure 8, however, the coherence holds for up to 20 rotations of the ion spoke about the anode ring. The motion of the electron spoke can be followed for at least 100 rotations and implies a substantially greater coherence. Another characteristic of the data in figure 8 is that both the ion and electron spokes rotate with a single very sharply defined frequency. In other data, not illustrated in figure 8, a very low and broad frequency peak was seen in the spectrum analyzer under more highly turbulent operating conditions. While the data in figure 8 are some of the most coherent taken during this investigation, these data are typical in having a relatively sharply defined frequency for both the electron and ion spoke rotation frequency.

The frequency of the spoke was measured as a function of radius and found to be constant. This observation, along with the nature of the spoke rotation as an E/B drift velocity, implies that the electric field in the sheath is proportional to radius. Otherwise, one would see a multitude of frequencies, each appropriate to a particular electric field. The nature of the sheath is discussed further in appendix C. In addition, the waveforms are visible over dozens to hundreds of cycles after the triggering waveform peaks in figure 8(a) and (b), before they fade out into turbulent noise or incoherence. This suggests that the radial velocity of the electrons and ions is much smaller than their azimuthal E/B drift velocity. If the radial velocities were as much as one-tenth of the azimuthal drift velocities, the ion and electron spokes would be expected to fade out into incoherence after making only one or two rotations about the inner circumference of the anode ring.

Equations of Electron Motion in Sheath

The guiding center equations of motion for electrons in the sheath may be written in terms of the coordinates defined in figure 14 as follows (ref. 48, p. 199, and ref. 49, pp. 2 to 3):

$$-\ddot{R}_e + \Omega_e^2 R = \frac{\omega_e E_r}{B} + \omega_e \Omega_e R + \nu_{ce} \dot{R}_e \tag{4}$$

$$R\dot{\Omega}_e + 2\Omega_e \dot{R}_e = -\frac{\omega_e E_\theta}{B} + \omega_e \dot{R}_e - \nu_{ce} R \Omega_e \tag{5}$$

The last term on the right side of these equations is the Langevin collision term, which

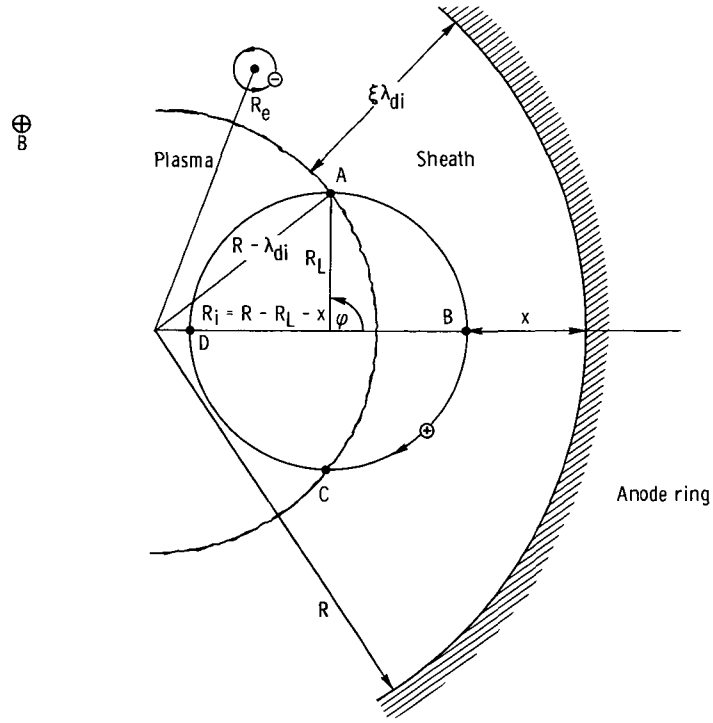

Figure 14. - Schematic diagram for derivation of quantity δ, which describes fraction of ion orbit spent in anode ring sheath.

normally represents the forces that result from electron collisions with the neutral atoms of the background gas (ref. 49, p. 15). In the present context, however, the electron-neutral collision frequency ν_{en} is not adequate to represent the forces acting on the electrons due to collisional processes.

It has been shown that the ion and electron spokes will interact with one another with frequencies generally higher than 1 megahertz. Such interaction frequencies are from one to two orders of magnitude higher than the frequencies of electron-neutral collisions in the present experiment. The strong electric fields associated with the interaction of the two spokes when they pass through one another will perturb the motion of individual particles at least as much as a collision with an individual electron, ion, or neutral gas molecule. For this reason, it is proposed to introduce a "mixmaster" collision frequency given by the following expression:

$$\nu_{ce} = \nu_{en} + \Omega_e - \Omega_i \tag{6}$$

This new collision frequency is the sum of (1) the conventional Langevin collision frequency of electrons (or ions) with the neutral molecules of the background gas, and (2) the number of times the spokes interact per second.

Introducing equation (6) into equation (4) and (5) yields

$$-\ddot{R}_e + \Omega_e^2 R = \frac{\omega_e E_r}{B} + \omega_e \Omega_e R + \dot{R}_e(\nu_{en} + \Omega_e - \Omega_i) \tag{7}$$

$$R\dot{\Omega}_e + 2\Omega_e \dot{R}_e = -\frac{\omega_e E_\theta}{B} + \omega_e \dot{R}_e - R\Omega_e(\nu_{en} + \Omega_e - \Omega_i) \tag{8}$$

where the radial and azimuthal positions and velocities refer to the guding center of the particle. One may utilize the experimentally observed coherence of the electron spoke waveform over many cycles of oscillation to justify the assumptions that

$$\dot{R}_e << R\Omega_e \tag{9}$$

and

$$\ddot{R}_e << R\Omega_e^2 \tag{10}$$

The observed constant frequency of spoke rotation illustrated in figure 8 justifies the assumption

$$\dot{\Omega}_e \approx 0 \tag{11}$$

In the present experiment, it is always the case that

$$\Omega_e << \omega_e \tag{12}$$

In light of these inequalities, the equations of motion for electrons in the sheath given by equations (7) and (8) may be written

$$\Omega_e R \approx -\frac{E_r}{B} + \frac{\Omega_e^2 R}{\omega_e} \tag{13}$$

$$\dot{R}_e \approx \frac{E_\theta}{B} \tag{14}$$

Equation (13) states that the electron azimuthal drift velocity is given by the ratio E_r/B plus a small centrifugal correction. In the present experiment the centrifugal force term is many orders of magnitude smaller than the other two terms in equation (13), and one can assume that the electron drift velocity is given by

$$\Omega_e R \approx \frac{E_r}{B} \tag{15}$$

Equations of Ion Motion in Sheath

The guiding center equations of motion for ions in the sheath may be written in terms of equation (6) as

$$\ddot{R}_i - \Omega_i^2 R = \frac{\omega_i \delta E_r}{B} + \omega_i R \Omega_i - \dot{R}_i(\nu_{in} + \Omega_e - \Omega_i) \tag{16}$$

and

$$R\dot{\Omega}_i + 2\Omega_i \dot{R}_i = \frac{\omega_i \delta E_\theta}{B} - \omega_i \dot{R}_i - R\Omega_i(\nu_{in} + \Omega_e - \Omega_i) \tag{17}$$

where ν_{in} is the ion-neutral collision frequency. The ion-neutral collision frequency is several orders of magnitude smaller than the spoke interaction frequency given by $\Omega_e - \Omega_i$. The effective sheath penetration δ is the fraction of the ion orbit located in the sheath, and δE is then the effective electric field experienced by the ions.

Although the ion spoke rotation frequency waveforms were not as coherent as those of the electrons, the coherence of the ion spoke rotation frequency over many cycles of oscillation and the relatively small radial ion currents noted during the data taking imply that the $\dot{R}_i$ terms in equations (16) and (17) may be neglected by comparison with the azimuthal ion velocity. By arguments and approximations analogous to those discussed for the electron equations of motion, the radial equation of motion for the ions is given by the following:

$$R\Omega_i \approx -\frac{\delta E_r}{B} - \frac{\Omega_i^2 R}{\omega_i} \tag{18}$$

The second term on the right side of equation (18) is the centrifugal force term for ions. This term may not be completely ignored under all experimental conditions. It is comparable to, but smaller than, the other terms in equation (18) at the ion cyclotron frequency, which was typically 3 megahertz in the present experiment. Typical ion spoke rotation frequencies were about 1 order of magnitude below ω_i at the magnetic field midplane.

If the definition of the electron spoke rotation frequency given by equation (15) is utilized, one may write equation (18) for the ion spoke rotation frequency as follows:

$$\Omega_i \approx \delta_o \Omega_e - \frac{\Omega_i^2}{\omega_i} \tag{19}$$

Equation (19) may be used to determine the observed effective sheath penetration δ_o in terms of the experimentally measured quantities Ω_i, Ω_e, and ω_i.

THEORETICAL EXPRESSIONS FOR SPOKE ROTATION AND THE ION HEATING PROCESS

Derivation of the Effective Sheath Penetration

A comprehensive theory of physical processes in the sheath, and particularly a theoretical derivation of the ion spoke rotation frequency, requires a scaling law for the parameter δ, which we have designated the "effective sheath penetration." Figure 14 is a schematic drawing of an ion orbit in the sheath in a coordinate system rotating with the ion spoke velocity. The anode ring has a radius R. The sheath thickness is assumed to be approximately equal to the ion Debye length λ_{di} multiplied by ξ, a numerical constant of order unity which is independent of the discharge operating conditions. It is assumed that the radial electric field is proportional to radius over the sheath thickness. This assumption is supported by the sharply defined frequencies observed in the potential waveform, which imply an electric field proportional to radius across the sheath to give a uniform E/B spoke frequency. A further discussion of this radial potential distribution is presented in appendix C. The ion gyroradius is designated R_L and the distance x is equal to the distance of closest approach of the ion orbit to the inner circumference of the anode ring.

Under the conditions existing in the present experiment, and also in a fusion reactor, the ion gyrodiameter is larger than the ion Debye length. As shown in figure 14,

the ion therefore will be in the sheath for only a fraction of its orbit. It is assumed that the sheath has a sharp boundary, so that the ion will experience the radial electric field of the sheath only in that part of its orbit along the arc ABC in figure 14 and will not experience any significant radial electric field when it is in the quasi-neutral plasma along arc CDA. The angle 2φ designates the angular fraction of the gyroorbit during which the ion is in the electric field of the sheath. The effective sheath penetration δ may be written in terms of the angle $\hat{\varphi}$ as follows:

$$\delta = \frac{\hat{\varphi}}{\pi} \tag{20}$$

where $\hat{\varphi}$ is the average over all ion orbits penetrating the sheath. From the law of cosines, the angle φ can be written in terms of the gyroradius R_L, the radius of the anode ring R, and the distance x as follows:

$$\left(R - \xi\lambda_{di}\right)^2 = \left(R - R_L - x\right)^2 + R_L^2 + 2R_L(R - R_L - x)\cos\varphi \tag{21}$$

It will also be assumed that ions are created uniformly across the thickness of the sheath, and their gyroorbits will therefore range from just grazing the inner circumference of the anode ring to grazing the inner circumference of the sheath. The parameter x will vary over the range

$$0 \leq x \leq \xi\lambda_{di}$$

for ions that are created in the sheath and not absorbed by impact with the inner circumference of the anode ring. It is useful to define the three dimensionless variables X, Y, and Z:

$$X \equiv \frac{x}{R_L} \tag{22}$$

$$Y \equiv \frac{\xi\lambda_{di}}{R_L} \tag{23}$$

$$Z \equiv \frac{R}{R_L} \tag{24}$$

Rewriting equation (21) in terms of these dimensionless variables, one obtains an expression for the angle φ as follows:

$$\varphi = \cos^{-1}\left[1 + \frac{(Y - X)(Y + X - 2Z)}{2(Z - 1 - X)}\right] \tag{25}$$

The average effective sheath penetration δ is given by an average over all ion orbits from those that graze the inner surface of the anode ring at $X = 0$ to those that graze the inner circumference of the sheath at $X = Y$. The effective sheath penetration distance δ may then be written

$$\delta = \frac{1}{\pi Y}\int_0^Y \varphi \, dX = \frac{1}{\pi Y}\int_0^Y \cos^{-1}\left[1 + \frac{(Y - X)(Y + X - 2Z)}{2(Z - 1 - X)}\right]dX \tag{26}$$

In a Cartesian geometry in which $R \to \infty$, then $Z \to \infty$ and equation (26) may be written

$$\delta = \frac{1}{\pi Y}\int_0^Y \cos^{-1}[1 - Y + X]dX \tag{27}$$

Equation (26) for the average effective sheath penetration δ cannot be integrated in closed form, but may be solved by numerical integration. Equation (27) for the Cartesian sheath may be integrated in closed form and is equal to

$$\delta = \frac{1}{\pi Y}\left[\sqrt{Y(2 - Y)} - (1 - Y)\cos^{-1}(1 - Y)\right] \tag{28}$$

Equation (26) has been solved for δ as a function of Y for various values of Z as a parameter. The results are plotted in figure 15. The limiting case of a Cartesian sheath is taken from equation (28) and is plotted in figure 15 as the line appropriate to $Z = \infty$. When $Z = 3$, the anode ring radius is equal to three times the gyroradius of the ions. For the conditions of this experiment, Z is generally greater than 3 or 4. When scaling to a fusion reactor, the curve labelled $Z = \infty$ would be most appropriate.

Figure 15 shows the scaling law for δ as a function of the ratio $Y = \xi\lambda_{di}/R_L$, of the effective sheath dimension to ion gyroradius. When $Y < 1$, a very good approximation for the effective sheath penetration δ is given by

$$\delta \approx \frac{1}{\pi}\sqrt{\frac{ZY}{Z - 1}} \qquad Z \gtrsim \infty \qquad \frac{Y^{1/2}}{\pi} = \frac{1}{\pi}\sqrt{\frac{\xi\lambda_{di}}{R_L}} \tag{29}$$

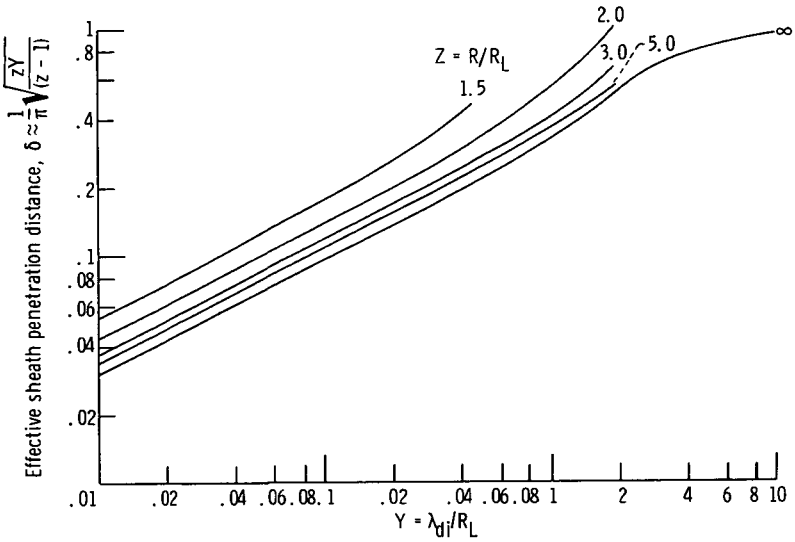

Figure 15. - Effective sheath penetration as function of parameter Y for various values of Z.

For large ratios of anode ring to cyclotron radius Z, the effective sheath penetration δ is proportional to the square root of the ratio of the ion Debye length divided by the gyroradius. The ion Debye length is given by

$$\lambda_{di} = \sqrt{\frac{\epsilon_o V_i}{e n_i}} = \frac{v_i}{e}\sqrt{\frac{\epsilon_o m_i}{n_i}} \tag{30}$$

Equation (29) may be written in terms of the microscopic parameters of the sheath by substituting equation (30) and the expression for gyroradius into equation (29) to yield

$$\delta = \frac{B^{1/2}}{\pi}\left(\frac{\xi^2 \epsilon_o}{2 n_i m_i}\right)^{1/4} \tag{31}$$

where n_i is the ion density in the sheath. The ratio δ is independent of the ion energy. In actual practice, equation (31) must be regarded as only an approximation to the actual fraction of the orbit spent by an ion in the sheath. The inner boundary of the sheath is probably not sharp, the parameter ξ may depend on operating conditions, and the ions may not be uniformly distributed across the sheath because of a tendency for them to diffuse radially inward. Nevertheless, these assumptions were made on an interm

basis, until further research reveals with what they should be replaced.

Relative Ion Number Density in Sheath

As is indicated in equation (31), one of the crucial parameters entering into the theory is n_i, the ion number density in the sheath. Absolute, as opposed to relative measurement of n_i, under the conditions of this experiment, is probably beyond the capability of existing diagnostic techniques. The ion density in the sheath is therefore estimated indirectly. The ion density measurement technique takes advantage of the fact that ions are lost along field lines. The ions that leave the sheath along field lines, and are lost through the magnetic mirrors, are detected by the retarding potential energy analyzer. It is observed that no more than a few percent of the particles lost through the mirrors are electrons. The electrical circuit to the power supply is completed by ions leaving through the magnetic mirror, rather than by electrons emitted into the plasma by hot cathodes.

The raw data from the retarding potential energy analyzer are reduced on the assumption that the ions are lost from the discharge in periodic pulses (ref. 10). This assumption gave the best theoretical fit to the raw retarding potential data and best represents the observed situation (ref. 10). The zero intercept of the retarding potential curve is proportional to the efflux of ions on the magnetic field line on which the retarding potential analyzer is located. This experimentally measured average current of ions from the plasma sheath was denoted Φ_i. The continuity equation for ions in the sheath may be written in the following simplified form:

$$\frac{\partial n_i}{\partial t} = n_e n_o \langle \sigma v \rangle_{ne} - \frac{\Phi_i}{V_p} \tag{32}$$

where the second term on the right is the flux of ions along the axis sampled by the analyzer, and V_p is the sheath volume sampled by the analyzer, which includes the aperture dimensions of the retarding potential energy analyzer, the expansion of the magnetic flux tube between the sheath and the analyzer, and the axial thickness of the sheath, assumed constant. The first term on the right side is the ionization rate of neutral molecules in the sheath due to electron-neutral impact ionization. If one averages equation (32) over times longer than the period of the continuity-equation oscillation, the time derivative on the left must average to zero. Because ions and electrons are created

in pairs, the time average allows one to replace n_e with n_i in equation (32). In averaging equation (32) over time, one therefore obtains

$$\Phi_i = n_i n_o \langle \sigma v \rangle_{ne} V_p \tag{33}$$

Hence, one has

$$n_i = \frac{\Phi_i}{n_o \langle \sigma v \rangle_{ne} V_p} = \frac{G\Phi_i}{n_o} \tag{34}$$

The electron energy is required to specify the ionization rate coefficient $\langle \sigma v \rangle_{ne}$. Measurement of the electron kinetic temperature in this plasma is very difficult. Previous work (ref. 47) has indicated, however, that the Penning discharge adjusts its operation so that the ionization rate coefficient is constant, near its maximum value. It is therefore expedient to introduce the constant factor G, which includes the product of the ionization rate coefficient and the sheath volume sampled by the analyzer.

Theoretical Expressions for Radial Electric Field and Electron Spoke Rotation Frequency

The theoretical expressions for ν_e, ν_i, and V_i are derived for two sets of assumptions. The first incorporates explicitly the observed sheath penetration parameter δ_o defined in terms of the ion and electron spoke velocities by equation (19) and hence does not rely on the assumptions which were necessary in deriving equation (31) for δ. This has the disadvantage, however, of introducing an additional experimentally determined parameter into the expressions for ν_e, ν_i, etc. with its attendant experimental error. Theoretical expressions which eliminate δ by substitution of equation (31) were also derived. These assume the validity of equation (31) but eliminate the experimental error associated with δ_o. As will become evident in the discussion of experimental results, expressions for ν_e and ν_i in which equation (31) was substituted for δ had the smallest relative standard deviations. This implies that equation (31) has the correct functional form, or at least that the errors associated with it were substantially less than the experimental errors associated with measuring δ_o.

The electron spoke rotation frequency is given by equation (15) above

$$\nu_e = \frac{E_r}{2\pi r B} \tag{35}$$

where E_r is the electric field in the sheath. It is observed that the plasma in this discharge rarely floats more than 1 kilovolt above ground potential, while the anode voltages are as high as 30 kilovolts. The electric field, therefore, may be written in terms of the applied anode voltage V_a and the sheath thickness:

$$E_r = \frac{rV_a}{R\xi\lambda_{di}} = \frac{rV_a}{R\xi}\sqrt{\frac{en_i}{\epsilon_o V_i}} = \frac{eV_a r}{v_i \xi R}\sqrt{\frac{n_i}{\epsilon_o m_i}} \tag{36}$$

where v_i is the velocity corresponding to the most probable ion energy. The expression for the ion Debye length is given by equation (30) and has been used in equation (36).

Substituting equation (36) into equation (35) for the electron spoke rotation frequency yields

$$\nu_{el} = \frac{E_r}{2\pi rB} = \frac{V_a}{2\pi RB\xi}\sqrt{\frac{en_i}{\epsilon_o V_i}} = \frac{eV_a}{2\pi RB\xi v_i}\sqrt{\frac{n_i}{\epsilon_o m_i}} \tag{37}$$

Equation (37) is a theoretical expression for the sheath electric field and electron spoke rotation frequency written in terms of the experimentally observable variables of the problem, with the exception of the ion density in the sheath n_i. If equation (34) is used to express n_i in terms of the experimentally observed parameters, equation (37) becomes

$$\nu_{el} = \frac{V_a}{2\pi RB\xi}\sqrt{\frac{Ge\Phi_i}{\epsilon_o V_i P p_o}} \tag{38}$$

where P is equal to 8.9×10^{16} molecules per torr in this experiment and relates the neutral density to the indicated vacuum tank pressure p_o,

$$n_o = Pp_o \tag{39}$$

Equation (38) may be written in terms of experimentally observed quantities and a constant:

$$\nu_{el} = C_1 \frac{V_a}{RB}\sqrt{\frac{\Phi_i}{V_i p_o}} \tag{40}$$

where

$$C_1 \equiv \frac{1}{2\pi\xi}\sqrt{\frac{Ge}{\epsilon_o P}} \tag{41}$$

The constant C_1 may be independently determined from equation (40) and the observed electron spoke rotation frequency ν_{eo}:

$$C_1 = \frac{\nu_{eo} RB}{V_a}\sqrt{\frac{V_i p_o}{\Phi_i}} \tag{42}$$

The constants C_k contain natural constants and the geometrical parameters ξ and G. These latter could not be unambiguously determined, and it was therefore necessary to restrict the scope of the present experiment to checking the functional dependence predicted by the theoretical expressions and to exclude a checking of the predicted absolute values.

A second scaling law for the electron spoke rotation frequency and the radial electric field in the sheath may be obtained by eliminating the ion energy from equation (38). The resulting expression will incorporate, implicitly, the effective sheath penetration δ. Equations (35) to (42) did not utilize it. Since in this experiment $\Omega_e >> \Omega_i^2/\omega_i$, and $\xi\lambda_{di}/R_L < 1$ at the discharge midplane, equations (19) and (31) may be combined to yield

$$\nu_i \approx \delta\nu_e = \frac{B^{1/2}\nu_e}{\pi}\left(\frac{\xi^2\epsilon_o}{2n_i m_i}\right)^{1/4} \tag{43}$$

Since it has been shown (fig. 10) that the ion spoke rotation velocity is proportional to the velocity corresponding to the most probable ion energy

$$v_i = 4\pi R\nu_i \tag{44}$$

one may write equation (43), by using equation (44), as

$$v_i = 4R\nu_e B^{1/2}\left(\frac{\xi^2\epsilon_o}{2n_i m_i}\right)^{1/4} \tag{45}$$

If equation (45) is substituted into equation (37), one obtains an expression for the electron spoke rotation frequency that is explicitly independent of the ion energy:

$$\nu_{e2} = \frac{V_a^{1/2}}{2\pi^{1/2} R B^{3/4}} \left(\frac{n_i^3 e^4}{8 m_i \xi^6 \epsilon_o^3} \right)^{1/8} \tag{46}$$

If we substitute equations (34) and (39) for n_i, equation (46) becomes

$$\nu_{e2} = \frac{V_a^{1/2}}{2 R B^{3/4} \pi^{1/2}} \left(\frac{e^4 G^3 \Phi_i^3}{8 P^3 p_o^3 m_i \xi^6 \epsilon_o^3} \right)^{1/8} \tag{47}$$

Equation (47) may be written in terms of experimentally determined quantities and a constant:

$$\nu_{e2} = C_2 \frac{V_a^{1/2}}{R B^{3/4}} \left(\frac{\Phi_i}{p_o} \right)^{3/8} \tag{48}$$

where

$$C_2 \equiv \frac{1}{2\pi^{1/2}} \left(\frac{e^4 G^3}{8 P^3 m_i \xi^6 \epsilon_o^3} \right)^{1/8} \tag{49}$$

The constant C_2 may also be written in terms of the observed electron spoke frequency ν_{eo}:

$$C_2 = \frac{\nu_{eo} R B^{3/4}}{V_a^{1/2}} \left(\frac{p_o}{\Phi_i} \right)^{3/8} \tag{50}$$

Theoretical Expressions for Ion Spoke Rotation Frequency

Equation (37) may be used to write a theoretical expression for the ion spoke rota-

tion frequency. Substituting equation (44) into equation (37) and rearranging, one obtains

$$\nu_{il} = \frac{eV_a}{8\pi^2 R^2 B \xi \nu_{eo}} \sqrt{\frac{n_i}{\epsilon_o m_i}} \tag{51}$$

Substituting equations (34) and (39) for n_i into equation (51), one obtains

$$\nu_{il} = \frac{eV_a}{8\pi^2 R^2 B \xi \nu_{eo}} \sqrt{\frac{G\Phi_i}{\epsilon_o m_i p_o P}} \tag{52}$$

Separating equation (52) into a constant and the experimental variables, one obtains

$$\nu_{il} = C_3 \frac{V_a}{R^2 B \nu_{eo}} \sqrt{\frac{\Phi_i}{p_o}} \tag{53}$$

where

$$C_3 \equiv \frac{e}{8\pi^2 \xi} \sqrt{\frac{G}{\epsilon_o m_i P}} \tag{54}$$

The constant C_3 may also be written in terms of the observed ion spoke rotation frequency and equation (53):

$$C_3 = \frac{\nu_{io} \nu_{eo} B R^2}{V_a} \sqrt{\frac{p_o}{\Phi_i}} \tag{55}$$

Equations (51) to (55) do not utilize the effective sheath penetration δ, nor do they incorporate the assumptions that went into its derivation. If the sheath penetration is utilized, one may substitute equation (37) into equation (45) to obtain

$$v_i = \frac{V_a^{1/2}}{B^{1/4}} \left(\frac{8e^4 n_i}{\pi^4 \epsilon_o \xi^2 m_i^3} \right)^{1/8} \tag{56}$$

Using equation (44), one obtains the ion spoke rotation frequency

$$\nu_{i2} = \frac{V_a^{1/2}}{4\pi RB^{1/4}} \left(\frac{8e^4 n_i}{\pi^4 \epsilon_o \xi^2 m_i^3} \right)^{1/8} \tag{57}$$

Substituting equations (34) and (39) for n_i into equation (57), one obtains

$$\nu_{i2} = \frac{V_a^{1/2}}{4\pi RB^{1/4}} \left(\frac{8e^4 G \Phi_i}{\pi^4 \epsilon_o \xi^2 P p_o m_i^3} \right)^{1/8} \tag{58}$$

If equation (58) is separated into a constant and the experimental variables, one obtains

$$\nu_{i2} = C_4 \frac{V_a^{1/2}}{RB^{1/4}} \left(\frac{\Phi_i}{p_o} \right)^{1/8} \tag{59}$$

where

$$C_4 \equiv \frac{1}{4\pi} \left(\frac{8e^4 G}{\pi^4 \epsilon_o \xi^2 P m_i^3} \right)^{1/8} \tag{60}$$

The constant C_4 may also be written in terms of the observed ion spoke rotation frequency ν_{io} and equation (59):

$$C_4 = \frac{\nu_{io} RB^{1/4}}{V_a^{1/2}} \left(\frac{p_o}{\Phi_i} \right)^{1/8} \tag{61}$$

Theoretical Expressions for Ion Temperature

A theoretical expression for the ion kinetic temperature is of great importance in order to assess the scaling laws appropriate to this ion heating method. An expression which ignores the centrifugal force term and incorporates the "observed" value of the

effective sheath penetration from equation (19) may be obtained by using equation (37) and (44) and the left members of equation (43). The result is

$$V_{il} = \frac{2V_a\delta_o}{\xi B}\sqrt{\frac{n_i m_i}{\epsilon_o}} \tag{62}$$

where V_i is the ion kinetic temperature in electron volts. If equations (34) and (39) are used to substitute for the ion density in the sheath, one obtains

$$V_{il} = \frac{2V_a\delta_o}{\xi B}\sqrt{\frac{m_i G\Phi_i}{\epsilon_o p_o P}} \tag{63}$$

If equation (63) is split into experimental variables and a constant C_5, one obtains

$$V_{il} = C_5\frac{V_a\delta_o}{B}\sqrt{\frac{\Phi_i}{p_o}} \tag{64}$$

where

$$C_5 \equiv \frac{2}{\xi}\sqrt{\frac{m_i G}{\epsilon_o P}} \tag{65}$$

The constant C_5 may also be written in terms of equation (64) and the observed ion energy V_{io}:

$$C_5 = \frac{V_{io}B}{V_a\delta_o}\sqrt{\frac{p_o}{\Phi_i}} \tag{66}$$

To remove the explicit dependence on the effective sheath penetration, one may substitute equation (31) into equation (62) to obtain

$$V_{i2} = \frac{V_a}{\pi B^{1/2}}\left(\frac{8m_i n_i}{\xi^2\epsilon_o}\right)^{1/4} \tag{67}$$

If equations (34) and (39) are used to substitute for the sheath ion density, one obtains

$$V_{i2} = \frac{V_a}{\pi B^{1/2}} \left(\frac{8 m_i G \Phi_i}{\xi^2 \epsilon_o P p_o} \right)^{1/4} \tag{68}$$

Equation (68) may be split up into a constant and the experimental variables:

$$V_{i2} = C_6 \frac{V_a}{B^{1/2}} \left(\frac{\Phi_i}{p_o} \right)^{1/4} \tag{69}$$

where

$$C_6 \equiv \frac{1}{\pi} \left(\frac{8 m_i G}{\xi^2 \epsilon_o P} \right)^{1/4} \tag{70}$$

The constant C_6 may also be written in terms of the observed ion energy V_{io} and equation (69) as

$$C_6 = \frac{V_{io} B^{1/2}}{V_a} \left(\frac{p_o}{\Phi_i} \right)^{1/4} \tag{71}$$

The constants C_k are summarized in table I.

Theoretical Expressions for Ion Heating Efficiency

The efficiency to be expected of the ion heating process is a matter of engineering importance. The ion kinetic temperature and the electron energies were both measured during the course of a series of experiments. The electron energies were observed to be between one and two orders of magnitude below the ion kinetic temperatures when measured with Langmuir probes 10 centimeters along the discharge axis from the anode rings. The Langmuir probes were located on a field line which passed within 0.5 centimeter of the anode ring. This state of affairs is in sharp contrast to ohmic heating and turbulent heating of ions, in which the electrons must have energies substantially

TABLE I. - SUMMARY OF PROPORTIONALITY

CONSTANTS C_i

$C_1 = \frac{1}{2\pi}\sqrt{\frac{eG}{\epsilon_o \xi^2 P}} = \frac{\nu_{eo} RB}{V_a}\left(\frac{V_i p_o}{\Phi_i}\right)^{1/2}$
$C_2 = \frac{1}{2\pi^{1/2}}\left(\frac{e^4 G^3}{8P^3 \xi^6 \epsilon_o^3 m_i}\right)^{1/8} = \frac{\nu_{eo} RB^{3/4}}{V_a^{1/2}}\left(\frac{p_o}{\Phi_i}\right)^{3/8}$
$C_3 = \frac{e}{8\pi^2 \xi}\left(\frac{G}{\epsilon_o m_i P}\right)^{1/2} = \frac{\nu_{io}\nu_{eo} R^2 B}{V_a}\left(\frac{p_o}{\Phi_i}\right)^{1/2}$
$C_4 = \frac{1}{4\pi}\left(\frac{8e^4 G}{\pi^4 \epsilon_o \xi^2 P m_i^3}\right)^{1/8} = \frac{\nu_{io} RB^{1/4}}{V_a^{1/2}}\left(\frac{p_o}{\Phi_i}\right)^{1/8}$
$C_5 = \frac{2}{\xi}\left(\frac{m_i G}{\epsilon_o P}\right)^{1/2} = \frac{V_{io} B}{V_a \delta_o}\left(\frac{p_o}{\Phi_i}\right)^{1/2}$
$C_6 = \frac{1}{\pi}\left(\frac{8 m_i G}{\xi^2 \epsilon_o P}\right)^{1/4} = \frac{V_{io} B^{1/2}}{V_a}\left(\frac{p_o}{\Phi_i}\right)^{1/4}$

greater than that of the ions in order to transfer their energy to the ions effectively.

In the present discharge, unlike Penning discharges with hot, electron emitting cathodes, the electrical circuit through the power supply is completed by ions which are lost through the magnetic mirrors to the grounded wall of the vacuum tank. Energy is also lost from this plasma by hot, charge-exchange neutrals that are lost perpendicular to the magnetic field. The total power deposited in the ion population is

$$P_o = P_{oi} + P_{ox} = V_i I_a + V_i I_n \tag{72}$$

where P_{oi} is the power transported by the ions through the mirrors, and P_{ox} is the power transferred to the charge-exchange neutrals. The power carried by the ions is the product of the ion kinetic temperature V_i and the current of ions lost through the two magnetic mirrors in this device, equal to the anode current I_a.

A population of slow charge-exchanged ions might be expected in the ion efflux. However, such ions were not observed on the retarding potential trace, either because

they were heated before being lost, or because they were a negligibly small fraction of the total ion current.

The power lost with charge-exchange neutrals and/or neutrals recombined on the anode ring surface is the product of the ion kinetic temperature and the equivalent current of charge-exchanged and recombined neutrals I_n. The heating efficiency of the modified Penning discharge may be written

$$\eta_i = \frac{V_i(I_a + I_n)}{P_{in}} \tag{73}$$

where P_{in} is the input power. Since the latter is in the form of high voltage direct-current electrical power, P_{in} is the product of the anode voltage V_a and the anode current I_a. A simplification results since the ions lost through the mirrors must be equal to the net electron current collected by the anode ring. The heating efficiency of the discharge may then be written in the form

$$\eta_i = \frac{V_i}{V_a}\left(1 + \frac{I_n}{I_a}\right) \geq \frac{V_i}{V_a} \tag{74}$$

where I_n is the current carried away by charge-exchange neutrals, and I_a is the anode current flowing to the power supply. It was not possible to make a quantitative measurement of the charge-exchange neutral current in this experiment. However, a lower limit to the ion heating efficiency is given by the ratio of the ion kinetic temperature to the applied direct-current anode voltage.

EXPERIMENTAL CONFIRMATION OF THEORETICAL EXPRESSIONS

Random and Systematic Errors of Experiment

The instruments used to measure the anode ring radius R, magnetic field B, anode voltage V_a, relative neutral gas pressure p_o, and spoke rotation frequencies ν_{eo} and ν_{io} had an accuracy of 1 percent or less. Variations in the data-gathering procedures over the 7-month period during which data were taken resulted in errors in the measured quantities which are believed to be within the following values: anode ring radius, an error of 3 percent; magnetic field B, 3 percent; anode ring voltage V_a, 3 percent; and relative neutral gas pressure p_o, 10 percent. Fluctuations of the neutral gas pressure during a given run were typically ±5 percent. An independent variable of the experiment

was the ion mass, which was deuterium in all runs of these experiments. Examination of spectral lines with an optical bench spectrometer showed no detectable impurities in the plasma. It is therefore presumed that the plasma consisted of ionized deuterium for the entire investigation described in this report.

The dependent variables, those not under the experimentalist's direct control, showed much larger random variations than the independent variables. The imprecision in the ion kinetic temperature has been discussed in reference 10 and is believed to be less than 15 percent. The imprecision in determining the relative ion current Φ_i is approximately ±50 percent. The imprecision associated with a measurement of the electron and ion spoke rotation frequency depends very much on the conditions of operation. When the frequencies of the electron and ion spoke rotation were as coherent and distinct as those illustrated in figure 8, the frequencies could be measured to within ±1 percent. Under highly turbulent conditions of operation, however, the signal-to-noise ratio was quite low, and the errors of measurement might have been as high ±20 percent. It is estimated that at least three-fourths of the data had random errors of measurement of less than ±5 percent for both ν_{i0} and ν_{e0}.

During the series of experiments in which the electron temperature was measured with Langmuir probes, the random and systematic errors were extreme, since the Langmuir probes were used in a highly turbulent, sheath-like plasma for which they could not be expected to give good data. It is estimated that the electron kinetic temperatures and particle number densities measured with Langmuir probes, T_e and n_e, are subject to combined random and systematic errors of +100 and -50 percent of the reading. The combined errors of measurement for the various theoretical relations are exhibited by calculating the constant parameters C_k. Any random or systematic errors will show up as a standard deviation in the quantity C_k. This method is discussed in appendix D. The median values and standard deviations of the parameters C_k were determined by plotting cumulative values of C_k on probability graph paper and reading these values off the best-fitting straight line.

Relation of Electron Energy to Electron Spoke Velocity

A preliminary series of measurements was made with a single loop, 15.24-centimeter-diameter anode ring. A diagnostic used only in that series of experiments was a Langmuir probe located 2.54 centimeter from the magnetic field axis at the magnetic mirror throat. This Langmuir probe was used to measure the electron kinetic temperature along a field line which projected to within 1 centimeter of the inner circumference of the anode ring. Some previous investigators of Penning discharges (see ref. 4) have reported an electron spoke, the rotation velocity of which corresponded to

an energy that was approximately equal to the ionization energy of the gas. It therefore was decided to see whether there existed a relation between the electron spoke rotation frequency and the electron kinetic temperature as measured by the Langmuir probe. The effective electron kinetic temperature was calculated from the expression

$$V'_e = \frac{16\pi^2 m_e \nu_{eo}^2 R^2}{e} \text{ eV} \tag{75}$$

and plotted in figure 16 as a function of V_{eo}, the electron kinetic temperature measured by the Langmuir probe. By analogy with equations (2) and (44) for the ions, it was as-

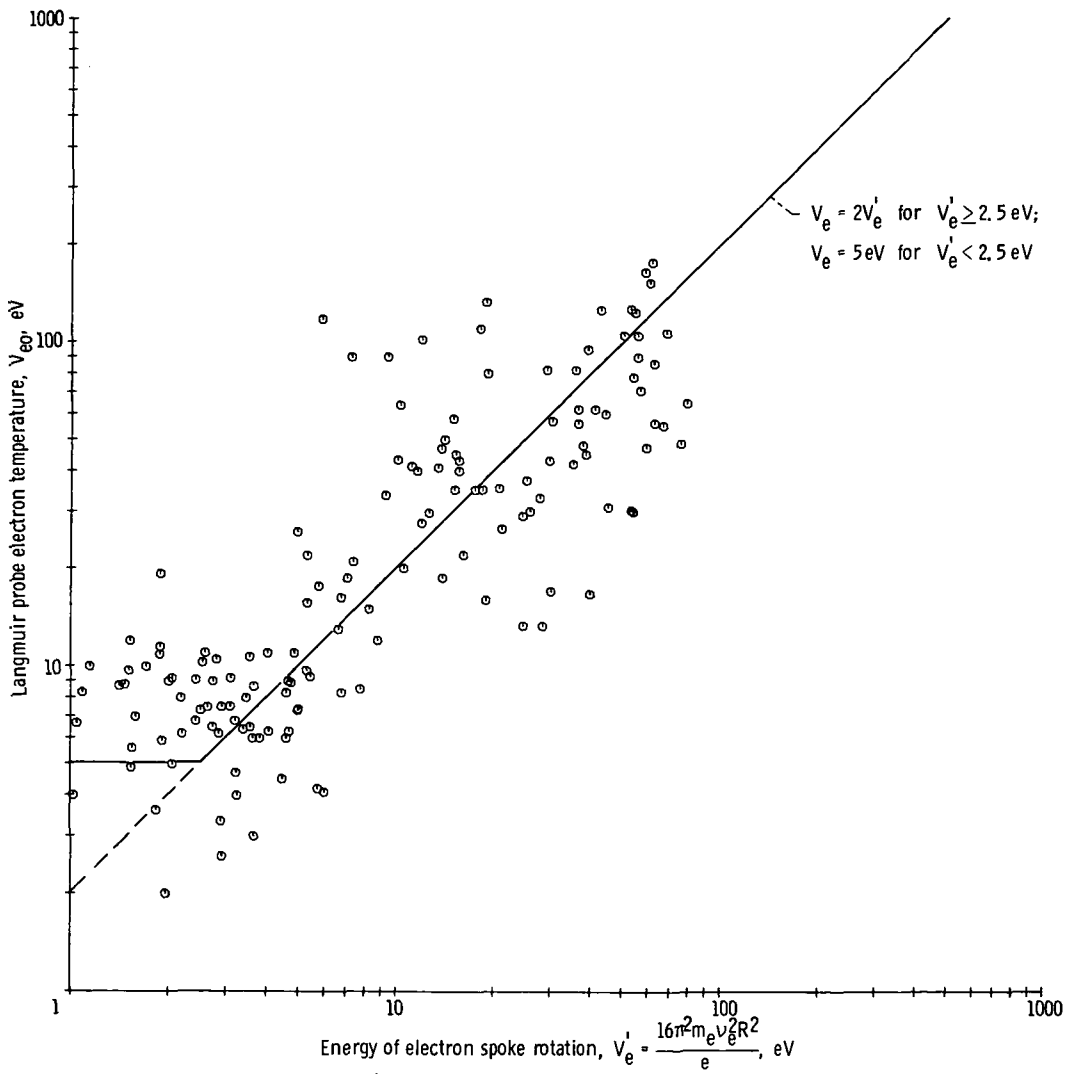

Figure 16. - Experimentally observed relation between electron temperature measured with Langmuir probes in plasma and electron spoke rotation frequency.

sumed that the electron velocity is given by

$$v_e = 4\pi R \nu_{eo} \tag{76}$$

There is obviously a very wide spread in the data of figure 16. However, these data were interpreted as follows. It appears that the electron energies are not less than about 5 eV in this plasma. This is to be expected, since the ionization rate coefficient for electron-neutral impact ionization falls off very rapidly below 5 eV. The highest electron kinetic temperatures are no more than a few hundred electron volts. This limit can be understood as an energy just above the maximum in the ionization rate coefficient $\langle \sigma v \rangle_{ne}$. The discharge appears to heat electrons to energies near the maximum of the ionization rate coefficient curve, about 100 eV for deuterium gas. Above an electron energy of 5 eV, as measured by the Langmuir probe, the data in figure 16 fall very roughly along a straight line of slope 45°, the electron energies of which are a factor of 2 higher than electron energies calculated from equation (75).

Experimentally Observed Functional Dependence of the Electron Spoke Rotation Frequency

The type of experimental run most frequently utilized consisted of holding the magnetic field constant and varying the anode voltage. A second type consisted of setting the anode voltage at a fixed value and varying the magnetic field. When the ion cyclotron frequency was higher in amplitude than the turbulent noise level, it was observed at a frequency appropriate to D^+ ions. This therefore appears to be the dominant ionic species in this plasma. The extreme and typical values of the parameters in this experiment are listed in table II. The methods used in measuring these experimental variables have been discussed in previous publications (refs. 8, 10, 25, 44, 46, and 47).

The random and systematic errors present in the experiment may be assessed by treating the parameter C_k as if it were a variable. Any imprecision in the experimentally measured quantities and any disagreement between theory and experiment will show themselves by creating a spread in the experimentally determined value of C_k, which should be a mixture of natural and geometrical constants. The parameters C_1 and C_2 have been obtained for the four anode ring radii from equations (42) and (50). The median, standard deviation, and relative standard deviation of all C_k are listed in table III for each anode ring radius and for the entire data population.

TABLE II. - EXTREME AND TYPICAL VALUES

OF DISCHARGE PARAMETERS

Parameter	Low value	Typical value	High value
Independent variables			
Radius of anode ring, R, cm	2.54	---	10.16
Anode voltage, V_a, kV	1.0	10	30
Background pressure, p_o, torr	7×10^{-7}	10^{-5}	4×10^{-5}
Ion mass, amu	2	2	2
Maximum magnetic field strength,[a] B_{max}, T	0.2	1.0	2.0
Midplane magnetic field strength,[a] B_{min}, T	0.08	0.4	0.8
Cyclotron frequency for electrons,[a] $\nu_{ce}(D^+)$, GHz	2.1	11	21
Cyclotron frequency for ions,[a] $\nu_{ci}(D^+)$, MHz	.58	2.9	5.8
Dependent variables			
Electron energy, [b]V_e, eV	2	30	200
Ion energy, V_i, eV	20	1000	7000
Number density, [b]n_e, cm^{-3}	3×10^5	2×10^7	5×10^8
Electron spoke rotation frequency, ν_e, MHz	0.3	2.5	10
Ion spoke rotation rotation frequency, [c]ν_i, kHz	40	300	800
Sheath penetration parameter, δ	0.022	0.2	0.45
Ion heating efficiency	0.014	0.086	0.40
Electron plasma frequency,[d] ν_{pe}, MHz	4.9	40	200
Ion plasma frequency,[d] $\nu_{pi}(D^+)$, MHz	0.08	0.66	3.2
Electron Debye length, λ_{de}, cm	0.47	0.92	2.1
Ion Debye length,[d] $\lambda_{di}(D^+)$, cm	2.8	5.3	6.1
Ion gyroradius,[a] R_{Li}, cm	0.38	1.70	24
Electron gyroradius,[a] R_{Le}, cm	0.0013	0.049	0.125

[a]At midplane, location of anode ring.

[b]As measured with Langmuir probe 2.5 cm from axis, at mirror throat.

[c]Data for R = 7.62 cm anode ring.

[d]Based on n_e measured with Langmuir probe at throat (see footnote b). Particle number densities at throat were at least two orders of magnitude smaller than densities at midplane when measurements were made at high density limit with a microwave interferometer at midplane.

TABLE III. - VALUES, STANDARD DEVIATIONS, AND RELATIVE STANDARD DEVIATIONS OF PROPORTIONALITY CONSTANTS

C_i	Anode ring diameter, cm	Constant					
		C_1	C_2	C_3	C_4	C_5	C_6
Median	5.08	0.0131	0.00975	0.000815	0.081	0.176	1.71
Standard deviation	5.08	.0056	.0020	.00035	.0245	.098	.88
Relative deviation	5.08	.427	.206	.430	.303	.557	.515
Median	10.16	.0187	.0130	.0011	.0835	.282	2.28
Standard deviation	10.16	.0161	.0044	.00082	.0422	.298	2.53
Relative deviation	10.16	.862	.338	.745	.505	1.06	1.11
Median	15.24	.0192	.0123	.00129	.0985	.271	2.54
Standard deviation	15.24	.0061	.0029	.00043	.0275	.111	1.32
Relative deviation	15.24	.318	.236	.33	.297	.410	.520
Median	20.32	.0095	.0091	.00061	.064	.134	1.09
Standard deviation	20.32	.0036	.0027	.00030	.0225	.065	.66
Relative deviation	20.32	.379	.297	.492	.352	.485	.605
Median	All data	.0155	.0111	.000995	.085	.212	1.87
Standard deviation	All data	.0094	.0030	.00058	.033	.138	1.63
Relative deviation	All data	.605	.270	.582	.388	.651	.873

The observed electron spoke rotation frequency and the relative ion number density calculated from

$$n_i \sim \frac{\Phi_i}{p_o} \tag{77}$$

are plotted as functions of V_a (at constant B_{min}) in figures 17 and 18, respectively, and as functions of B_{min} (at constant V_a) in figures 19 and 20, respectively. Data are shown for the 15.2-centimeter-diameter anode ring. Plotted also in figures 17 and 19 are theoretical values of the electron spoke rotation frequency obtained from equations (40) and (48), with the constants C_1 and C_2 obtained from table III for the 15.2-centimeter-diameter anode ring. The functional dependence of the electron spoke frequency on anode voltage is correctly predicted by the theoretical expression, even though the ion number density is varying with V_a and B_{min} in the manner illustrated in figures 18 and 20.

Although figures 17 and 19 demonstrate good agreement between the observed and theoretically predicted functional relation, for the conditions specified in the figure, they represent only 2 out of 88 run series taken during this investigation and only one of

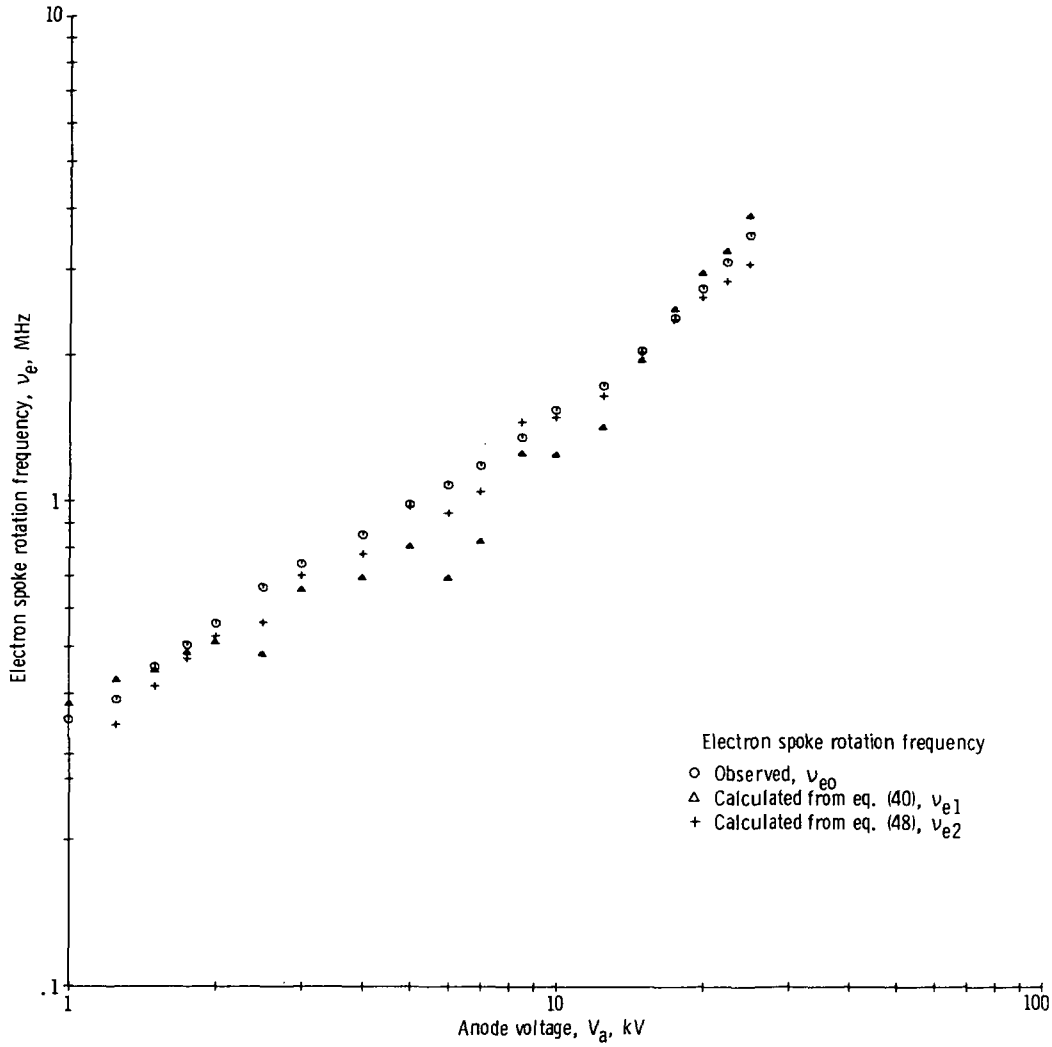

Figure 17. - Observed electron spoke rotation frequency, calculated electron spoke rotation frequency from equation (40), and calculated electron spoke rotation frequency from equation (48) as functions of anode voltage. Neutral gas pressure, 5×10^{-6} torr; anode ring diameter, 15.2 centimeters; midplane magnetic field strength, 0.38 tesla.

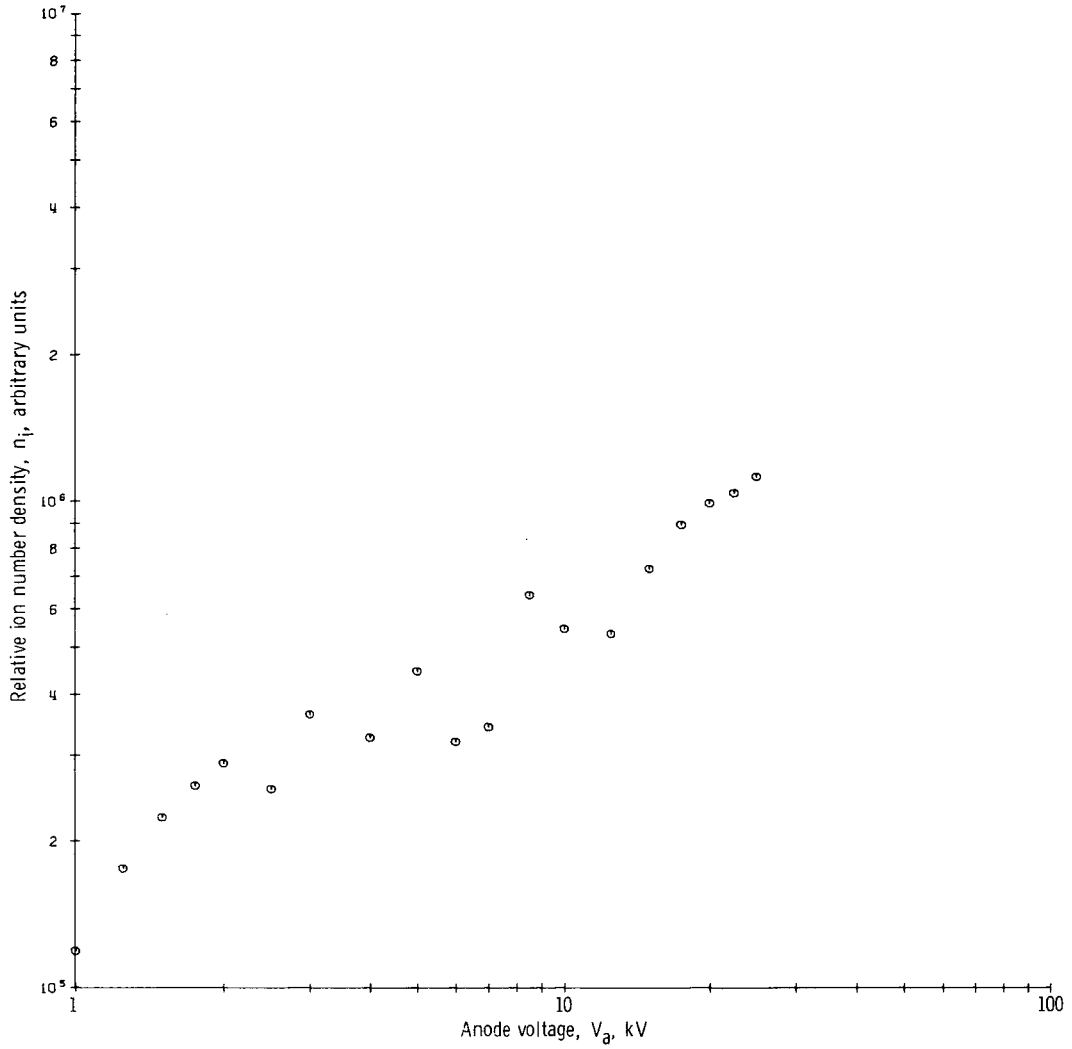

Figure 18. - Relative ion number density as function of anode voltage. Neutral gas pressure, 5×10^{-6} torr; anode ring diameter, 15.2 centimeters; midplane magnetic field strength, 0.38 tesla.

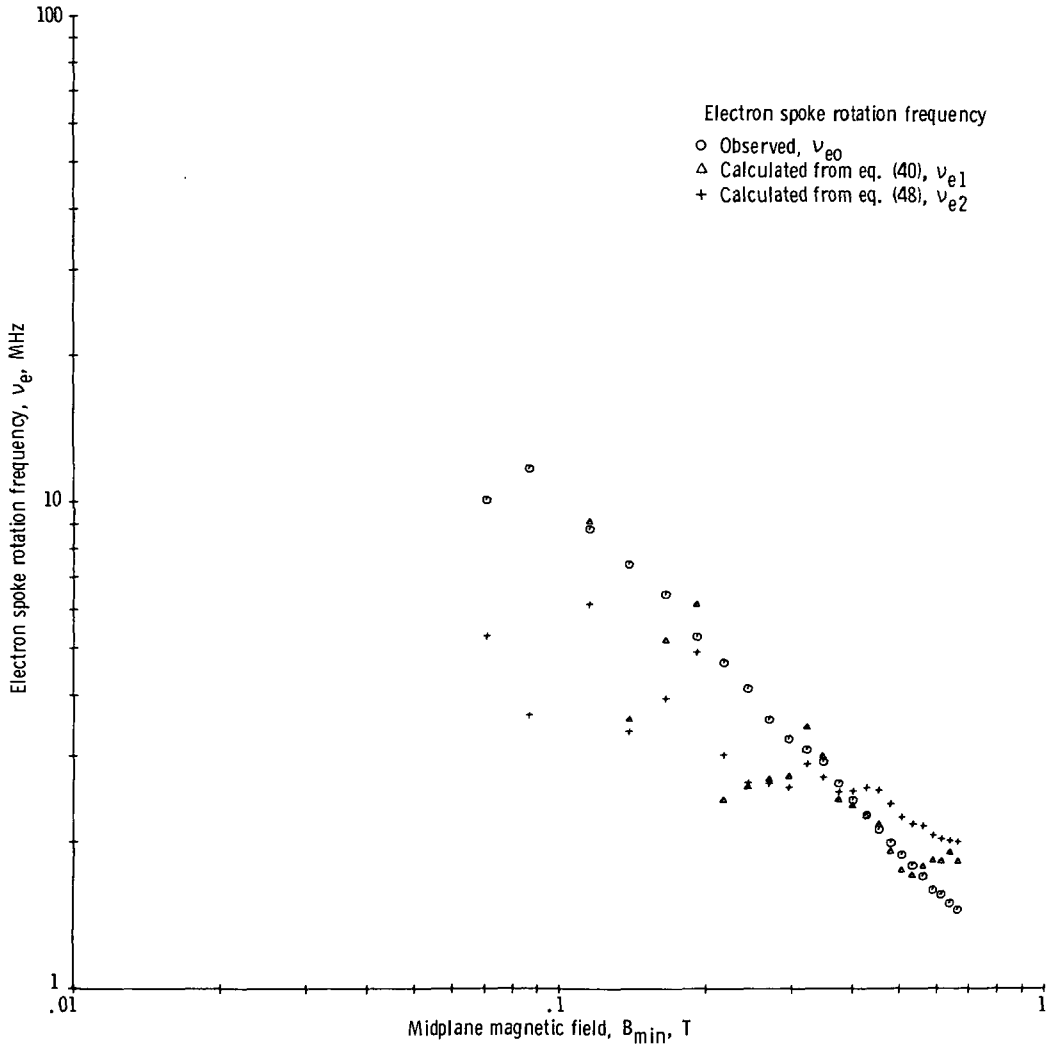

Figure 19. - Observed electron spoke rotation frequency, calculated electron spoke rotation frequency from equation (40), and calculated electron spoke rotation frequency from equation (48) as functions of midplane magnetic field. Neutral gas pressure, 1.6×10^{-6} torr; anode ring diameter, 15.2 centimeters; and anode voltage, 20 kilovolts.

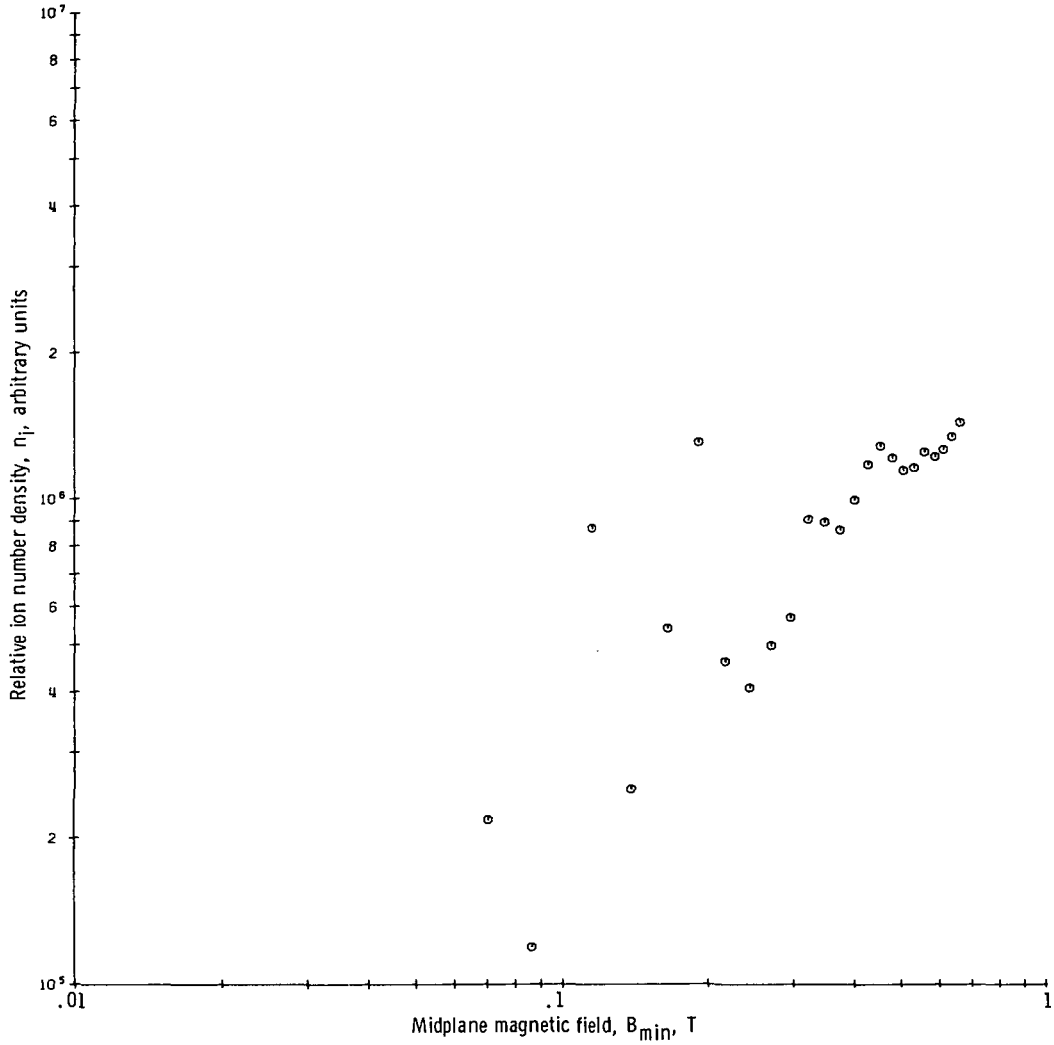

Figure 20. - Relative ion number density as function of midplane magnetic field. Neutral gas pressure, 1.6×10^{-6} torr; anode ring diameter, 15.2 centimeters; and anode voltage, 20 kilovolts.

the four anode ring diameters used. Another method used to demonstrate agreement betweeen observed and predicted electron spoke frequencies for the entire data population was the elimination of V_a or B_{min} as a parameter and the direct plotting of observed frequencies against predicted frequencies, with the constants C_k taken as the median values listed for the entire data population in table III.

In figure 21 is plotted the observed value of the electron spoke rotation frequency ν_{eo} as a function of the theoretical expression in equation (40), ν_{e1}, for the entire data population. The trend of the data along a straight line of slope 45^o confirms the functional dependences predicted by equation (38) over the range of data taken.

A second theoretical expression for the electron spoke rotation frequency is given by equation (48). This expression does not contain the measured ion kinetic tempera-

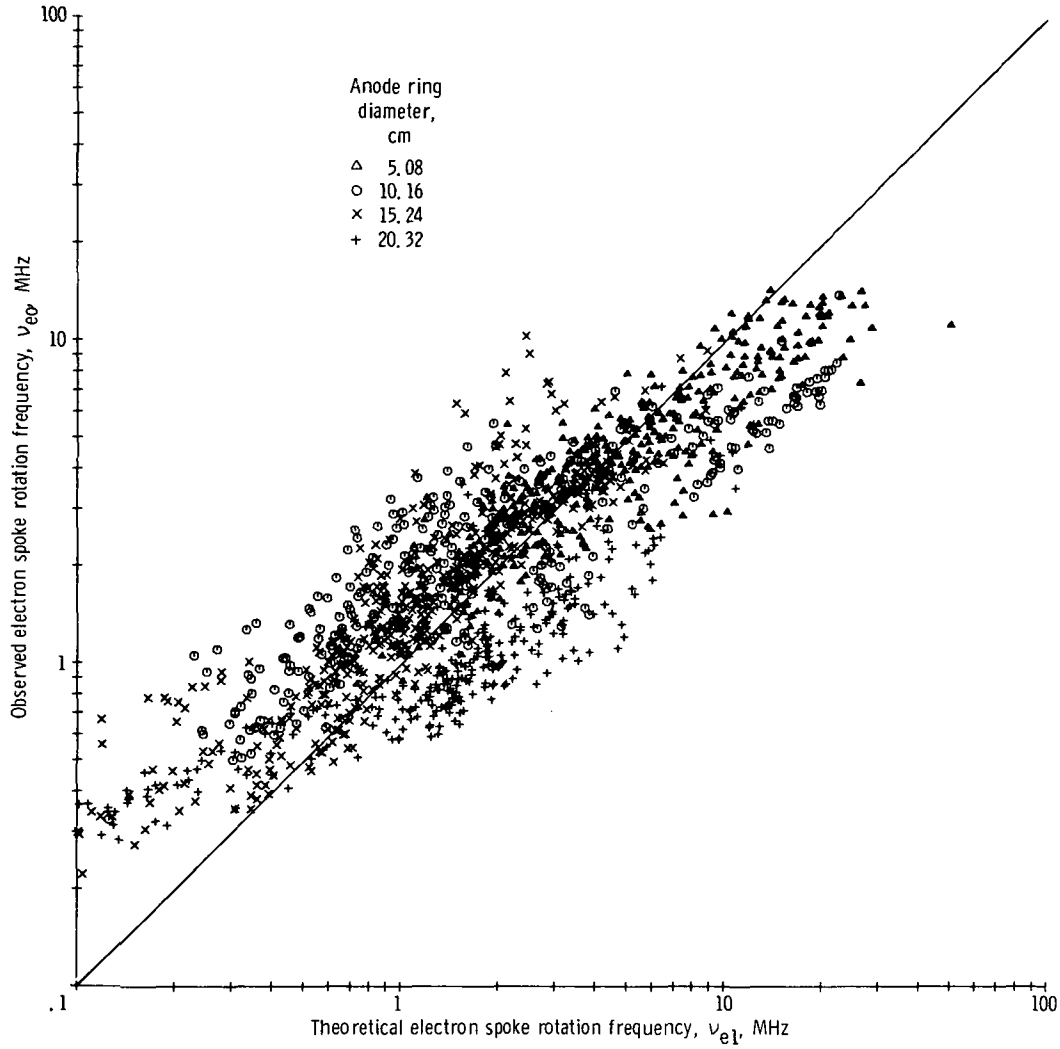

Figure 21. - Observed electron spoke rotation frequency as function of theoretical electron spoke rotation frequency calculated from equation (40) for entire data population. Median value of constant C_1 for entire data population taken from table III.

ture and incorporates the effective sheath penetration implicitly. The parameter C_2 given by equation (50) therefore contains one less experimental variable (V_i, or equivalently, δ_o is missing), and one would therefore expect the relative standard deviation of C_2 to be smaller than that of C_1, provided that equation (31) for δ is correct. Comparison of the relative standard deviations of C_1 and C_2 in table III shows that C_2 has a significantly smaller relative standard deviation and thus supports the assumptions required in the theoretical derivation of δ. The observed electron spoke rotation frequency is plotted against ν_{e2} given by equation (48) in figure 22. The substantially smaller standard deviation of the data, relative to figure 21, is evident. Except possibly for the data below 0.4 megahertz, there is no systematic deviation from a straight line of slope 45^o, and this fact confirms equation (48) over the range of data taken.

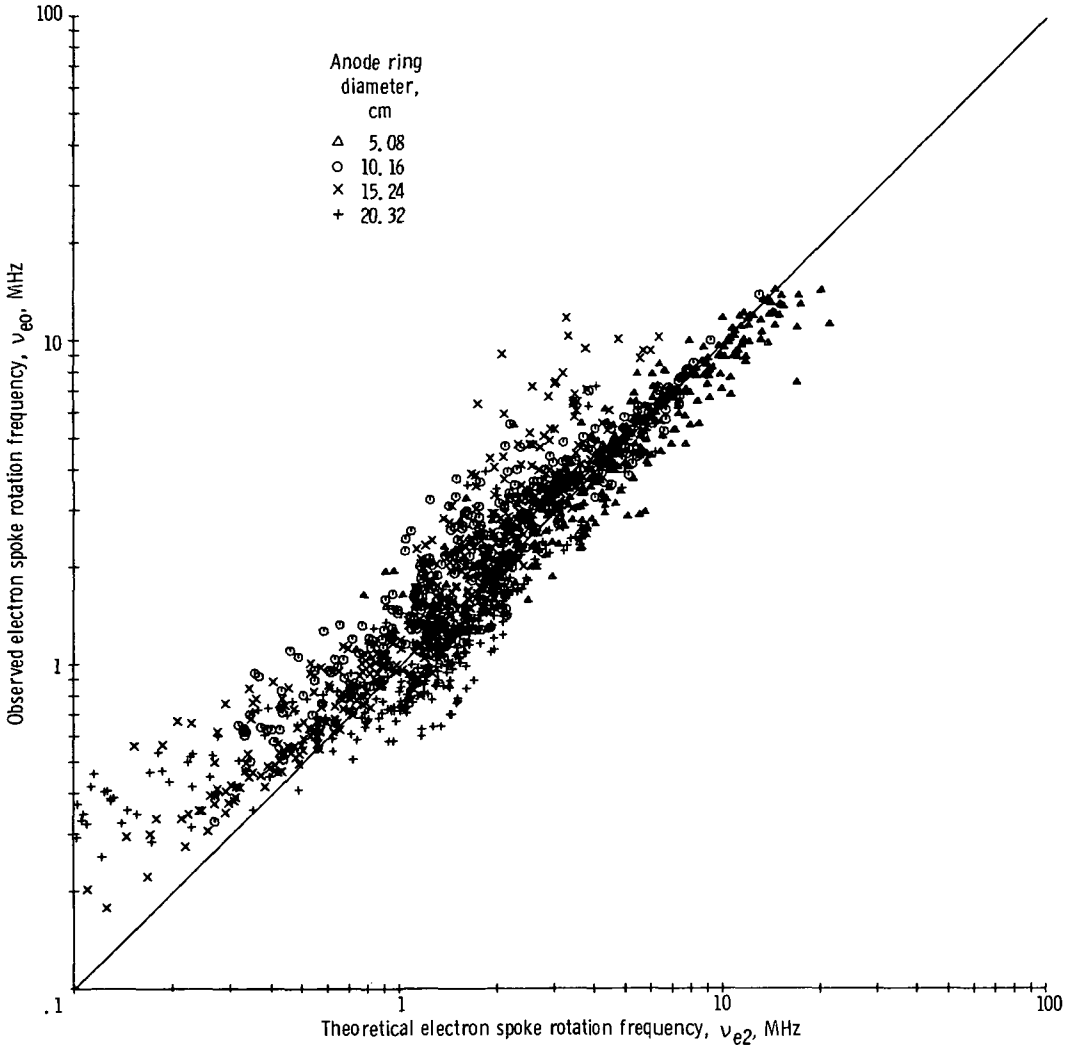

Figure 22. - Observed electron spoke rotation frequency as function of theoretical electron spoke rotation frequency calculated from equation (48) for entire data population. Median value of constant C_2 for entire data population taken from table III.

Experimentally Observed Functional Dependence of the Ion Spoke Rotation Frequency

The ion spoke rotation frequency given by equation (53) incorporates the observed electron spoke rotation frequency as one of the experimental parameters, which is equivalent to its containing the effective sheath penetration δ_0 explicitly. Equation (59) for the ion spoke rotation incorporates δ implicitly and therefore contains one less experimental variable. The parameters C_3 and C_4 for these two expressions have been calculated from the experimental variables by using equations (55) and (61). The median, standard deviation, and relative standard deviation of C_3 and C_4 are listed in table III for each anode ring radius and for the entire data population.

The observed ion spoke rotation frequency is plotted as a function of V_a (at con-

stant B_{min}) in figure 23 and as a function of B_{min} (at constant V_a) in figure 24. Data are shown for the 15.2-centimeter-diameter anode ring and for the same run plotted in Figures 17 to 20 for the electron spoke rotation velocity. Plotted also in figures 23 and 24 are theoretical values of the ion spoke rotation frequency obtained from equations (53) and (59) with the constants C_3 and C_4 from table III for the 15.2-centimeter-diameter anode ring. The functional dependence of the ion spoke rotation frequency on anode voltage and B_{min} is approximately given by the theoretical expressions, except at low values of magnetic field and high ion energies, where nonadiabatic effects must be expected (refs. 50 and 51). At a magnetic field B_{min} = 0.38 tesla, nonadiabatic losses of D^+ ions must be expected above ion energies of 300 eV (refs. 49 and 50). Nonadiabatic effects apparently do not come into play in this experiment until

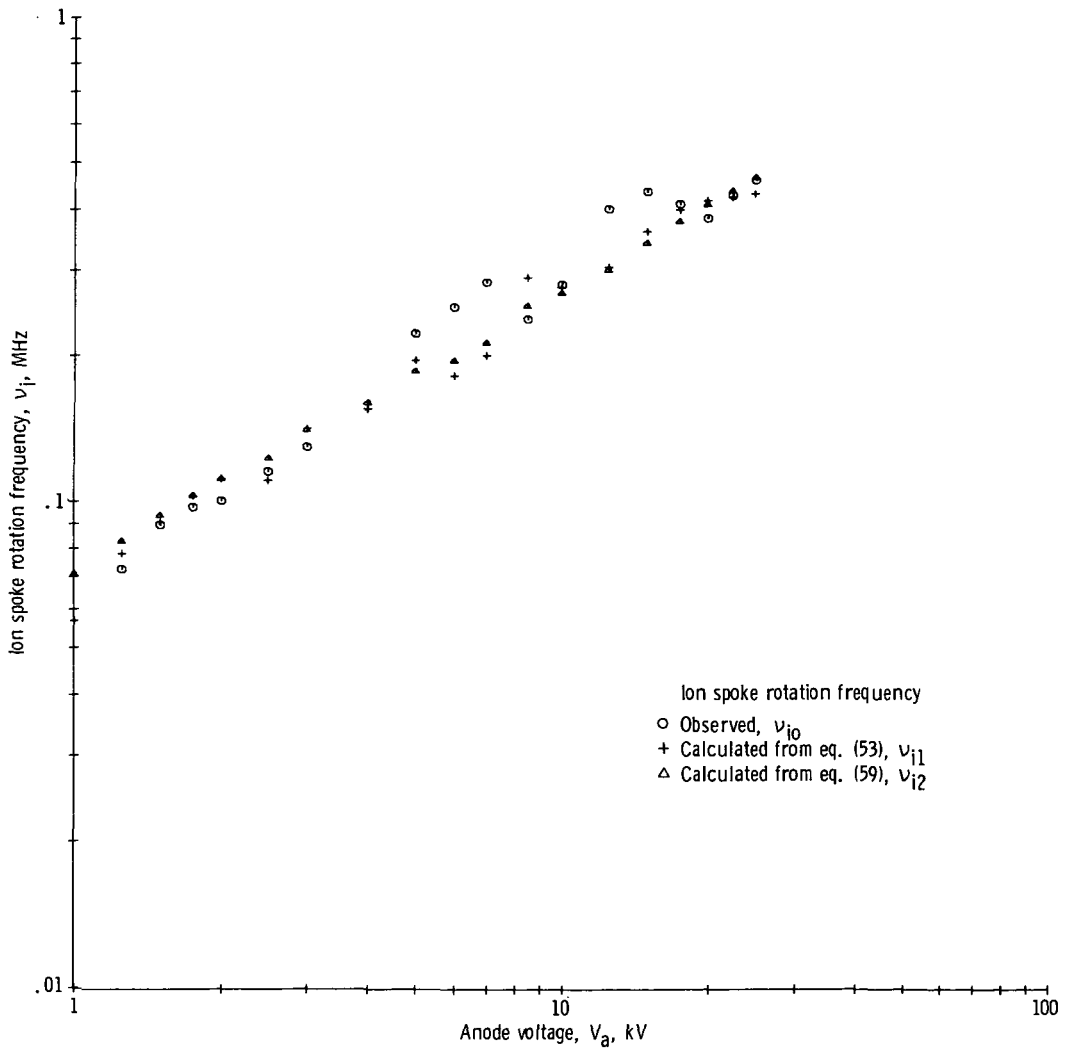

Figure 23. - Observed ion spoke rotation frequency, calculated ion spoke rotation frequency from equation (53), and calculated ion spoke rotation frequency from equation (59) as functions of anode voltage. Neutral gas pressure, 5×10^{-6} torr; anode ring diameter, 15.2 centimeters; midplane magnetic field strength, 0.38 tesla.

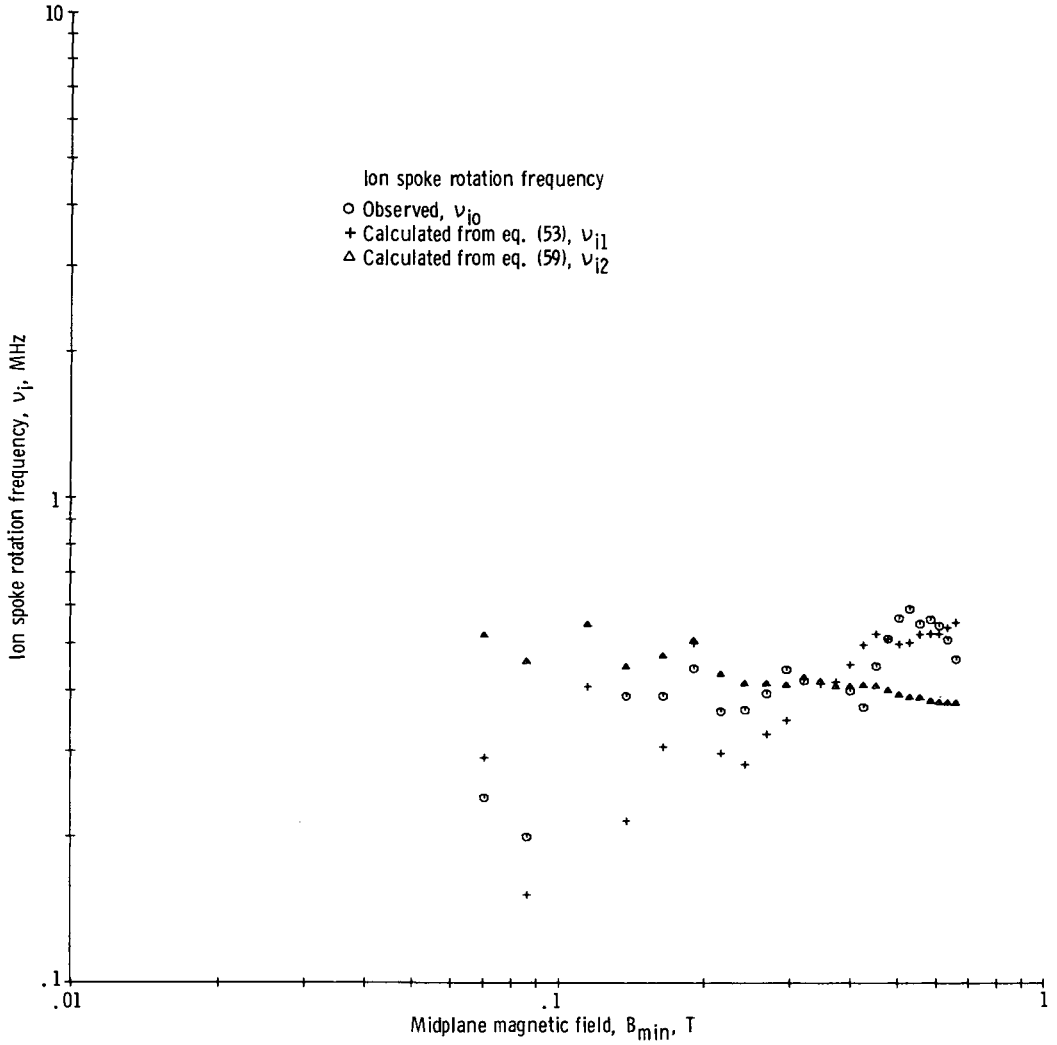

Figure 24. - Observed ion spoke rotation frequency, calculated ion spoke rotation frequency from equation (53) and calculated ion spoke rotation frequency from equation (59) as functions of midplane magnetic field. Neutral gas pressure, 1.6×10^{-6} torr; anode ring diameter, 15.2 centimeters; and anode voltage, 20 kilovolts.

well above this limit, presumably because the energetic ions have $v_\perp >> v_{||}$ and occupy a region in velocity space well away from the boundary of the escape cone.

In figure 25 is plotted the observed ion spoke rotation frequency ν_{io} as a function of the theoretical expression given in equation (53) for the entire data population. The trend of the data to lie along a straight line of slope 45^o confirms the functional dependence in the theoretical expression of equation (53) over the range of data taken. The apparent wide scatter of the data is in part a consequence of the large data population shown. A significant number of data points more than two standard deviations from the mean are present, which results in an apparent data spread much larger than the 0.582 relative standard deviation which is actually characteristic of the data.

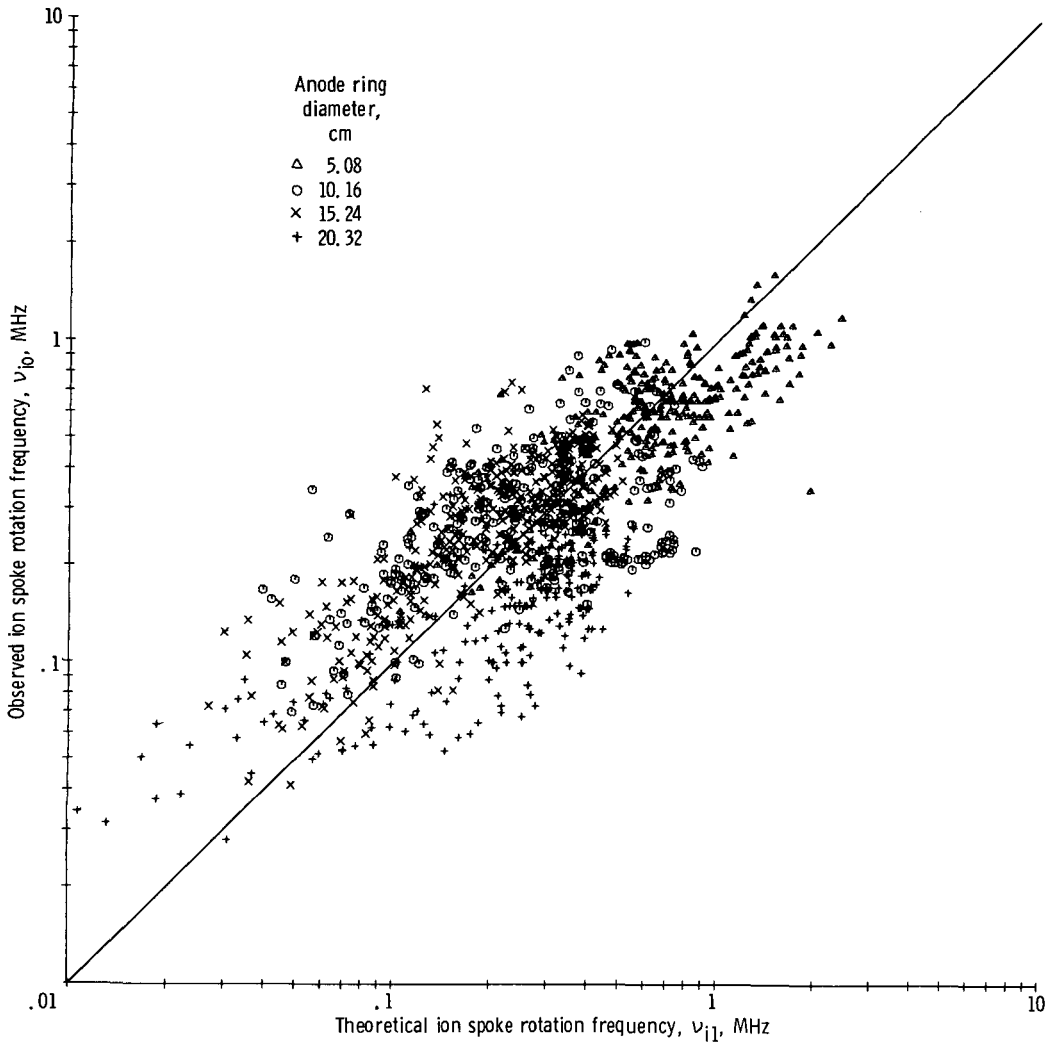

Figure 25. - Observed ion spoke rotation frequency as function of theoretical ion spoke rotation frequency calculated from equation (53) for entire data population. Median value of constant C_3 for entire data population taken from table III.

A second theoretical expression for the ion spoke rotation frequency is given in equation (59). This expression does not contain the effective sheath penetration as an explicit parameter, and the determination of C_4, therefore, requires one less experimental variable. Comparison of the relative standard deviations of C_3 and C_4 in table III shows that C_4 has a significantly smaller relative standard deviation and thus supports the assumptions required in the theoretical derivation of δ. The observed ion spoke rotation frequency ν_{io} is plotted as a function of ν_{i2}, given by equation (59), in figure 26. The smaller spread of the data points, relative to figure 25, is evident. There is no systematic deviation from a straight line with slope 45^{o}, which tends to confirm equation (59) over the range of data taken.

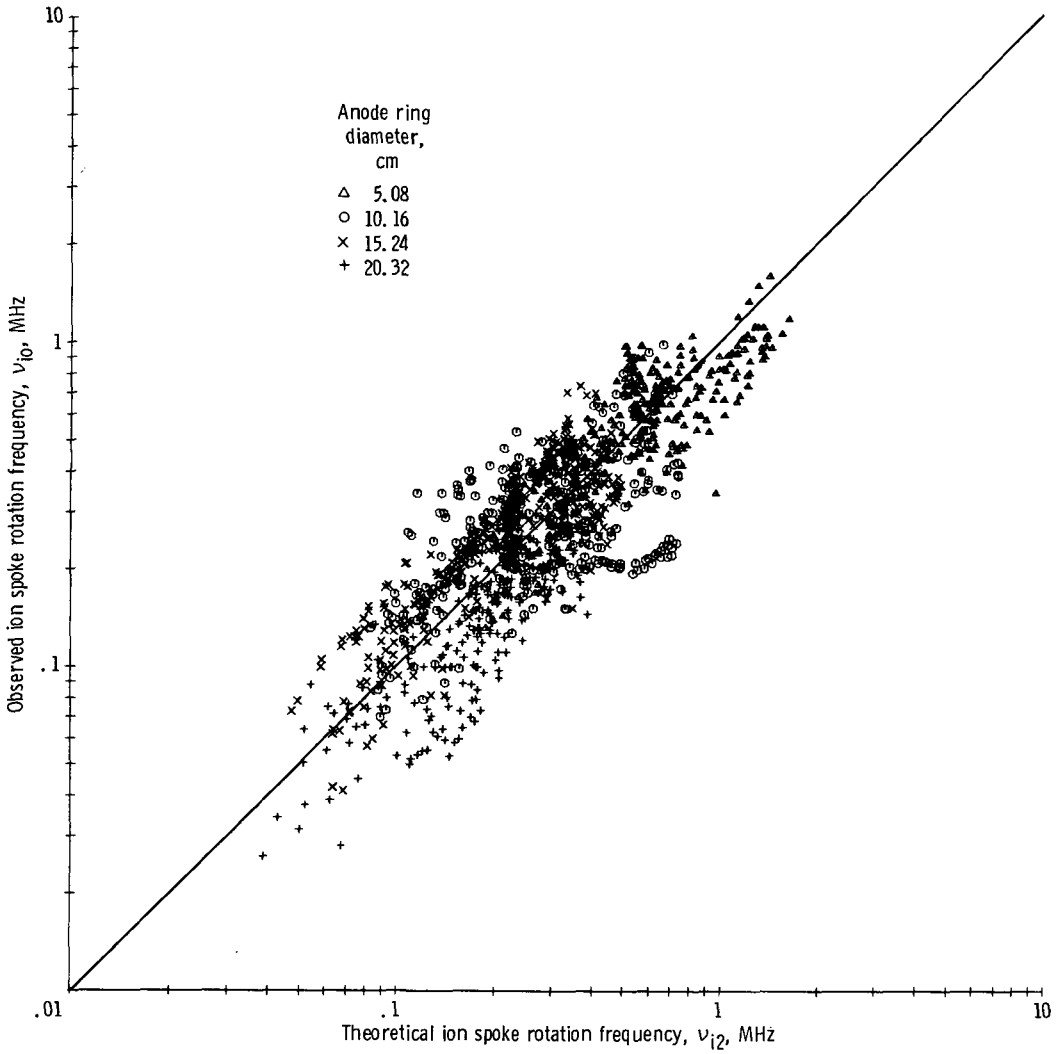

Figure 26. - Observed ion spoke rotation frequency as function of theoretical ion spoke rotation frequency calculated from equation (59) for entire data population. Median value of constant C_4 for entire data population taken from table III.

Experimentally Observed Functional Dependence of the Ion Kinetic Temperature

The ion kinetic temperature given by equation (64) incorporates the observed effective sheath penetration δ_o as one of the experimental parameters, while equation (69) for the ion kinetic temperature contains it implicitly. The parameters C_5 and C_6, obtained from equations (66) and (71), are listed in table III for each anode ring radius and for the entire data population.

The observed ion kinetic temperature V_{io} is plotted as a function of V_a (at constant B_{min} = 0.38 T) in figure 27 and as a function of B_{min} (at constant V_a) in figure 28. The data are shown for the 15.2-centimeter-diameter anode ring and for the

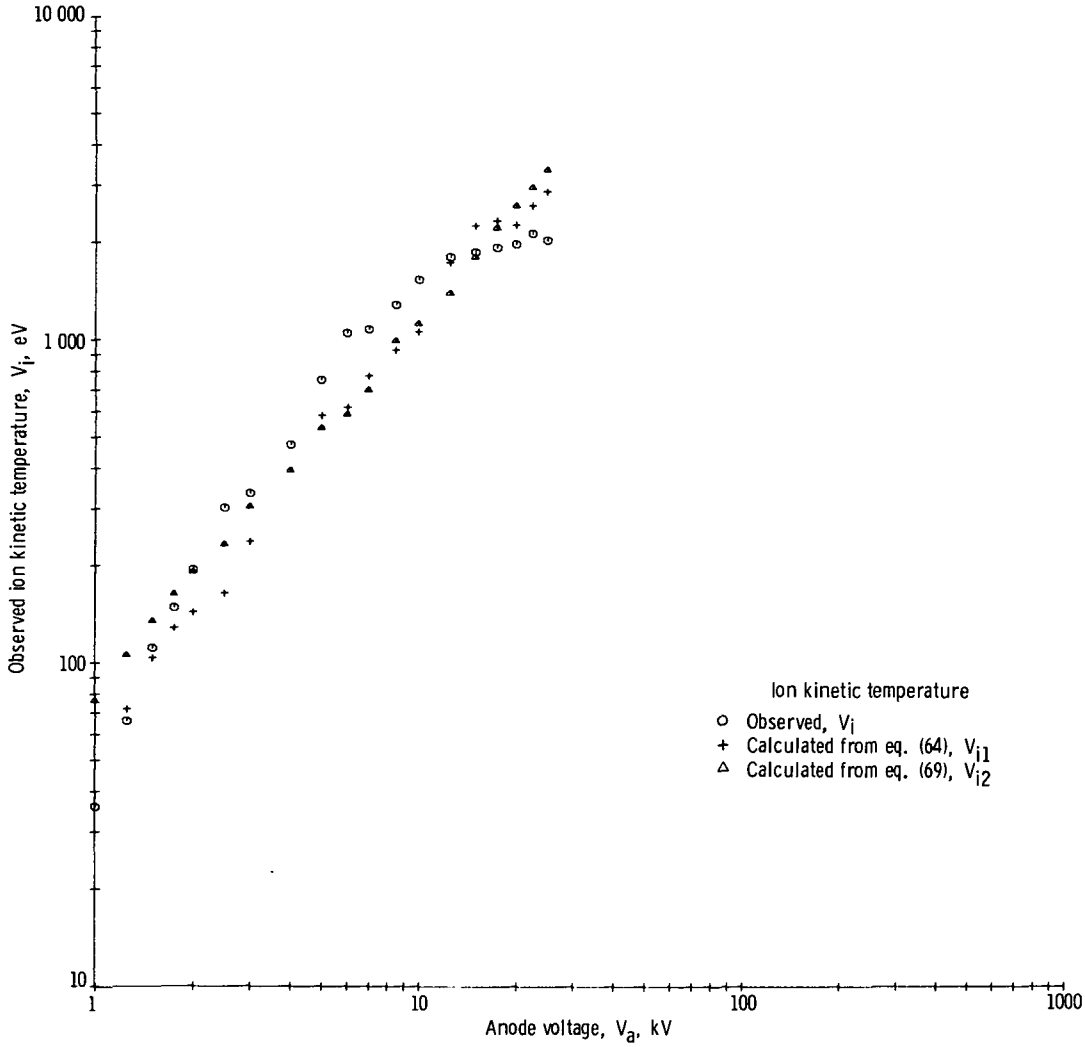

Figure 27. - Observed ion kinetic temperature, calculated ion kinetic temperature from equation (64), and calculated ion kinetic temperature from equation (69) as functions of anode voltage. Neutral gas pressure, 5×10^{-6} torr; anode ring diameter, 15.2 centimeters; midplane magnetic field strength, 0.38 tesla.

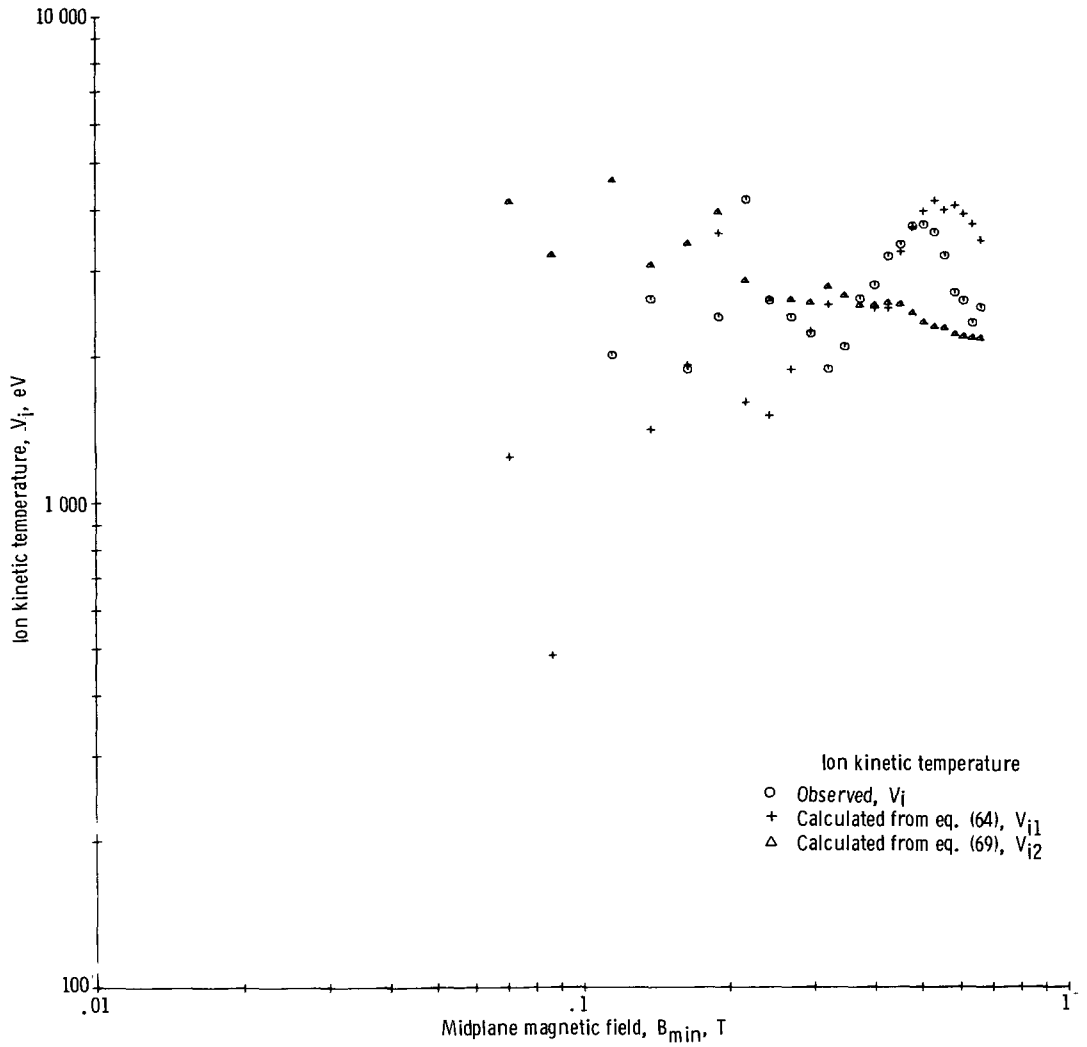

Figure 28. - Observed ion kinetic temperature, calculated ion kinetic temperature from equation (64), and calculated ion kinetic temperature from equation (69) as functions of midplane magnetic field. Neutral gas pressure, 1.6×10^{-6} torr; anode ring diameter, 15.2 centimeters; and anode voltage, 20 kilovolts.

same experimental run plotted in figures 17 to 20, 23, and 24. Plotted also in figures 27 and 28 are theoretical values of the ion kinetic temperature obtained from equations (64) and (69), with the constants C_5 and C_6 obtained from table III for the 15.2-centimeter-diameter anode ring. There is rough agreement between the observed and theoretical values, except at high ion energies and/or low magnetic fields, where nonadiabatic effects must be expected (refs. 49 and 50).

In figure 29 is plotted the observed ion kinetic temperature V_{io} as a function of the theoretical V_{il}, given in equation (64), for the entire data population. The trend of the data to lie along a straight line of slope 45^o confirms the functional dependence in equation (64). The relative standard deviation of the data is large because equation (64) is, in effect, the square of equation (53) for the ion spoke rotation frequency, and the error

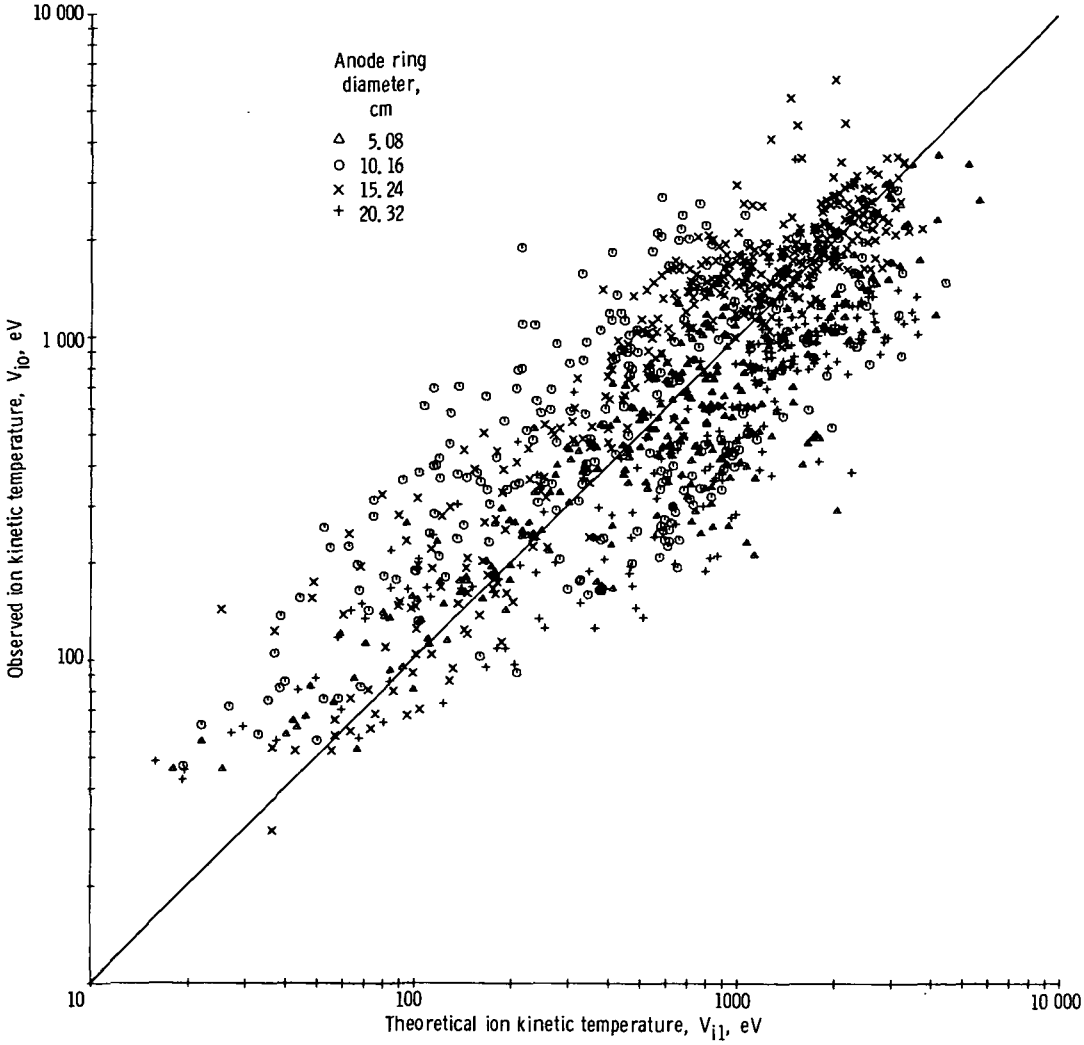

Figure 29. - Observed ion kinetic temperature as function of theoretical ion kinetic temperature calculated from equation (64) for entire data population. Median value of constant C_5 for entire data population taken from table III.

spread tends to increase at faster than a linear rate (quadratically for very large error spreads).

A second theoretical expression for the ion kinetic temperature is given by equation (69), which does not contain the effective sheath penetration explicitly. Comparison of the relative standard deviations of C_5 and C_6 in table III shows that both have approximately the same spread of error. This result may have come about because the error introduced by including the effective sheath penetration in C_5 was not larger than the quadratic increase in error caused by squaring the error associated with C_4.

The observed ion kinetic temperature V_{io} is plotted as a function of the theoretical ion kinetic temperature V_{i2} given by equation (69) in figure 30 for the entire data population. The data spread is great because of the quadratic increase in the error rela-

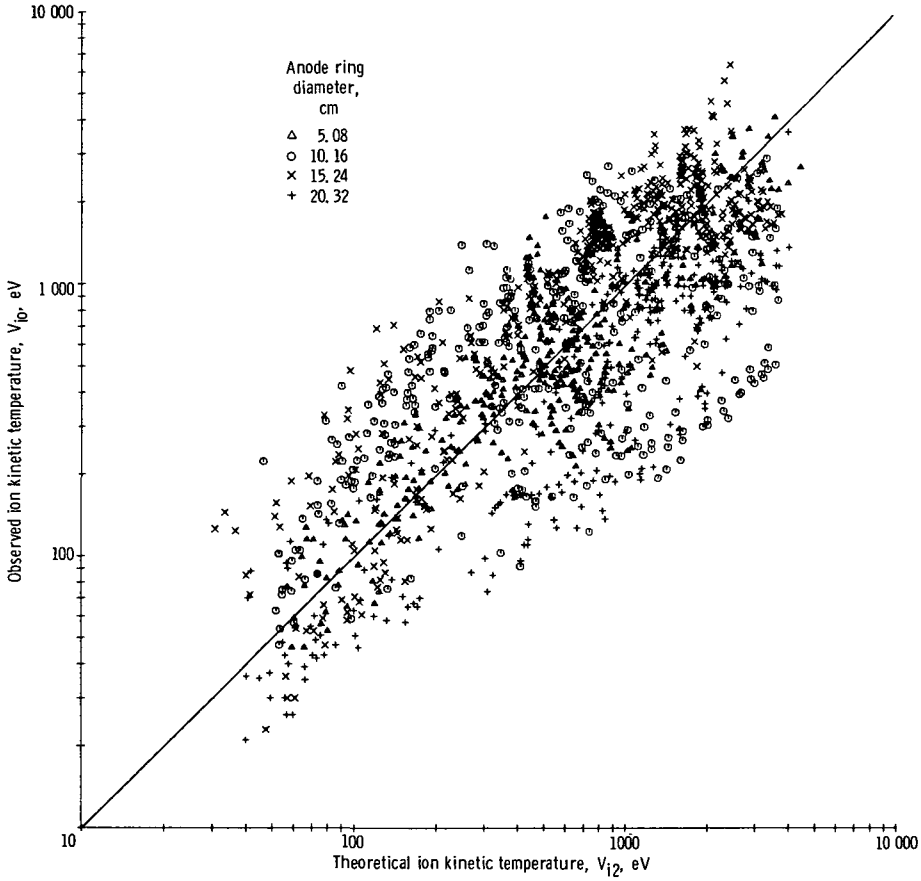

Figure 30. - Observed ion kinetic temperature as function of theoretical ion kinetic temperature calculated from equation (69) for entire data population. Median value of constant C_6 for entire data population taken from table III.

tive to figure 26, but the data tend to fall along a slope of 45° and thus confirm equation (69) over the range of data taken. The functional dependence of V_i upon the experimental variables given in equation (69) was confirmed by a statistical test described in appendix D. It is shown in appendix D that equation (69) minimizes the relative standard deviation of the experimental data.

Experimentally Observed Functional Dependence of the Ion Heating Efficiency

The observed ion heating efficiency is defined as

$$\eta_{io} = \frac{V_{io}}{V_a} \tag{78}$$

although this is really a lower bound on this efficiency. In order to obtain an impres-

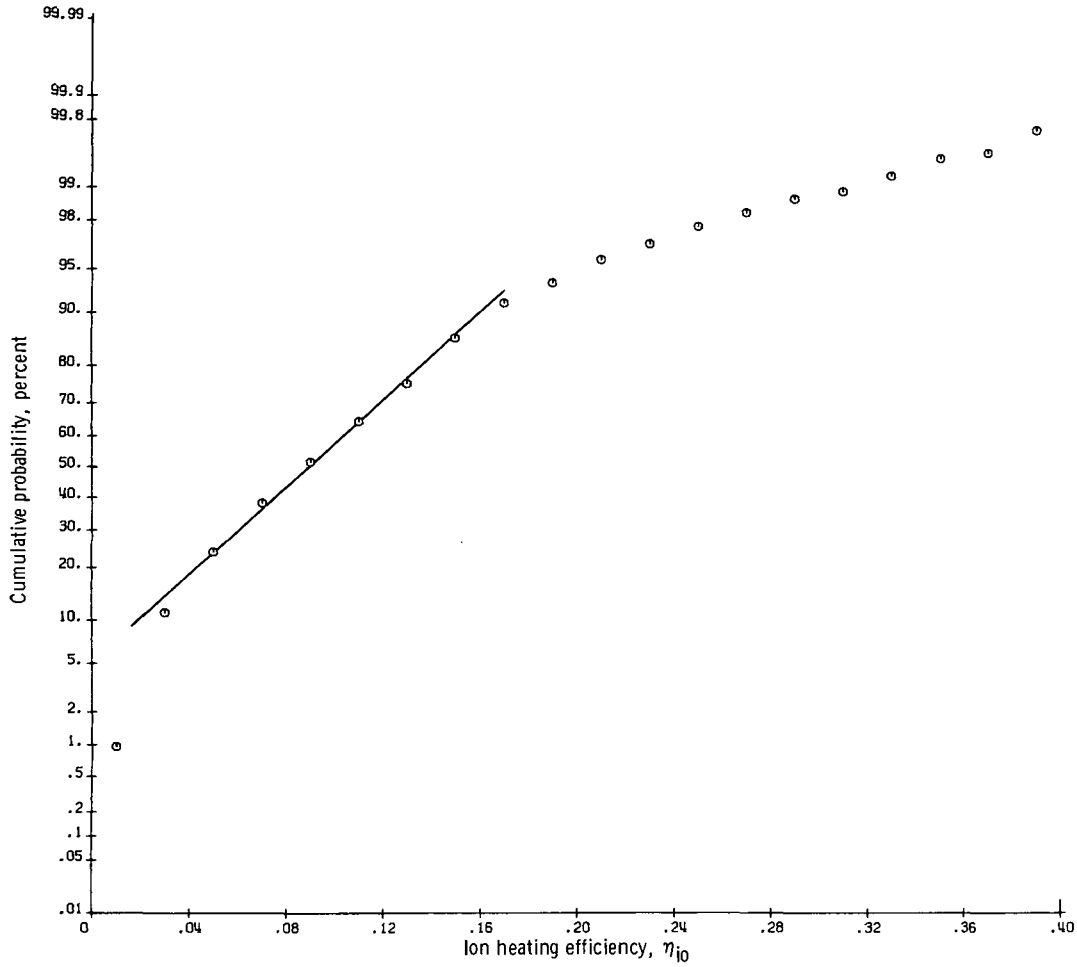

Figure 31. - Cumulative probability of ion heating efficiency as defined by equation (78) for entire data population. Median efficiency, 8.7 percent; highest ion heating efficiency, more than 40 percent.

sion of the magnitude of the efficiency observed in this discharge, the cumulative probability of the observed heating efficiency, from equation (78), was plotted against the observed efficiency in figure 31 for the entire data population. The median efficiency in this investigation was 8.6 percent, with the observed efficiencies ranging from 1 to 40 percent.

Observed Mode Phenomena

One type of mode phenomenon exhibited by this discharge has been mentioned previously and is illustrated by the data in figure 11. The spoke-like nature of these modes is shown schematically in figure 12. These higher-mode spokes result from a tendency for the ion spoke, particularly in the higher energy and density regimes of operation, to

break up into either two or four equally spaced radial spokes. It has not been possible to predict theoretically the conditions under which the higher order spokes will appear. However, it has been observed that the higher order modes are associated with high ion kinetic temperatures and with high neutral and charged particle number densities.

Another mode phenomenon appeared in the electron spoke motion. The data presented in figures 17 to 31 refer to the double anode rings shown in figure 3. The electron spoke which appeared in these double anode rings was, with no more than a dozen exceptions, a single $m = 1$ rotating electron spoke. Some preliminary data were taken with a single anode ring such as that shown in figure 2. It was found that the electron spokes in the single anode ring tended to operate in either an $m = 3$ or $m = 5$ mode of operation. That is, instead of a single electron rotating spoke, there were either 3 or 5 equally spaced electron spokes around the circumference of the sheath.

It was not possible to predict the circumstances under which a given type of mode would be observed, except that the single anode ring apparently favored the existence of higher modes, relative to the double anode ring. This might be very crudely analogous to the situation existing in metallic membranes, in which it is easier to excite a higher order mode in a thin plate than it is in a thick plate. Analogously, it might be easier to excite a higher electron spoke mode in the axially thin sheath of the single anode ring pictured in figure 2, than it is to excite a higher order mode mode in the thicker sheath created by the double anode rings shown in figure 3. In addition to this observation, there was some tendency for the very few higher electron spoke modes observed with the double anode rings to be observed at conditions of very high neutral and charged particle number densities.

DISCUSSION

Agreement of Experiment With Theory

There appears to be generally good agreement between the data in this series of experiments and the theoretical expressions which are based on the physical model illustrated in figure 9. Other physical models, based on sheath thicknesses given by the electron Debye length or the ion gyroradius, yielded larger relative standard deviations - a wider data spread about the theoretical expressions - than those presented in this report. The data for the four anode ring radii in figures 10 and 11 confirm the hypothesis that the high ion kinetic temperatures result from the thermalization of an ion spoke which results from E/B drift in the anode sheath. The dynamics of the sheath, the spoke rotation frequencies for both ions and electrons, the ion kinetic temperatures, and the ion heating efficiencies are summarized by the theoretical expressions described

in equations (30) to (78). These expressions appear to be in agreement with the experimentally observed data to the extent illustrated by figures 17 to 30.

It is not possible to separate the extent to which the spread of data in figures 17 to 30 is due to imprecision and inaccuracy of the experimental data from the extent to which it is due to the assumptions made in deriving the theoretical model. It can, however, be said that theoretical models based on the ion gyroradius or the electron Debye length as sheath thicknesses result in either "constants" C_i which are functions of n_i, B, V_a, etc. (implying scaling laws not in agreement with the data) and/or relative standard deviations significantly larger than those associated with figures 17 to 30 and listed in table III. Moreover, perturbing the exponents of the experimental parameters in equations (31) to (78) did not lead to a significant reduction of the relative standard deviation of the data. This analysis of the data is presented in appendix D. This implies that even if there were a plausible physical model associated with the other scaling law exponents investigated, the data would not fit such a model any better than the model actually adopted.

Possible Presence of Other Ion Heating Mechanisms

In references 11 and 32 to 37 various mechanisms have been suggested for the ion heating process in Penning discharges (ref. 11) or in ion magnetron devices (refs. 32 to 37). These mechanisms include beam-plasma interactions (refs. 11 and 32 to 34) and also a variety of instabilities near the ion plasma frequency (refs. 35 to 37).

In the present experiment, the heating of the ions can be understood as a result of their acceleration and drift in the electric field of the sheath. The thermalization of the ions can be understood as resulting from the interaction of the electron and ion spokes that rotate in the sheath. In the present experiment it is not necessary to invoke phenomena occurring at frequencies above a few megahertz, nor is it necessary to invoke beam-plasma interactions.

It appears that processes occurring at the ion-cyclotron frequency and/or the ion-plasma frequency can be ruled out as causative agents of the high ion kinetic temperatures on observational grounds. Spatial variation of n_i and B within the discharge volume produces spatial variation of the ion-cyclotron and ion-plasma frequencies. Hence, observed fluctuations which are z-coherent cannot relate simultaneously to all local ion plasma and cyclotron frequencies. It seems reasonable to expect that, if instabilities at either the ion-plasma frequency or the ion-cyclotron frequency played a significant role in heating the ions, then such frequencies would be very prominent in the spectrum of electrostatic potential fluctuations. In fact, the ion-plasma and ion-cyclotron frequencies were usually observed to be either faint or absent by comparison

with the amplitude of the background turbulent spectrum and by comparison with the peaks at the ion and electron spoke rotation frequencies. Only in a minority of cases were the ion-cyclotron frequency or the ion-plasma frequency identifiable in the spectrum of electrostatic potential fluctuations. In less than two dozen cases out of approximately 1500 individual runs were the amplitudes of the ion cyclotron or the ion plasma frequency higher than that of the electron spoke rotation frequency. The ion cyclotron frequency in this experiment, for a maximum magnetic field of 1.0 tesla, was 2.9 megahertz at the anode ring and 7.6 megahertz at the mirror throat, where the capacitive probes were located. These frequencies were always scanned while searching for the electron spoke rotation frequency. Similarly, for densities below about 10^{10} particles per cubic centimeter in the sheath, the ion plasma frequency in the sheath would have been below 10 megahertz and would have been observed if present. A weak peak at a frequency which may have been the ion plasma frequency was observed in a small minority of runs. The ion and electron spoke rotation frequencies could not have been misidentified, since all runs were monitored with two probes at opposite ends of a diameter. It was verified that the signals identified as spokes were 180° out of phase at opposite ends of the diameter. There is no reason to expect either the ion-cyclotron frequency or the ion-plasma frequency to be 180° out of phase in this way for all the data observed.

Importance of Ion Centrifugal Force Term

It has been suggested (refs. 35 to 37) that the centrifugal force might slow down the ions relative to the E/B velocity of the electrons and might be entirely responsible for the observed relative velocity of ions and electrons. The effect of the ion centrifugal force term is illustrated in equation (19):

$$\Omega_i = \delta\Omega_e - \frac{\Omega_i^2}{\omega_i} \tag{19}$$

If we define the dimensionless electron and ion spoke rotation frequencies as

$$\Omega_i' \equiv \frac{\Omega_i}{\omega_i} \tag{79}$$

$$\Omega_e' \equiv \frac{\Omega_e}{\omega_i} \tag{80}$$

equation (19) may be written

$$\Omega_i' = \delta\Omega_e' - \Omega_i'^2 \tag{81}$$

Equation (81) is plotted in figure 32. The straight line of slope 45^o is appropriate when there is no centrifugal force term to be considered. The curving line just below it is

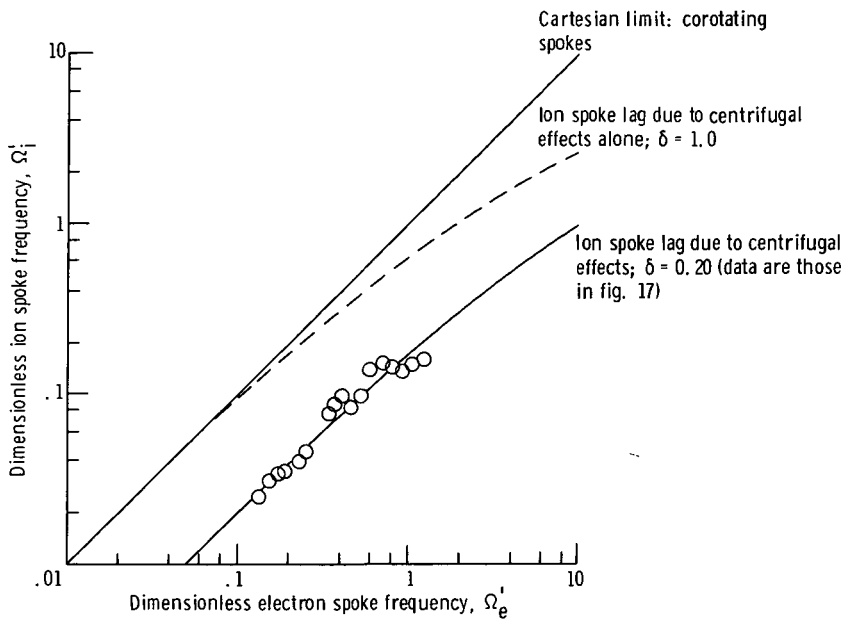

Figure 32. - Dimensionless ion spoke rotation frequency as function of dimensionless electron spoke rotation frequency showing effects of centrifugal force term. Neutral gas pressure, 5×10^{-6} torr; anode ring diameter, 15.2 centimeters.

plotted from equation (81) and includes the centrifugal force term for $\delta = 1.0$, when the ions gyrate entirely within the electric field of the sheath. Also shown in figure 32 is the curve from equation (81) appropriate to $\delta = 0.20$.

The set of experimental runs from figures 17 and 23 are replotted in figure 32. These data lie in a regime where the ion centrifugal force term accounts for only a small part of the difference between the electron and ion spoke rotation frequencies. It therefore seems reasonable to attribute the difference between the spoke frequencies to the ions spending only a portion of their orbit in the sheath ($\delta = 0.2$), rather than to the effect of the centrifugal force term.

Comparison of Data With Fahleson-Lehnert Limit

The ion spoke velocities and ion energies observed in the present series of experiments are substantially higher than the empirically determined limit of Fahleson (ref. 29) and Lehnert (refs. 30 and 31). On the basis of pulsed experiments at neutral gas pressures higher than those employed in the present experiment (i.e., above 10^{-3} torr), these authors suggest a limitation on the ion energy obtainable with devices employing $E \times B/B^2$ drift. They find that the limiting ion energy is of the order of the ionization potential V^* of the gas used. This would imply an ion spoke rotation frequency given by

$$\nu = \frac{1}{4\pi R} \sqrt{\frac{eV^*}{m_i}} \tag{82}$$

where V^* equals 15.6 eV for the present case, and $R = 7.62$ centimeters. If this limiting velocity were applicable to the present experiment, the spoke rotation frequency calculated from equation (82) would be 9 kilohertz for the $R = 7.62$ centimeter anode ring. As inspection of figure 10 shows, the observed ion velocities are from one to two orders of magnitude above this limit. Thus, the phenomenological limit of Fahleson (ref. 29) and Lehnert (refs 30 and 31) does not appear to be applicable to the conditions of the present experiment.

Comparison of Data With Datlov-Bannenberg and Brakenhoff Limit

Datlov (ref. 18) and Bannenberg and Brakenhoff (ref. 24) have pointed out that, if the electron spoke rotates with a velocity corresponding in energy to the ionization potential of the gas and if the ion spoke is dragged along with the electron spoke at this same velocity, the ions would then possess very high energies given by

$$V_i = \frac{m_i}{m_e} V^* = 57.4 \text{ kV} \tag{83}$$

Equation (83) would imply rotation frequencies for the ion spoke given by

$$\nu = \frac{1}{4\pi R} \sqrt{\frac{eV^*}{m_e}} \tag{84}$$

This limiting rotation frequency would be 1.7 megahertz for the 15.2 centimeter diameter anode ring. As inspection of figure 11 shows, the ion spoke rotation frequency for the 15.2-centimeter anode ring falls below 1.0 megahertz in this experiment. This lower ion spoke velocity can be understood as a result of the ions passing through the electric field of the sheath for only a part of their orbit. It is probable that the ion spoke velocity cannot be equal to the electron drift velocity, since the magnetic fields are seldom strong enough, or the densities low enough, to make the ion gyrodiameter smaller than the sheath thickness.

Implications for Scale-Up to Fusion Reactor Regime

The ion heating process in a modified Penning discharge is a very simple means for converting high-voltage, direct-current electrical power to ion energy. Since the electron and ion drift velocities are generally within an order of magnitude of one another, their large mass ratio assures that the input energy will not be wasted in heating the electrons. The ion heating efficiency was observed to be as high as 40 percent, and the lowest observed efficiency was still about 1.0 percent. The latter is higher than the highest ion heating efficiency observed in "turbulent heating" experiments, and this range of heating efficiencies is somewhat above that characteristic of ohmic heating.

Another significant advantage of the modified Penning discharge is that the presence of the anode ring at the magnetic field midplane produces a radially inward electric field, which may be expected to stabilize the plasma. In addition, this electric field provides an electrostatic potential well that tends to drive the positive ions inward across the sheath and into the bulk of the plasma. Heating and confinement schemes employing the modified Penning discharge may then provide a mechanism for infusing ions into the plasma, to replace classical or anomalous diffusion of the ions.

The scaling law for the ion kinetic temperature, in terms of the conditions in the sheath, is given by equation (67a):

$$V_i \sim \frac{V_a n_i^{1/4}}{B^{1/2}} \tag{67a}$$

The ion kinetic temperature is directly proportional to the anode voltage, to the fourth root of the ion number density in the sheath, and inversely proportional to the square root of the magnetic field employed. This scaling law was found to hold over the entire range of operating conditions in the present experiment, the extreme values of which are indicated in table II. Consideration is given to other possible exponents in appen-

dix D. If no other physical process intervenes, this ion heating mechanism may be capable of being scaled to fusion reactor conditions. The forseeable difficulties are practical ones, having to do with heat transfer to the anode ring, maintaining the integrity of the anode ring under high electron and particle bombardment, and preventing contamination of the plasma by impurities removed from the surface of the anode ring. These difficulties may not be crucial if the modified Penning discharge scheme is used only to ignite the thermonuclear reactor, after which the anode rings would be retracted into the walls of the vessel.

CONCLUSIONS

The experimental evidence discussed in this report appears to justify the following conclusions about the ion heating process in a modified Penning discharge:

1. Over a very wide range of operating conditions, hot, Maxwellianized ions with kinetic temperatures from 20 to 7000 eV were generated in the discharge. The observed electron energies were below the ion energies, typically by an order of magnitude or more.

2. Two distinct, rotating, spoke-like structures were observed in the sheath between the anode ring and the plasma. The faster rotating spoke consists of electrons rotating with the E/B drift velocity in the electric field of the sheath, where E is the electric field strength. The slower spoke typically has velocities from 5 to 50 percent of the electron spoke and consists of ions. The rotational velocity of the ion spoke was shown to be directly proportional to the ion thermal velocity over more than an order of magnitude in these quantities. The ion heating process, therefore, consists of accelerating newly ionized ions to a high drift velocity in the electric field of the sheath.

3. The spectrum of turbulent, electrostatic potential fluctuations, at frequencies below the ion cyclotron and plasma frequencies, was observed to have a prominent peak at the ion spoke rotation frequency. The spectrum was considerably enhanced above this peak, which suggested that energy cascades upward in frequency and downward in scale size as the energy of spoke rotation is degraded into thermal motions of the plasma constituents.

4. The rotational velocity of the electron spoke was observed to be directly proportional to the electron thermal velocity, although there was a large spread in the relevant data. The electron energies were typically from 2 to 200 eV. It appears that the electrons receive energy just sufficient to ionize the background gas from their E/B drift in the electric field of the sheath.

5. The ion and electron spokes pass through or near each other with periods that typically are microseconds or less. These strong electrostatic interactions provide a sufficiently swift and powerful mechanism to explain the observed Maxwellianization of the particle energies.

6. Theoretical expressions have been derived for the effective sheath penetration δ (the fraction of time that the ions spend in the electric field of the sheath), the ion and electron spoke rotation frequencies ν_i and ν_e, the ion kinetic temperature V_i, and the ion heating efficiency η_i. These theoretical expressions were shown to be consistent with data from a population of 1495 individual runs.

The sheath between the anode ring and the plasma has a thickness which is proportional to the ion Debye length. Other candidate sheath thicknesses, such as the electron Debye length and the ion gyroradius, were not consistent with the experimental data. The ratio of the ion Debye length to the ion gyrodiameter is less than unity in this plasma, with the result that the ions were in the electric field of the sheath for only part of their orbits. The ions, therefore, experience an effective radial electric field smaller than that which the electrons experience, since the latter gyrate entirely within the sheath. Centrifugal effects alone cannot explain the large difference between the electron and ion spoke velocities in this discharge.

8. The median efficiency of converting direct-current electric power to ion energy in this series of 1495 individual experimental runs was 8.6 percent.

9. The ion spoke velocities observed in this experiment were from one to two orders of magnitude larger than the phenomenological limit suggested by Fahleson and Lehnert.

10. The observed ion spoke velocities were typically 20 percent of the value required by corotation with the electron spoke. Such corotation was suggested by Datlov and Bannenberg and Brakenhoff as an ion heating mechanism.

11. It is not necessary to invoke phenomena at the ion plasma or the ion cyclotron frequencies as causative agents to explain the ion heating or thermalization in this discharge. Phenomena at these frequencies appeared to play only a secondary role in the heating and thermalization processes, if any.

12. The ion and electron spokes obey Ferraro's law of isorotation along the discharge axis.

13. The radial electric field in the sheath of a modified Penning discharge may promote macroscopic stability of the plasma confined inside the sheath and also may promote the infusion of ions from the sheath into the bulk of the confined plasma.

14. The modified Penning discharge provides a simple, efficient method for the conversion of direct-current electrical power into high ion kinetic temperatures.

15. The theoretical expressions which describe the experimental results of this investigation reveal no impediment to scaling this ion heating mechanism to fusion reactor conditions.

Lewis Research Center,
National Aeronautics and Space Administration,
Cleveland, Ohio, July 13, 1972,
503-10.

APPENDIX A

SYMBOLS

B	magnetic field strength, T
C_i	constant parameters defined in text
E	electric field volts/m
e	charge on electron
G	geometrical constant describing fraction of total ion flux intercepted by retarding potential energy analyzer
I	electrical current, A
m	particle mass or spoke mode number
n_i	ion number density in sheath
n_o	neutral number density
P	constant defined by eq. (39) relating neutral density to gage pressure; or electrical power, W
p_o	neutral gas pressure, units of 10^{-6} torr
R	anode ring inner radius, cm, or radius of gyroorbit
R_e	radius of electron gyroorbit defined in fig. 14
R_i	radius of ion gyroorbit defined in fig. 14
R_L	ion gyroradius defined in fig. 15
V	particle energy, eV or electrostatic potential, volts
V_a	anode potential, volts
V_p	plasma sheath volume sampled by retarding potential energy analyzer
V^*	ionization potential of gas, electron volts
v	particle velocity
W	particle energy
X	defined by eq. (22)
x	ion orbit approach distance defined in fig. 15, cm
Y	defined by eq. (23)
Z	defined by eq. (24)

δ	effective sheath penetration distance defined by eq. (20)
ϵ_o	permitivity of free space
η_i	efficiency of ion heating
λ_{di}	ion Debye length
ν_c	particle-neutral collision frequency
ν_{ce}	cyclotron frequency for electrons
ν_{ci}	cyclotron frequency for ions
ν_e	electron spoke frequency
ν_{en}	electron-neutral collision frequency
ν_i	ion spoke rotation frequency
ν_{in}	ion-neutral collision frequency
ν_p	plasma frequency
ν_1	calculated ion spoke frequency defined by eq. (3)
ξ	dimensionless sheath thickness parameter
$\langle \sigma v \rangle_{ne}$	ionization rate parameter for electron-neutral ionization
τ	collision time for particle-neutral collision
Φ_i	measured ion flux from plasma
φ	gyration angle defined in fig. 15
Ω_e	electron spoke angular frequency
Ω_i	ion spoke angular frequency
ω	cyclotron frequency of particles

Subscripts

a	anode ring
c	cyclotron motion
d	drift velocity
e	electrons
i	ions
in	input
k	fiduciary index

n	neutral background gas
o	observed quantity or neutral gas
oi	ions
ox	charge-exchange neutral
r	radial direction
s	spoke
θ	azimuthal direction
$\parallel$	direction along magnetic field
$\perp$	direction perpendicular to magnetic field

APPENDIX B

DETAILED MODEL OF ANODE SHEATH

Experimental data have been taken which make it clear that the angular frequency of the electron and ion spokes are independent of radius. Frequencies which were a function of the radial probe position were not observed. The frequency of the electron spoke may be written

$$\nu_e = \frac{E_r}{2\pi rB} \tag{B1}$$

Since the midplane magnetic field is essentially independent of radius, a frequency independent of radius implies an electric field proportional to radus:

$$E_r \sim C_7 r \tag{B2}$$

We also require that, in the Cartesian limit, when

$$\frac{r}{R} \to 1 \quad \text{and} \quad R \approx r \to \infty \tag{B3}$$

the radial electric field be given by the anode voltage divided by a multiple of the ion Debye length,

$$E_r \to \frac{V_a}{\xi \lambda_{di}} \tag{B4}$$

An expression for the electric field which is consistent with equation (B2) and (B4) is

$$E_r = - \frac{V_a r}{\xi \lambda_{di} R} \tag{B5}$$

A boundary condition which must be satisfied by the potential is

$$V(R) = V_a \tag{B6}$$

A potential distribution which is consistent with equations (B5) and (B6) is

$$V = \frac{V_a\left(R^2 - 2\xi R\lambda_{di} - r^2\right)}{2\xi\lambda_{di}R} \tag{B7}$$

Equation (B7) predicts that the potential will drop off to zero (the cathode potential in this experiment) at a position

$$r_{min} = \sqrt{R(R - 2\xi\lambda_{di})} \tag{B8}$$

Thus, the total sheath thickness

$$\Delta = R - r_{min} = R\left[1 - \sqrt{1 - \frac{2\xi\lambda_{di}}{R}}\right] \tag{B9}$$

is equal to the Cartesian sheath thickness $\xi\lambda_{di}$ when the sheath is thin. Even when $r_{min} = R/2$, Δ differs by only 25 percent from $\xi\lambda_{di}$, so the latter was taken as the sheath thickness in the text.

The radial distribution of electric field and potential represented by equations (B5) and (B7) look qualitatively as shown in sketches (a) and (b). Potential and electric field

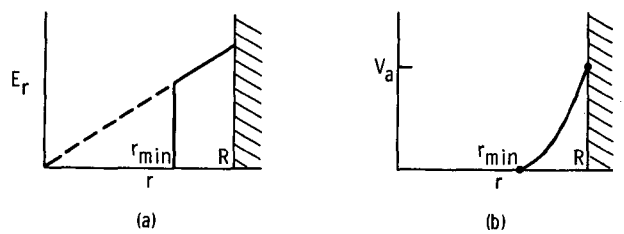

distributions qualitatively similar to sketches (a) and (b) have been observed in the literature (refs. 4 and 23).

It is clear on observational grounds that equipartition between ions and electrons is absent. The ion energies are typically an order of magnitude or more greater than that of the electrons. This result is consistent with the vary small ion-electron binary collision cross sections which exist under the experimental conditions.

It is consequence of the model proposed in this report that all of the electrons comprising the electron spoke are within the sheath, while only about 20 percent (δ is equal to this percentage) of the ions are typically in the sheath at any given time, because of

their larger gyroradii. The mean radius of the ion spoke is, therefore, smaller than that of the electrons, and only a fraction of the ions are involved with any given interaction of the two spokes. Another factor which may lead to randomization of the energies and velocity vectors of both species is that both ions and electrons will possess velocities parallel to the magnetic field. Successive reflections between the magnetic mirrors will surely result in a given particle experiencing the electric field of the sheath for different periods of time.

In scaling this sheath model to fusion densities, the sheath thickness will become much thinner relative to the plasma radius. In this limit, the Cartesian approximation to the sheath kinematics becomes exact, and the time-averaged electric field used in calculating the drift velocity becomes exact, in that centrifugal effects are no longer significant. It appears plausible that the interaction of the ion and electron spokes may give rise to quasi-resonant coupling conditions. An example of such coupling might be ion and electron spoke velocities that were related by a small integer factor. There appeared to be no obvious evidence for this in the experimental data, although one cannot rule out at this time such a coupling effect as an influence on determining the mode number of the spokes.

APPENDIX C

DATA ON INDIVIDUAL MODES OF ION SPOKE ROTATION

Figure 11 contains approximately 1500 data points. Some of these were for $m = 4$, with four rotating ion spokes; some for $m = 2$, with two spokes; and most for $m = 1$, with a single spoke. The $m = 1$ data for the four anode ring diameters are plotted in figure 33. The data lie somewhat above the theoretical $m = 1$ line, as a result of the finite gyroradius of the ions. The $m = 2$ data are shown in figure 34 and again lies somewhat above the theoretical line. The two isolated points below the rest of the data apparently were $m = 1$ modes which were misidentified in the laboratory. The $m = 4$ data are shown in figure 35. It is not known why no $m = 3$ modes were observed.

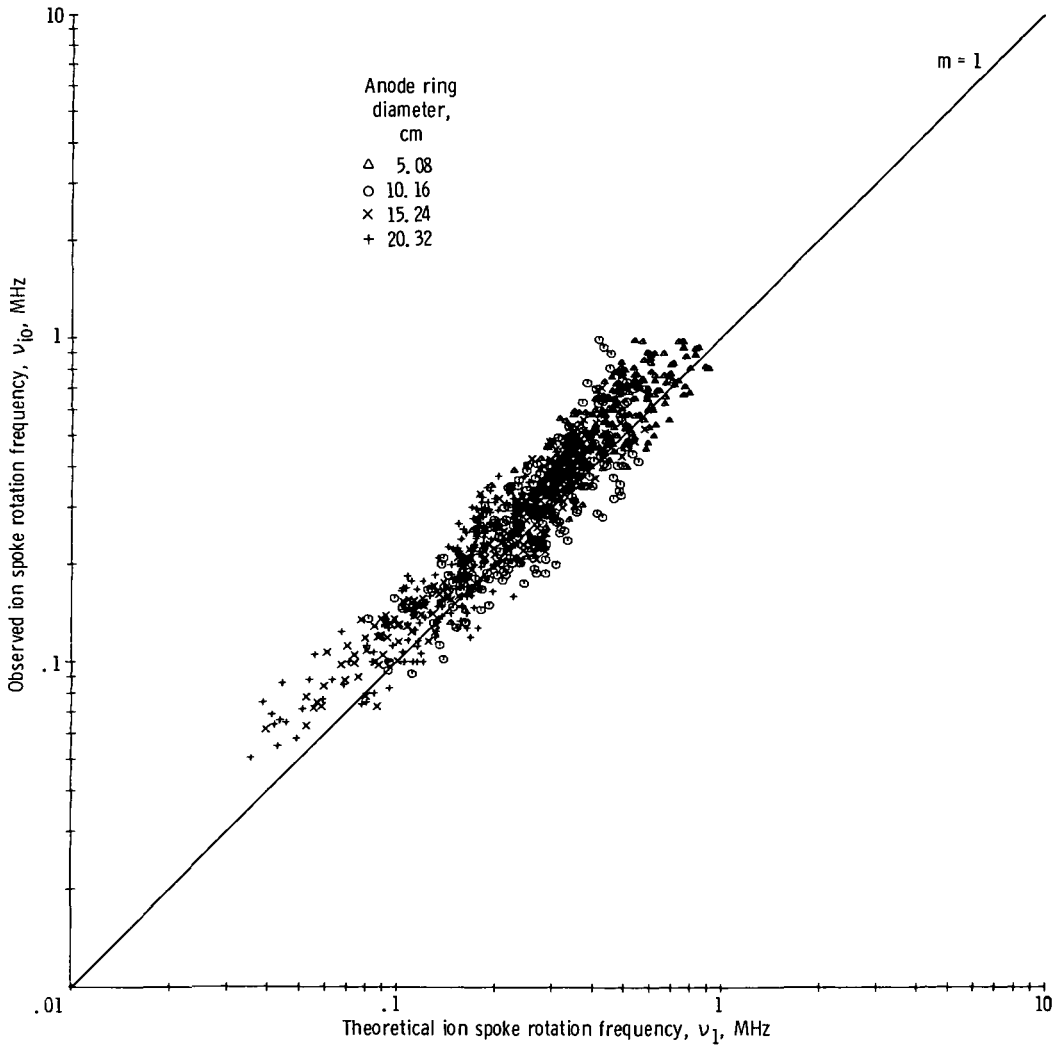

Figure 33. - Observed ion spoke rotation frequency as function of theoretical ion spoke rotation frequency given by equation (3) for single rotating spoke. Mode number, $m = 1$.

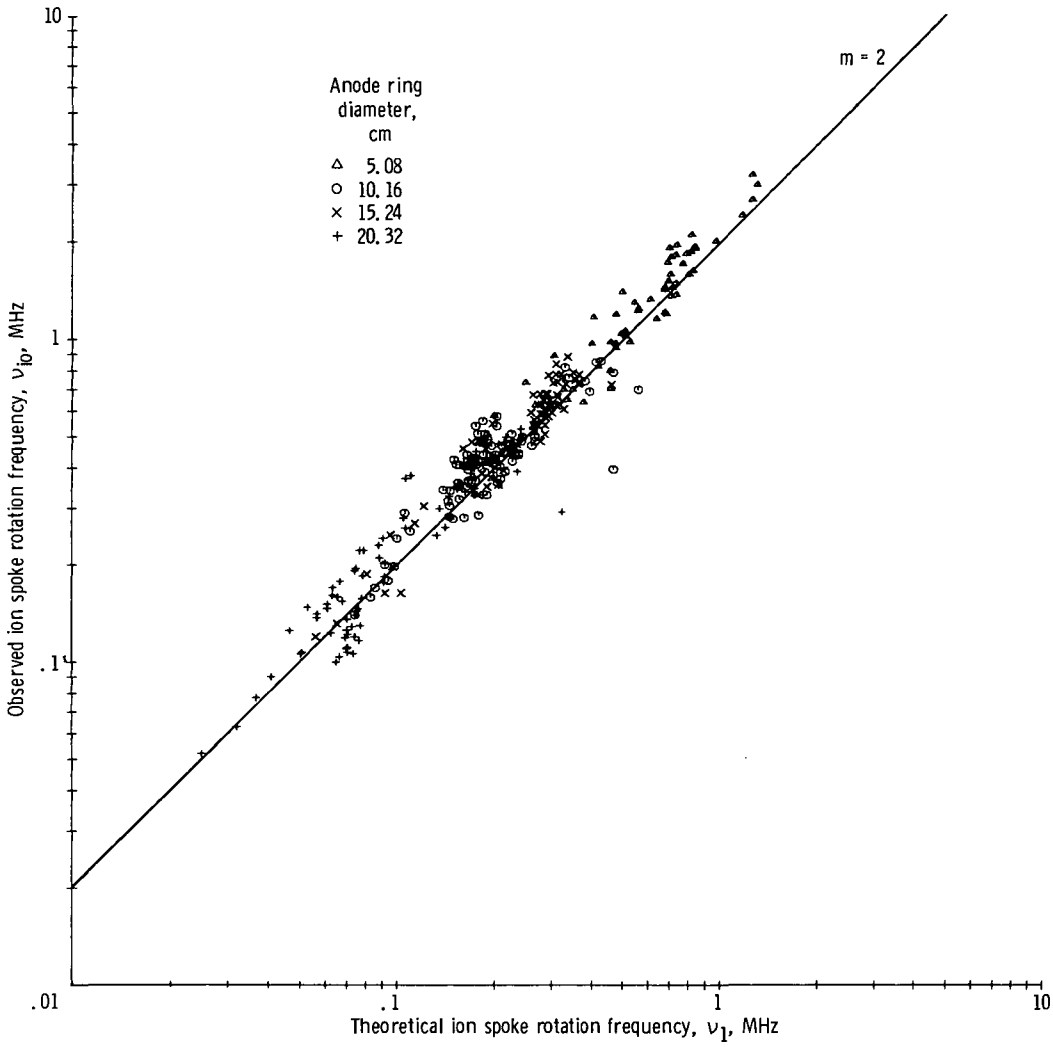

Figure 34. - Observed ion spoke rotation frequency as function of theoretical ion spoke rotation frequency given by equation (3) for two spokes with mode number m = 2. Two points well below m = 2 line apparently were m = 1 data which were misidentified in the laboratory.

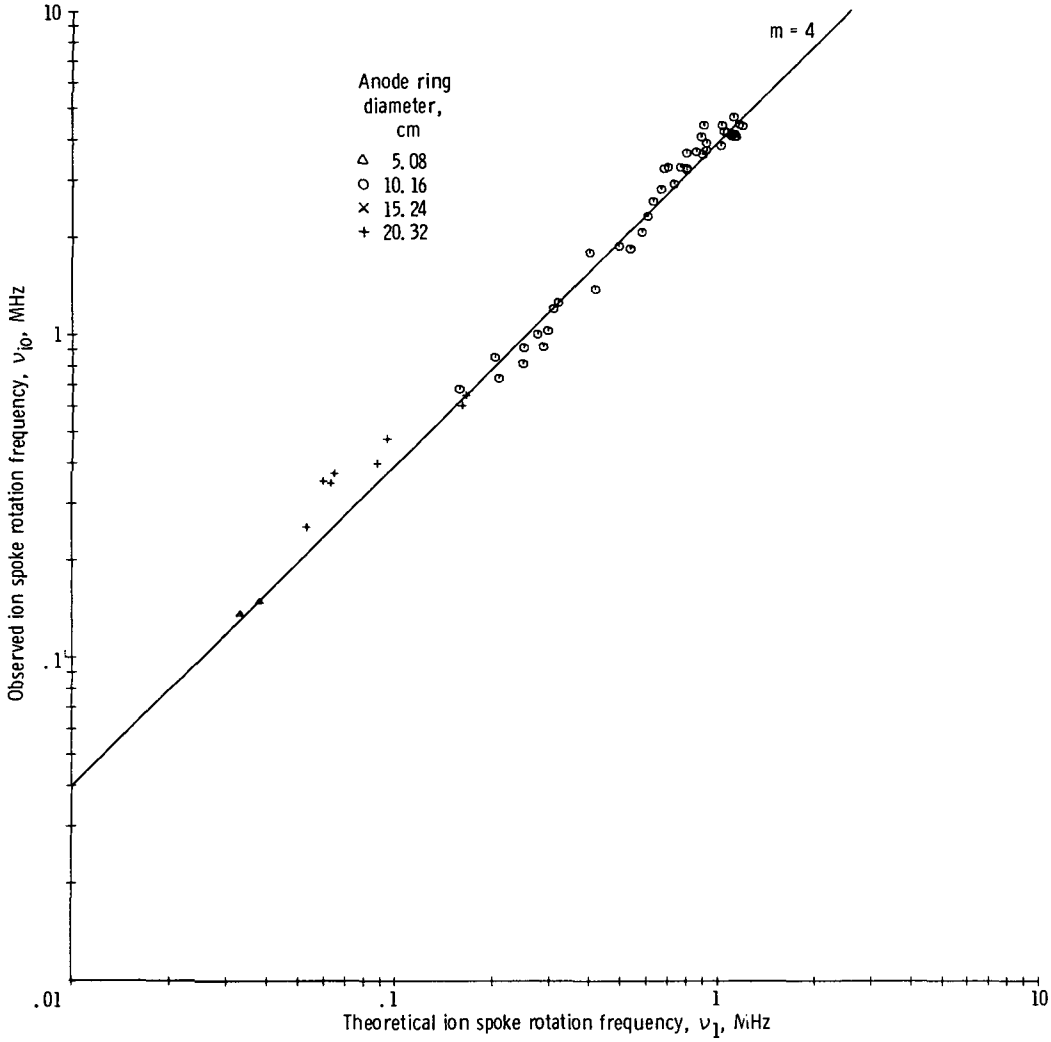

Figure 35. - Observed ion spoke rotation frequency as function of theoretical frequency given by equation (3) for four ion spokes, with mode number m = 4.

APPENDIX D

STATISTICAL COMPARISON OF THEORY AND EXPERIMENT

The data population of the present experiment is large enough that one may use statistical methods to compare theory and experiment. This method relies on the fact that, if the theory is valid, the standard deviation of the data should be minimized when the data are correlated with the theoretical expression. The method will be illustrated using the theoretical expression for ion kinetic temperature given by equation (69). This expression is important for scaling this ion heating mechanism to fusion reactor conditions, and it also appears most questionable, in view of the large data spread evident in figure 30. It is the contention of the author that this spread is due to the quadratic increase in error associated with squaring the ion spoke rotation frequency and not due to an attempt to force a fit to an inappropriate theoretical expression.

One may test other candidate theoretical expressions by adopting the following generalization of equation (69):

$$V_i = C_6' \frac{V_a^{\alpha}}{B^{\gamma}} \left(\frac{\Phi_i}{p_o}\right)^{\epsilon} \tag{D1}$$

One may then allow the exponents α, γ, and ϵ to range between selected limits and test whether the standard deviation of the data is minimized for the theoretically predicted values $\alpha = 1.0$, $\gamma = 1/2$, and $\epsilon = 1/4$. The standard deviation of the constant C_6' has been calculated from

$$C_6' = \frac{V_{io} B^{\gamma}}{V_a^{\alpha}} \left(\frac{p_o}{p_i}\right)^{\epsilon} \tag{D2}$$

and read off plots of the cumulative probability of C_6' on probability paper. The equivalent standard deviation was defined as the geometric mean of the values of C_6' one standard deviation above and below the median value. The relative equivalent standard deviation was defined as the equivalent standard deviation of C_6' divided by the median value of C_6'. The data population chosen for purposes of illustration was that for the 15.2-centimeter-diameter anode ring. Only those experimental runs for which the parameter in question varied from run to run (B, V_a, or n_i) were included in the population.

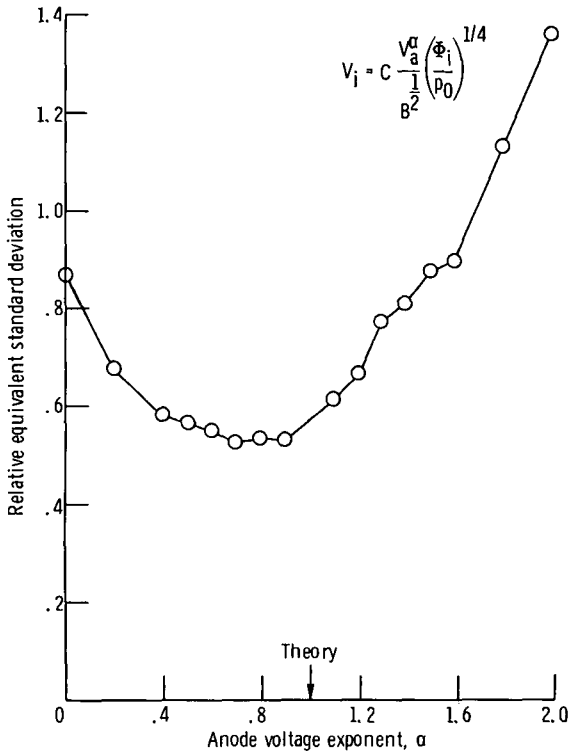

Figure 36. - Relative equivalent standard deviation for 15.2-centimeter diameter-anode-ring data population as function of anode voltage exponent. Magnetic field exponent, 1/2; ion density exponent, 1/4; ion kinetic temperature, V_i; anode voltage, V_a; magnetic field strength, B; measured ion flux from plasma, Φ_0; neutral gas pressure, p_0.

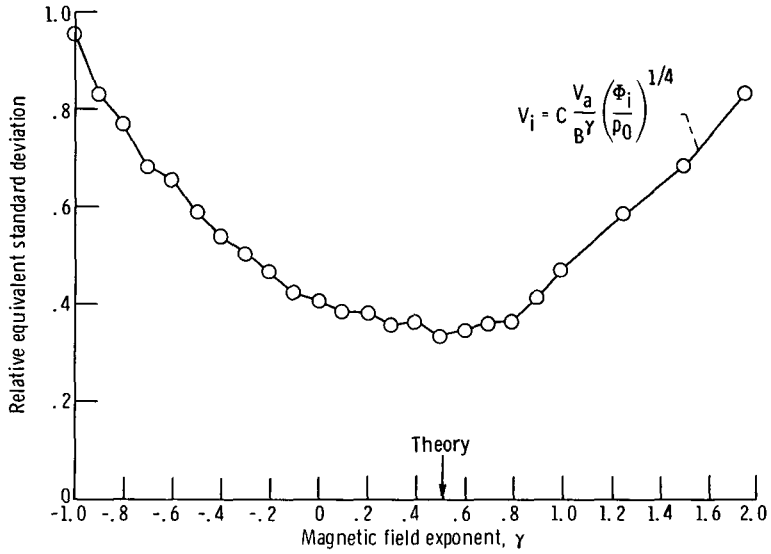

Figure 37. - Relative equivalent standard deviation for 15.2-centimeter-diameter-anode-ring data population as a function of magnetic field exponent. Anode voltage exponent, 1.0; ion density exponent, 1/4; ion kinetic temperature, V_i; anode voltage, V_a; magnetic field strength, B; measured ion flux from plasma, Φ_0; neutral gas pressure, p_0.

In figure 36 the values $\gamma = 1/2$ and $\epsilon = 1/4$ were held constant, and the anode voltage exponent α was permitted to vary over the range $0 \leq \alpha \leq 2.0$. The relative standard deviation has a minimum in the vicinity of $0.7 \leq \alpha \leq 1.0$, which is consistent with the theoretical prediction that the ion energy is directly proportional to anode voltage. In figure 37 the magnetic field exponent is permitted to vary over the range $-1.0 \leq \gamma \leq 1.75$, while the other parameters assume their theoretically predicted values. The relative standard deviation has a minimum in the vicinity of the theoretically predicted value of $\gamma = 0.5$. In figure 38 the relative standard deviation is plotted as a function of the ion density exponent ϵ over the range $-1.0 \leq \epsilon \leq 1.5$, with the other two exponents set at their theoretical values. The relative standard deviation has a minimum in the vicinity of the theoretically predicted value of $\epsilon = 1/4$, but it probably is not possible to rule out exponents in the range $-0.1 \leq \epsilon \leq 0.3$ with the available data.

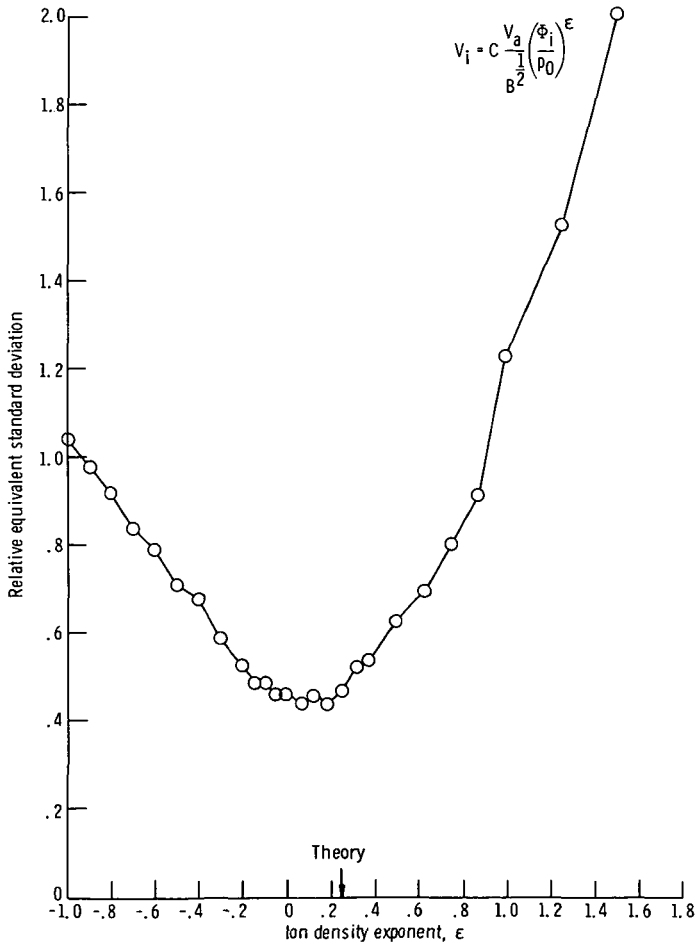

Figure 38. - Relative equivalent standard deviation of 15.2-centimeter-diameter-anode-ring data population as function of ion density exponent. Anode voltage exponent, 1.0; magnetic field exponent, 1/2; ion kinetic temperature, V_i; con-anode voltage, V_a; magnetic field strength, B; measured ion flux from plasma, Φ_0; neutral gas pressure, p_0.

REFERENCES

1. Penning, F. M.; and Nienhuis, K.: Construction and Applications of a New Design of the Philips Vacuum Gauge. Philips Tech. Rev., vol. 11, no. 4, Oct. 1949, pp. 116-122.

2. Gow, J. D.; and Foster, J. S., Jr.: A High-Intensity Pulsed Ion Source. Rev. Sci. Inst., vol. 24, no. 8, Aug. 1953, pp. 606-610.

3. Meyerand, Russell G., Jr.; and Brown, Sanborn C.: High-Current Ion Source. Rev. Sci. Inst., vol. 30, no. 2, Feb. 1959, pp. 110-111.

4. Hooper, E. B., Jr.: A Review of Reflex and Penning Discharges. Advances in Electronics and Electron Physics. Vol. 27. Academic Press, Inc., 1969, pp. 295-343.

5. Hopfgarten, N.: Glow and Arc-Type Penning Discharges. Rep. TRITA-EPP-71-12, Royal Inst. Tech., Stockholm, June 1971.

6. George, K. A.: Confining a Plasma in Steady Electric and Magnetic Fields. Nature, vol. 190, Apr. 22, 1961, p. 334.

7. Angerth, B.; Ehrensvärd, J.; and Persson, H.: Production of a Hot Plasma by Discharge in a Strongly Inhomogeneous Magnetic Field. Plasma Physics and Controlled Nuclear Fusion Research. Vol. 2. IAEA, Vienna, 1966, pp. 901-911.

8. Roth, J. Reece: Modification of Penning Discharge Useful in Plasma Physics Experiments. Rev. Sci. Inst., vol. 37, no. 8, Aug. 1966, pp. 1100-1101.

9. Hopfgarten, N.; Johansson, R. B.; Nilsson, B.; and Persson, H.: Penning Discharge in a Strongly Inhomogeneous Magnetic Mirror Field. Phys. Fluids, vol. 11, no. 10, Oct. 1968, pp. 2272-2277.

10. Roth, J. Reece; and Clark, Marion: Analysis of Integrated Charged Particle Energy Spectra from Gridded Electrostatic Analyzers. Plasma Phys., vol. 11, no. 2, Feb. 1969, pp. 131-143.

11. Fumelli, M.; Dei-Cas, R.; Girard, J. P.; and Valckx, F. P. G.: Chauffage des Ions Dans Une Decharge Penning. Plasma Phys., vol. 12, no. 6, June 1970, pp. 423-433.

12. Roth, J. Reece: Experimental Study of Spectral Index, Mode Coupling, and Energy Cascading in a Turbulent, Hot-Ion Plasma. Phys. Fluids, vol. 14, no. 10, Oct. 1971, pp. 2193-2202.

13. Hopfgarten, N.; Johansson, R. B.; Nilsson, B. H.; and Persson, H.: Hot Ions and Differential Rotation in a Non-Maxwellian Plasma with a Static Parallel Electric Field. Rep. 70-27, Royal Inst. of Tech., Stockholm, Sept. 1970. Also presented at the Fourth European Conference on Controlled Fusion and Plasma Physics Rome, Aug. 31-Sept. 4, 1970, p. 91.

14. Batten, H. W.; Smith, H. L.; and Early, H. C.: Pl: ma Fluctuations in Crossed Electric and Magnetic Fields. J. Franklin Inst., vol. 262, no. 1, July 1956, pp. 17-30.

15. Knauer, W.: Mechanism of the Penning Discharge at Low Pressures. J. Appl. Phys., vol. 33, no. 6, June 1962, pp. 2093-2099.

16. Knauer, W.; Fafarman, A.; and Poeschel, R. L.: Instability of Plasma Sheath Rotation and Associated Microwave Generation in a Penning Discharge. Appl. Phys. Letters, vol. 3, no. 7, Oct. 1, 1963, pp. 111-112.

17. Drawin, H. W.; and Fumelli, M.: Spectroscopic Measurement of Plasma Rotation in a Penning Discharge. Proc. Phys. Soc., vol. 85, pt. 5, May 1965, pp. 997-1005.

18. Dǎtlov, J.: The Inverted Ion Magnetron Principle and Its Usefulness in Laboratory Plasma Physics and Cosmical Electrodynamics. Czech. J. Phys., Ser. B, vol. 15, no. 11, 1965, pp. 858-860.

19. Vlasov, M. A.; Dobrokhotov, E. I.; Zharinov, A. V.: Instability of a Hot Cathode Discharge in a Magnetic Field at Low Pressures. Nucl. Fusion, vol. 6, no. 1, Mar. 1966, pp. 24-34.

20. Naumovets, V. G.; Romanyuk, L. I.; and Slobodyan, V. M.: Low Frequency Oscillations in the Hot Cathode Penning Discharge Plasma. NASA TT F-13641, 1971.

21. Berezin, A. B.; Bulyginskii, D. G.; Vil'dzhyunas, M. I.; and Rodichkin, V. A.: Correlation Study of a Penning Discharge. Soviet Phys. - Tech. Phys., vol. 15, no. 1, July 1970, pp. 101-105.

22. Hooper, E. B., Jr.: Parasitic Instability Generated by Steady State Oscillations in a Reflex Arc Plasma. Plasma Phys., vol. 12, no. 12, Dec. 1970, pp. 990-996.

23. Smirnitskaya, G. V.; and Nosyreva, I. A.: Oscillations in a Low-Pressure Penning Discharge. Soviet Phys. - Tech. Phys., vol. 15, no. 11, May 1971, pp. 1832-1838.

24. Bannenberg, J. G.; and Brakenhoff, G. J.: Energy Measurements on a Rotating Plasma. Plasma Phys., vol. 13, no. 7, July 1971, pp. 587-605.

25. Roth, J. Reece: Origin of Hot Ions Observed in a Modified Penning Discharge. NASA TM X-67956, 1971; see also Bull. Am. Phys. Soc., vol. 16, no. 11, p. 1265.

26. Bishop, Amasa S.: Project Sherwood. Addison-Wesley Publ. Co., 1958, pp. 67-68, 127-131.

27. Neidigh, R. B.; and Weaver, C. H.: Effect of an Applied Pressure Gradient on a Magnetically Collimated Arc. Theoretical and Experimental Aspects of Controlled Nuclear Fusion. Vol. 31 of Proceedings of the Second United Nations International Conference on the Peaceful Uses of Atomic Energy. United Nations, 1958, pp. 315-318.

28. Boyer, K.; Hammel, J. E.; Longmire, C. L.; Nagle, D.; Ribe, F. L.; and Riesenfeld, W. B.: Theoretical and Experimental Discussion of Ixion, a Possible Thermonuclear Device. Theoretical and Experimental Aspects of Controlled Nuclear Fusion. Vol. 31 of Proceedings of the Second United Nations International Conference on the Peaceful Uses of Atomic Energy. United Nations, 1958, pp. 319-324.

29. Fahleson, Ulf V.: Experiments with Plasma Moving through Neutral Gas. Phys. Fluids, vol. 4, no. 1, Jan. 1961, pp. 123-127.

30. Lehnert, B.: Fusion Devices for Plasma Rotating at Super-Critical Velocities. Rep. 70-33, Royal Inst. Tech., Stockholm, Sept. 1970.

31. Lehnert, B.: Rotating Plasmas. Nucl. Fusion, vol. 11, 1971, pp. 485-533.

32. Alexeff, I.; Neidigh, R. V.; and Peed, W. F.: Beam-Plasma Interaction Experiments and Diagnostics. Phys. Rev., vol. 136, no. 3A, Nov. 2, 1964, pp. A689-A695.

33. Alexeff, I.; Jones, W. D.; Neidigh, R. V.; Peed, W. F.; and Stirling, W. L.: Plasma Heating and Burnout in Beam-Plasma Interaction. Plasma Physics and Controlled Nuclear Fusion Research. Vol. 2. IAEA, Vienna, 1966, pp. 781-799.

34. Alexeff, I.; Jones, W. D.; and Neidigh, R. V.: Production of d-d Reactions by Beam-Plasma Interaction in the Steady State. Phys. Rev. Letters, vol. 18, no. 25, June 19, 1967, pp. 1109-1112.

35. Alexeff, I.; Estabrook, K.; A.; Jones, W. D.; Neidigh, R. V.; Olsen, J. N.; Scott, F. R.; Stirling, W. L.; Widner, M. M.; and Wing, W. R.: Understanding Turbulent Ion Heating in the Oak Ridge Mirror Machine, "Burnout V." Phys. Rev. Letters, vol. 25, no. 13, Sept. 28, 1970, pp. 848-851.

36. Alexeff, I.; Berry, L. A.; Dudley, J. M.; Estabrook, K. G.; Hirose, A.; Jones, W. D.; Neidigh, R. V.; Olsen, J. N.; Scott, F. R.; Stirling, W. L.; Widner, M. M.; and Wing, W. R.: Understanding Turbulent Ion Heating in the Oak Ridge Mirror Machine, "Burnout V." Rep. CN-28/E-14, CONF-710607-67, Oak Ridge National Lab., June 17, 1971.

37. Alexeff, I.; Berry, L. A.; Neidigh, R. V.; and Hirose, A.: The Absence of Relative Drift Velocity Limitations on Ion Heating in the BO VI Mirror Machine. Phys. Canada, vol. 27, no. 4, 1971, p. 23.

38. Rayle, Warren D.; Reinmann, John J.; Roth, J. Reece; and Sigman, Donald R.: Magnetic Fields in Propulsion and Power Research. NASA SP-226, 1970, pp. 94-99.

39. Krawec, Roman; Prok, George M.; and Swett, Clyde C.: Evaluation of Two Direct-Current Methods of Plasma Production for Use in Magnetic Mirror Experiments. NASA TN D-2862, 1965.

40. Kribel, R.; Eckdahl, C.; and Lovberg, R.: Properties of the Rotating Spoke in an Unstable Pulsed MPD Arc. AIAA J., vol. 9, no. 5, May 1971, pp. 893-899.

41. Roth, J. Reece: Plasma Stability and the Bohr-Van Leeuwen Theorem. NASA TN D-3880, 1967.

42. Roth, J. Reece; Rayle, Warren D.; and Reinmann, John J.: Technological Problems Anticipated in the Application of Fusion Reactors to Space Propulsion and Power Generation. NASA TM X-2106, 1970.

43. Roth, J. Reece; Freeman, Donald C., Jr.; and Haid, David A.: Superconducting Magnet Facility for Plasma Physics Research. Rev. Sci. Inst., vol. 36, no. 10, Oct. 1965, pp. 1481-1485.

44. Roth, J. Reece; and Krawczonek, Walter M.: Paired Comparison Tests of the Relative Signal Detected by Capacitive and Floating Langmuir Probes in Turbulent Plasma from 0.2 to 10 MHz. Rev. Sci. Inst., vol. 42, no. 5, May 1971, pp. 589-594.

45. Alfvén, Hannes; and Fälthammar, Carl G.: Cosmical Electrodynamics. Second ed., Clarendon Press, Oxford, 1963, pp. 109-111.

46. Roth, J. Reece: Experimental Observation of Low-Frequency Oscillations Described by the Plasma Continuity Equations. Phys. Fluids, vol. 12, no. 1, Jan. 1969, pp. 260-262.

47. Roth, J. Reece: Experimental Observation of Continuity-Equation Oscillations in Slightly Ionized Deuterium, Neon and Helium Gas. Plasma Phys., vol. 11, no. 9, Sept. 1969, pp. 763-777.

48. Rose, David J.; and Clark, Melville, Jr.: Plasmas and Controlled Fusion. John Wiley & Sons, Inc., 1961, p. 162.

49. Allis, W. P.: Motions of Ions and Electrons. Rep. 299, Massachusetts Inst. Tech., Res. Lab. of Elec., June 1956, p. 15.

50. Roth, J. Reece: Experimental Investigation of Single Interaction Nonadiabatic Losses from Axisymmetric Magnetic Mirrors. Phys. Fluids, vol. 9, no. 12, Dec. 1966, pp. 2538-2540.

51. Roth, J. Reece: Correlation of Magnetic Moment Variation in Axisymmetric and Multipolar Magnetic Mirrors. Plasma Phys., vol. 10, no. 9, Sept. 1968, pp. 809-818.

NASA-Langley, 1972 — 25 E-7003

NATIONAL AERONAUTICS AND SPACE ADMISTRATION
WASHINGTON, D.C. 20546

OFFICIAL BUSINESS
PENALTY FOR PRIVATE USE $300

FIRST CLASS MAIL

POSTAGE AND FEES PAID
NATIONAL AERONAUTICS AND
SPACE ADMINISTRATION

U.S.MAIL

NASA 451

POSTMASTER: If Undeliverable (Section 158 Postal Manual) Do Not Return

"The aeronautical and space activities of the United States shall be conducted so as to contribute . . . to the expansion of human knowledge of phenomena in the atmosphere and space. The Administration shall provide for the widest practicable and appropriate dissemination of information concerning its activities and the results thereof."

— NATIONAL AERONAUTICS AND SPACE ACT OF 1958

NASA SCIENTIFIC AND TECHNICAL PUBLICATIONS

TECHNICAL REPORTS: Scientific and technical information considered important, complete, and a lasting contribution to existing knowledge.

TECHNICAL NOTES: Information less broad in scope but nevertheless of importance as a contribution to existing knowledge.

TECHNICAL MEMORANDUMS: Information receiving limited distribution because of preliminary data, security classification, or other reasons.

CONTRACTOR REPORTS: Scientific and technical information generated under a NASA contract or grant and considered an important contribution to existing knowledge.

TECHNICAL TRANSLATIONS: Information published in a foreign language considered to merit NASA distribution in English.

SPECIAL PUBLICATIONS: Information derived from or of value to NASA activities. Publications include conference proceedings, monographs, data compilations, handbooks, sourcebooks, and special bibliographies.

TECHNOLOGY UTILIZATION PUBLICATIONS: Information on technology used by NASA that may be of particular interest in commercial and other non-aerospace applications. Publications include Tech Briefs, Technology Utilization Reports and Technology Surveys.

Details on the availability of these publications may be obtained from:

SCIENTIFIC AND TECHNICAL INFORMATION OFFICE

NATIONAL AERONAUTICS AND SPACE ADMINISTRATION

Washington, D.C. 20546